Curling Deformations in Cement Paste Slabs and Effects of Shrinkage Reducing Admixtures

by

Eloy E. Martinez

Bachelor of Science in Civil Engineering
University of New Mexico, 1994

Submitted to the Department of Civil and Environmental
Engineering in partial fulfillment of the requirements for
the degree of

Master of Science of Civil and Environmental Engineering

at the

MASSACHUSETTS INSTITUTE OF TECHNOLOGY

February 1998

Author ....
Department of Civil and Environmental Engineering
January 16, 1998

Certified by ....
Professor Oral Buyukozturk
Professor of Civil and Environmental Engineering

Accepted by ....
Joseph M. Sussman
Chairman, Departmental Committee on Graduate Studies

Curling Deformations in Cement Slabs and Effects of Shrinkage Reducing Admixtures

by

Eloy E. Martinez

Submitted to the Department of Civil and Environmental
Engineering in February 1998, in partial fulfillment of the
requirements for the degree of
Master of Science in Civil and Environmental Engineering

Abstract

Curling stresses in concrete slabs poured on grade may be caused by both non-uniform temperature and moisture distributions through the slab thickness. If the gradients of temperature or moisture content are sufficiently high, very large stresses are induced which surpass the tensile strength of the material. Cracking results which then may serve as initiator sites for the ingress of external corrosive materials. Structural integrity may not be lost but serviceability of the structure is lessened due to the unsightly cracks. If corrosion of the reinforcement proceeds, staining and spalling of the concrete may ensue, further reducing the structures serviceability.

Due to the complexity of studying concrete slabs, such as the variation in effects of constituent materials such as coarse and fine aggregate type, quality and content, and the variation of temperature due to varying external conditions, cement paste slabs were investigated with the goal to predict curling stresses as a function of mix design, and time. A three phase study was developed to address: the design of new testing procedures to quantify curling deformations due to non-uniform moisture content in the slabs thickness, evaluation of the effects of a shrinkage reducing admixture on the curling phenomenon and moisture profile, and the development of a theoretical model to predict curling deformations and stresses resulting from uneven drying conditions of cement slabs.

Experiments were conducted using both normal and high strength paste mix designs with 0, and 5% replacement of mixture water by weight with a shrinkage reducing admixture (SRA), and 0, and 7.5% silica fume content. The time dependent mechanical and material properties measured were modulus of elasticity, compressive strength, shrinkage strains, and curling deformations. The addition of the SRA had varying effects on mechanical properties depending on the specific mix. The addition of the SRA reduced shrinkage strains by 40% in a 90 day period, and curling deformations by 60% up to 90 days. However for very low water-to-cementitious ratios (W/C = 0.25), the admixed specimens curled more than the companion control specimens. A computer model was developed which predicts curling deformations.

Thesis Supervisor: Oral Buyukozturk
Title: Professor of Civil and Environmental Engineering

ACKNOWLEDGEMENTS

TABLE OF CONTENTS

TABLE OF CONTENTS

TABLE OF CONTENTS

LIST OF FIGURES

LIST OF FIGURES

LIST OF FIGURES

LIST OF FIGURES

LIST OF FIGURES

LIST OF TABLES

LIST OF TABLES

Chapter 1

Introduction

1.1 Background

Deterioration experienced by infrastructure due to unforeseen modes of failure in concrete structures has significant social and economic implications. Durability is one of the most important considerations that an engineer must address when planning and designing new structural systems. Cyclic loadings due to mechanical and temperature effects can cause the initiation and propagation of cracks. These cracks then serve as rapid transport sites for external corrosive agents such as carbon dioxide, carbon monoxide, de-icing and/or marine salts, and sulfates. Once these agents penetrate the cover layer of concrete and reach the steel reinforcement corrosion may initiate and then propagate. Since the products from the corrosion reaction occupy a greater volume than the original material hydraulic stresses develop further cracking the cover concrete. This may lead to unsightly cracking, staining, and at later stages spalling. Structural integrity may not be compromised, but serviceability certainly is. Therefore, designers should account for any sources of premature cracking of structural members.

One source of cracking typically not accounted for in conventional design practice are those cracks caused by excessive curling stresses due to restraint of curling deformations. These deformations arise due to non-uniform moisture and/or temperature profiles through the slab thickness. Although there have been several studies conducted with regards to temperature related curling problems [Westergaard, 1926, Bradbury, 1938], there is a gap in knowledge for curling in slabs due to moisture movement. Therefore the focus of this research is to study the fundamental mechanisms related to curling of cement slabs and use this information to develop an analytical model to predict curling deformations due to moisture changes through the thickness of slab structures.

1.2 Problem Statement

The modeling of deformations of concrete slabs poured on grade due to external environmental conditions is a topic area of interest for the construction industry for the prevention of excessive cracking. Floor systems such as parking garages, industrial storage facilities, bridge decks, and even residential floors are affected by the early age curling deformations associated with moisture movement in slabs. Exposed surfaces dry at different rates than those insulated by subgrades. As drying proceeds a very non-uniform moisture profile occurs which results in differential shrinkage through the thickness of the slab.

The differential shrinkage occurs because the cement matrix in concrete expands slightly when saturated and shrinks when dried. Therefore in order to study the curling phenomenon, one must first understand the mechanisms of drying shrinkage and expand the knowledge gained from that field to curling. Recent advances in cement additive technologies have occurred and several different types of shrinkage reducing admixtures (SRA's) have been developed. Hence, in order to fully address the problem of curling deformations this study will focus on both conventional as well as admixed neat cement slabs. Concrete is not addressed due to several complicating factors which arise due to the size, gradation, and quality of coarse and fine aggregate.

1.3 Need for Enhanced Modeling Approaches

The analysis of rigid pavements subjected to transverse loads and temperature variations has been conducted by many researchers [Westergaard 1926, Westergaard 1927, Bradbury 1938, Pickett 1946, Harr and Leonards 1959, Al-Nasara and Wang 1994, Mohamed and Hansen 1997], but the problem of variational moisture conditions through the thickness of the slab must still be addressed in detail. One of the earliest stress analysis for temperature effects on pavements was conducted by Westergaard in 1926. Later in 1938 Bradbury improved the analysis of Westergaard by developing a simple design chart to evaluate curling stresses in finite slabs with free edges. Moisture content was considered of secondary importance in both analyses and nonlinear temperature effects were treated as equivalent linear distributions through the slab thickness. The stresses calculated with this assumption can grossly underestimate actual stresses [Mohamed and Hansen 1997]. Both

Westergaard and Bradbury modeled the slabs as plates fully supported on Winkler foundations which maintain full support during the lifetime of the structure. Many researchers have documented that full support of slabs does not occur [Harr and Leonards 1959]. Instead partial support is the rule, and the resulting stresses developed coupled with mechanical and temperature effects may be several orders of magnitude larger than those caused by simple wheel loads. Although Westergaard and Bradbury had to make the simplifying assumption of full contact and support, many designers to date use their theory as a design guideline to calculate curling stresses and deformations due to temperature effects.

There is insufficient research on the mechanisms of curling deformations caused by moisture, and there is a considerable need to fill this void of knowledge. There is also a need to take mechanistic work and translate it into readily available computational tools and guidelines so that the engineering community can address this important design problem.

1.4 Objectives of the Research

Many modern designers have access to very sophisticated computational design tools, i.e. packaged finite element programs for the analysis of structural elements, but those in smaller design firms may not have the same access or expertise to use the available software. So these designers rely on the simplified theory postulated by Westergaard and Bradbury and most continue the practice of linearizing temperature distributions when conducting analyses and few bother to account for moisture effects at all. Therefore, the objective of this study is to develop in an evolutionary fashion a computational model to accurately predict curling deformations in cement slabs which may then be extrapolated to concrete slabs poured on grade.

Deformations are dramatically affected by the use of modern chemical admixtures that change the unrestrained drying shrinkage behavior of concrete. Therefore, a large portion of the study will address the basic mechanisms that these shrinkage reducing admixtures, (SRA), have on the microstructure of the cementitious composite, and how this then effects macroscopic response.

1.5 Research Approach

The planned course of study shall involve multiple phases conducted in parallel. The first phase is the study of the mechanisms involved in drying shrinkage and differential shrinkage induced by non-uniform moisture profiles in cement paste slabs. Cement paste was chosen as a simpler model than concrete which has natural variations in behavioral response due to the restraining components, i.e. type, quality, content, and grading of coarse and fine aggregate. The second phase provides the analytical modeling requisite to establish a computational tool to quantitatively predict changes in curling behavior as a function of mix design and time. The third and final phase is the implementation of the knowledge learned into the computational model. Comparisons are made between experimental and modeling results in this stage, and final conclusions drawn with suggestions for further research are given.

To address the drying shrinkage-curling problem from a phenomenological approach an extensive experimental program is designed with varied material parameters affecting bulk macroscopic properties such as compressive strength, modulus of elasticity, and modulus of rupture, as well as microstructural properties such as pore size distribution and permeability. Measurements are taken under varying environmental conditions to establish a relationship between moisture content and free shrinkage. Mass loss measurements will also be useful to determine rates of moisture flow from different mixes. To establish the shape of the moisture profiles for varying mixes, electrochemical impedance spectroscopy techniques will be used to establish trends on changes in cement dielectric properties as a function of curing condition, storage environment, and time. Curling deformations are induced in plate specimens by sealing five sides and allowing moisture movement only from the top surface. Measurements are taken in time and the specimens are stored in a constant environmental condition. The information obtained from the experimental program will be used to verify the analytical analysis to be conducted in the second phase.

The second phase of the study is to develop an analytical model of drying behavior of cement and correlate this information with drying shrinkage to calculate the residual stresses and deformations experienced slabs. Considerable work has been previously done in the area of uniform and linear temperature gradients in slabs to calculate induced

responses. Moisture effects are therefore modeled using similar assumptions, except non-uniform moisture profiles are accounted for. This portion of the study treats the slab response independent of restraint and boundary conditions due to subgrade reactions.

The final phase of the study is to use the analytical model as the basis for computational model which can accurately predict the curling behavior of cement slabs accounting for mix design and the passage of time. The requisite comparisons with experimental results are conducted.

1.6 Thesis Organization

Chapter 2 of this thesis provides a succinct literature review of factors affecting drying shrinkage and curling deformations. Current analysis techniques will be presented and problems associated with the simplifying assumptions used for these techniques will be discussed.

Chapter 3 presents the experimental aspects of this work. New testing techniques for quantifying drying shrinkage as a function of moisture content, curling deformations, and moisture profiles as well as standardized testing for mechanical properties will be presented. Chapter 4 discusses interesting trends found in the results for both conventional mixes and those admixed with SRA's.

Chapter 5 describes the analytical modeling of drying and the relations used to correlate moisture content to shrinkage strains. The computational model will also be presented. This Chapter also compares experimental results with the predicted curling behavior given by the computational model. Any discrepancies are discussed as well as further suggestions to obtain additional required data.

The final chapter will summarize the work accomplished, draws conclusions and makes recommendations concerning future work. Comments on further possible refinements of the newly developed testing techniques as well as possible applications of the moisture profile technique to field conditions are made.

Chapter 2

Literature Review

2.1 Introduction

This chapter presents the necessary background information. Basic definitions of technical terms are presented first. A discussion of general background information concerning concrete and cement paste and then the key models proposed for drying shrinkage are presented. A short discussion pertaining to shrinkage reducing admixtures is presented, and then correlation between drying shrinkage and curling deformations is discussed. Finally, some of the modeling assumptions and restrictions presented by previous researchers to predict curling deformations in plate structures are discussed.

2.2 Definitions

2.2.1 Curling

Curling, also called warping, is the distortion of an originally planar member into a curved surface. For concrete or cement slabs the curling deformations are induced by non-uniform moisture or temperature profiles through the slab thickness [Ytterberg, B 1987].

2.2.2 Shrinkage/Swelling

Neville defines shrinkage/swelling as the volumetric change in concrete or cement [Neville 1996]. Drying causes a decrease in volume, i.e. shrinkage, while wetting causes in increase in volume, i.e. swelling. This volumetric change may be induced by several different mechanisms and so is further subdivided as: autogeneous shrinkage, plastic shrinkage, chemical shrinkage, and drying shrinkage.

2.2.2.1 Autogeneous Shrinkage

Autogeneous shrinkage occurs due to the consumption of internal moisture content from hydration reactions also referred to as self-desiccation. According to the Power's model of cement paste, mixes with water-to-cement ratios greater than 0.38 contain sufficient water to completely hydrate [Soroka 1972]. For lower water-to-cement ratios Neville reports

that autogeneous shrinkage may increase depending on the rigidity of the microstructure. One can expect higher values of autogeneous shrinkage with increasing temperature, higher cement contents, finer ground paste, and pastes which contain high values of trical-cium aluminate and tetracalcium aluminoferrite. Due to the restraint of aggregate particles and the hydrated structure of paste the autogeneous shrinkage in concrete is often an order of magnitude lower than in paste [Czernin 1962]. Pickett addressed this problem in the early forty's and developed a the following relation:

$$S = S_o(1 - g)\alpha \qquad (2.1)$$

where S is the shrinkage of the mortar or concrete, S_o is the shrinkage of the paste, g is the proportion by volume of aggregate in the unit volume of concrete, and finally α is the constant derived from the compressive modulus of elasticity of the aggregate and the cement paste. Hence the model for shrinkage and curling deformations for paste should account for autogeneous shrinkage while for concrete it may be ignored.

2.2.2.2 Plastic Shrinkage

Plastic shrinkage describes the shrinkage that occurs prior to cement setting caused by moisture loss, i.e. bleeding and evaporation from the top surface of the slab and capillary suction in subgrades at lower moisture contents than the slab. The rate of moisture loss is affected by temperature, convective forces, and ambient relative humidity. Plastic shrinkage occurs when the mix still acts like a very viscous liquid. As soon as the rigidity of the matrix is sufficiently high, plastic shrinkage ceases. Surface crazing or cracking may occur, but can be prevented if the structural member is wet cured. Dry subgrades should be avoided to prevent moisture loss from the bottom surface of the slab. The interest of this thesis is on the material behavior of cement after setting has occurred, so this type of shrinkage is not addressed in the modeling section.

2.2.2.3 Chemical Shrinkage

Chemical shrinkage is a blanket terms used to describe shrinkage or swelling changes resulting from chemical reactions, such as thermal shrinkage, dehydration shrinkage, crystallization shrinkage, and carbonation shrinkage. Since these types of shrinkage predominately occur close to the setting time they also shall not be included in the analytical modeling section. Carbonation shrinkage will only effect the outermost layers of speci-

mens and so plays a small role in typical sized specimens, however for very small specimen it may play a larger role. The small scale specimens used in this study were not sealed in a CO_2 free environment and hence may experience some problems due to this phenomenon.

2.2.2.4 Drying Shrinkage

The final type of shrinkage to be defined plays the largest role in the typical environments of interest for this study. The environment range of interest is between 40-100% relative humidity (RH). This type of environment is typical of moderate climates such as those experienced in the Eastern United States. Drying shrinkage is defined as the negative volumetric change induced by the removal of moisture. Drying shrinkage is composed of two parts, reversible and irreversible drying shrinkage. Irreversible drying shrinkage is that portion of drying shrinkage is not recoverable. Most of the irreversible drying shrinkage occurs during the initial drying period, with subsequently smaller percentages from additional wetting-drying-rewetting cycling [Neville 1996, Czernin 1972, Soroka 1979]. This may occur due to reorganization of microstructural bonds when gel particles come in close enough contact. Soroka comments that the reorganization of bonds occurs to reduce the free surface energy of the system [Soroka 1979]. This idea is also postulated by Scherer, but with respect to sol-gels [Scherer 1992, A, B]. For very low external relative humidity environments, the percentage of irreversible drying shrinkage increases. Reversible drying shrinkage is caused by the alternating storage of specimens under dry and wet conditions and is the portion of drying shrinkage which is recoverable. Figure 2.2.1 depicts the shrinkage behavior of a paste due to typical drying rewetting drying cycles [Adaptation of figure given by Soroka 1979, Neville 1996]. One should note that since a primary source of moisture movement in cement paste is diffusion, there is a size effect which must be accounted for when comparing data from different sized specimens.

Typical values of drying shrinkage for concrete are between 400 to 800 millionths [Ytterberg 1987, A]. Larger ranges are possible depending on a number of different factors. The factors which affect shrinkage include water-to-cementitious ratio, water and cement content, the microstructure of paste, the use of chemical admixtures, aggregate content, type and quality, the degree of hydration, and the curing conditions [Soroka 1979,

Neville 1996]. These factors will be further discussed in the overview portion of this section.
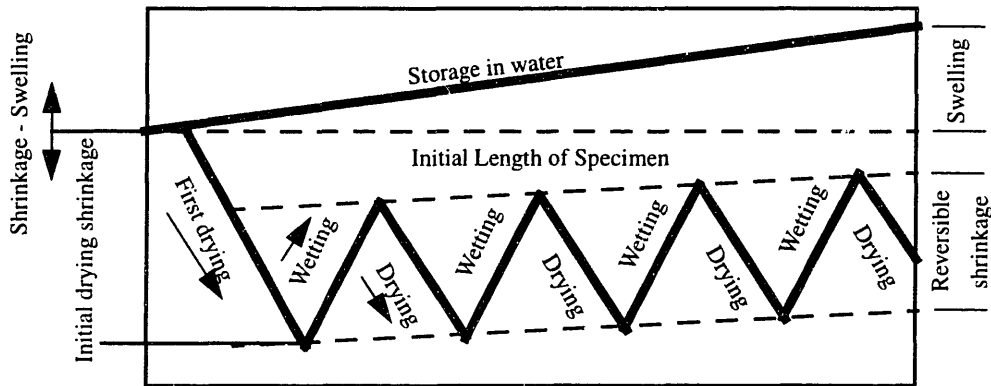
Figure 2.2.1. Shrinkage behavior due to drying then wetting cycles.

2.2.3 Cracking Stress

Cracking in cement takes place whenever the general state of stress exceeds the intrinsic strength of the matrix. Due to the heterogeneity of the paste structure, the failure envelope for cement is radically different than that of metals. Cement paste is able to carry significant loads in compression while its tensile strength is typically one-tenth of its compressive strength. From classical linear elastic fracture mechanics, the theoretical strength of a material is dependent on the strength and type of intermolecular forces and intermolecular spacing. This calculated value typically exceeds measured values by three orders of magnitude.

The difference in strengths is due to the presence of cracks or flaws in the material which experience very high stress concentrations when subjected to external loads [Griffith 1920]. Griffith developed a criterion for cracking of brittle materials based upon energy release rates. He considered an elliptical crack, and calculated the associated decrease in elastic strain energy in a plate due to the formation of this type of crack. Next he suggested that in order for a crack to propagate that a critical energy release rate must be reached, i.e. the strain energy release rate must equal the energy release rate associated with creating new crack surfaces. This is succinctly represented by the expression

$$\frac{\partial}{\partial a}\left(\frac{\pi a^2 \sigma^2}{E}\right) = \frac{\partial}{\partial a}(4\gamma_{sv}a) \qquad (2.2)$$

which upon simplification results in the classic Griffith equation

$$\sigma = \sqrt{\frac{2\gamma_{sv}E}{\pi a}} \qquad (2.3)$$

where σ is the applied stress, a is the crack half size, E is the materials modulus of elasticity, and γ_{sv} is the solid-vapor interfacial surface energy. Since the flaw size is in the denominator of the expression, it is expected that larger flaw sizes will decrease the strength of the material. Also, the solid-vapor interfacial energy should decrease as a function of increasing internal relative humidity, thereby decreasing the strength of the material. The interfacial energy is measured indirectly by comparing the strengths of specimens subjected to different relative humidity environments. The failure criterion is clearly represented in Figure 2.2.2 [adapted from Soroka 1979].
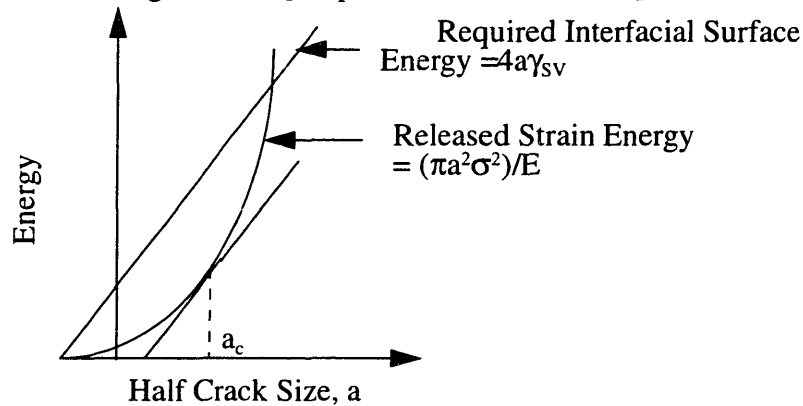
Figure 2.2.2. Energy release rate failure criterion for a brittle material.

When the energy release rate becomes critical, that is at impending motion of the crack, the slope of the required interfacial energy equals the slope of the parabolic relation for critical strain energy release.

The significant difference between the strength in tension versus compression in cement paste is the fact that in tension the energy release rate increases with crack size, and the first activated crack is the critical crack. In compression, the release rate is constant and independent of crack length, so multiple cracks may grow in a stable manner until the multiple cracks grow and/or coalesce to a sufficient size to cause failure [Soroka 1979].

2.3 Overview

2.3.1 General Background

Concrete is a complex particulate composite composed of stones and sand (the aggregates up to 70% of composite) that are held together by an adhesive. This adhesive is generally a

Portland cement mixed with water and a few specialty admixtures added to obtain specific enhanced material properties. Portland cement is manufactured by firing a controlled mixture of chalk, $CaCO_3$, and clay at high temperatures. The clay is made up of Alumina, Silica, and water.

To describe the processes and reactions more succinctly, a reduced nomenclature is introduced: Lime, CaO, is denoted by C, Alumina, Al_2O_3, by A, Silica, SiO, by S, Ferrite, Fe_2O_3, by F, and water, H_2O, by H. When the Portland cement is mixed with water during the batching process, a hydration reaction occurs that changes the microstructural character of the cement and binds the system together. The main constituents of cement clinker are tricalcium aluminate, C_3A, Dicalcium Silicate, C_2S, Tricalcium Silicate, C_3S, Tetracalcium Aluminoferrite, C_4AF, and gypsum, CS. The first hydration reaction involves the constituents C_3A, gypsum, and water. The reaction produces ettringite, $C_6AS_3H_{32}$, in an exothermal reaction. Ettringite is a crystalline structure and is responsible for the setting and early strength of concrete (first 2 - 4 hours). Hydration reactions involving C_2S, C_3S, and water produce calcium silicate hydrates, CSH, calcium hydroxide, $Ca(OH)_2$ or CH, and heat [Soroka 1979, Neville 1996, Czernin 1962]

Cement gel is what is responsible for the long term strength of the composite. It is the main bonding material and occupies approximately 70% of the solid matter in pure cement pastes specimens. The gels formed are covalently bonded in sheets and experience high surface forces between sheets. The gel pores are formed when fribillar rods grow from cement grains and interlock leaving areas with small microvoids exposed. Calcium hydroxide forms in small crystals that grow in interfacial regions. It can provide some strength to the composite, but usually orders of magnitude below the corresponding strength of gel particles.

What follows is a succinct review of the parameters which affect the microstructural character of typical mix designs. These same factors play roles in the response of mixes to drying shrinkage and hence curling deformations.

2.3.2 Water-to-Cement Ratio, Cement Content, and Water Content

Several authors have commented on the effects of water-to-cement ratio (w/c), cement content, and water content on shrinkage [Soroka 1979, Bazant and Whittmann 1982, Nev-

ille 1996] The trend for w/c ratios is that mix designs with higher values shrink more than those with smaller values at later time periods (in excess of 90, days). Mixes containing high cement contents usually experience increased shrinkage. Higher water content mixes also experience greater shrinkage values. All three factors have a profound impact on the microstructure.

2.3.3 Microstructure

The pore structure of the composite governs the effects of both bulk and microstructural properties. One of the most important measures of microstructure quality is permeability. Permeability is a measure of the ease or rate of transport of matter, solid, liquid, or gas, in a porous media. From electro-chemistry we know that the surface region of any body is, in a thermodynamic sense, more reactive than the interior. This fact is especially true where ratios of surface area to volume are very large, as in the porous networks of cementitious composites. Porosity is dependent on: curing temperatures, the size, shape and roughness of aggregate inclusions, the water to cementitious material ratio, the degree of hydration of the cementitious paste, and the uniformity of hydration products and inclusions in the mix after batching and setting [Neville 1996].

Three separate types of porous structures are generated during batching and setting: gel pores, capillary pores, and air voids. The state of water in the pores of a hardened cementitious composite matrix are described as: chemically bound, physically adsorbed, and/or free. Gel pores range in size from less than 0.5 nm to 10 nm. These micro-pores experience surface forces that intensely adsorb water and prevent it from forming a meniscus. Capillary pores range in size from 10 nm to 15 μm. Water in these pores experience moderate surface forces. Finally macro-pores or air voids range in size from 15μm and larger. The water in these pores have the properties of its body phase. Air voids and capillary pores affect the macro-mechanical properties of strength, shrinkage and permeability. Gel pores strongly affect shrinkage and creep of the cementitious composite [Neville 1996].

2.3.4 Chemical Admixtures

The addition of pozzolanic particles to the mix causes an additional set of hydration reactions to occur. The pozzolanic admixtures (fly ash and silica fume) react with calcium

hydroxide to form more CSH. Again, this reaction is exothermic and caution must be used to insure that excessive shrinkage and microcracking does not occur. Pozzolanic additives may be much finer particles than cement grains increasing the overall density of the matrix and reducing the size of the interfacial transition zone [Neville 1996].

Other admixtures generally used for manufacturing high performance cementitious composites are superplasticizers, air entraining agents, and recently drying shrinkage reducing admixtures. The data available for superplasticizers is indecisive. This may be due to the fact that the use of these admixtures allows mix designs to have decreased water and/or cement contents which increases shrinkage yet the rigidity of the microstructure matures quicker so it may be able to resist the higher tendencies to shrink. Air entrainment has little or no effect on shrinkage, because the pores size of these air voids are sufficiently large that when moisture is removed, surface forces of high intensity are not generated [Soroka 1979 Neville 1996]. However, excessively air-entrained mixes (i.e. > 10%) will have decreased rigidities which may allow for larger shrinkage values. Recent publications on shrinkage reducing admixtures demonstrate that very significant reductions are possible in the order of 20-50% depending on mix design [Berke et al. 1996]. That is why these types of admixtures are a key focus of the present study.

2.3.5 Aggregate Content, Type, and Quality

The aggregate particles in concrete or mortar serve as restraining agents against which the shrinking paste must conform. The content of and grading of both coarse and fine aggregates is important, because poorly graded mixes with low aggregate contents allow higher concentrations of free paste which may shrink and crack. Certain types of aggregates shrink less than others (i.e. granite, limestone, or quartz vs. dolerites, basalts, or mudstones) and may also imbibe water from the mix further increasing volumetric shrinkage strains. The quality of the aggregates is dependent on the location from a quarry or other source that it is taken from and the weathering that it has been subjected to. Dirty aggregates, or aggregates covered with clay type materials will exhibit much greater shrinkage strains than equivalent cleaned aggregates since clay has a great propensity to shrink [Soroka 1979, Neville 1996].

2.3.6 Degree of Hydration

Soroka has reported a positive correlation between the degree of hydration and the amount of shrinkage that a given mix experiences. The higher the degree of hydration, the higher the gel content and the lower the capillary pore content. Since moisture loss from larger voids induce small or no shrinkage strains, the more mature microstructure shrinks greater [Soroka 1979]. Yet he cautioned that the effect is small since one requires a low relative humidity environment to empty the smallest pores and induce the shrinkage strains. Therefore the degree of hydration is of second order effects and may not need to be accounted for in an analysis.

2.3.7 Curing Conditions

The curing conditions and storage environments of mix designs play a major role in the development of microstructure, but a lesser role for drying shrinkage. Longer periods of curing delays drying shrinkage strains and allows the microstructure to mature by increasing matrix rigidity. Greater percentage content of gel pores in neat cement pastes due to longer curing periods may increase shrinkage values because there is less restraining material to resist the shrinkage, but these values may be offset by the fact that the matrix is quite rigid. So curing condition may also be of second order effects.

According to Neville, the length of curing is not important for concrete mixes. Steam curing dramatically reduces drying shrinkage values due to the increase in percentage of larger capillary and air pores. External storage environmental conditions affect drying rates and the ability of the generated stresses to be relieved by creep. Moist cured slabs exposed to very low ambient relative humidities may crack. The hygral conductivity in cement and concrete is very low and so for extended exposure conditions, evaporation due to convective currents plays a minimal role.

2.4 Shrinkage Models

There are four mechanisms which affect drying shrinkage [Soroka 1979]. These are: capillary tension, surface tension, swelling pressures, and the movement of interlayer water. The four most commonly referenced models associated with drying shrinkage and which make use of these mechanisms are attributed to: Power, Ishai, Feldman and Serada, and

27

Wittmann.

A succinct description of the four mechanisms and the relative humidity ranges of interest are first given then more detailed discussions as to a combination of the models for use in the course of this paper follows.

(1) Capillary tension [Taken from Soroka 1979]

> The formation of a meniscus on drying results in tensile stresses in the capillary water. The tension in the water is balanced by compression in the solids causing, in turn, elastic decreases in the volume of the paste, i.e. shrinkage. This mechanism is reversible and is considered to be operative when the relative humidity exceeds 40%.

(2) Surface tension [Soroka 1979]

Surface tension may produce very high compressive stresses inside solid particles of colloidal size. Depending on the size and type of material of the particles, the effect of surface tension varies. It has been demonstrated that surface tension is dependent on the amount of physically adsorbed water. Lower adsorption of water molecules induces higher surface tensions in gel particles while higher adsorption reduces the surface tension. This inverse relationship is due to the fact that the solid vapor interface is thermodynamically much more active, i.e. contains more energy, than the solid liquid or liquid vapor interfaces. Therefore, on drying the compression in the gel particles increases causing shrinkage strains to occur. On rewetting, the surface tension decreases, and some of the compression in the solids is relieved, and the material swells.

(3) Swelling pressure [Soroka 1979]

The thickness of the adsorbed water layer is determined by the ambient vapor pressure and temperature. The interparticle spacing of gel plates may be less than the required thickness to accommodate adsorption of water layers, so a 'swelling' or 'disjoining' pressure is developed which tends to separate gel particles. When drying occurs this pressure is relieved because the thickness of the adsorbed layer decreases.

(4) Movement of interlayer water [Taken from Soroka 1979]

> Exit and re-entry of water into the layered structure of the gel particles causes volume changes due to resulting

changes in the spacing of layers, i.e. exit of water on drying causes volume decrease (shrinkage) and re-entry of water on wetting causes volume increase (swelling).

The dominant mechanisms related to the Power's shrinkage model are variations in swelling pressure augmented by the effects of capillarity. According to his model, these mechanisms covers the full range of relative humidity (0-100%). Ishai uses a different approach, applying variations in surface energy in the range of 0-40% RH and capillary tension affects from 40-100% RH. Feldman and Serada make use of the mechanisms of movement of interlayer water in the range of 0-35% RH and both capillary tension and variations in surface energy for relative humidities in excess of 35%. Finally Wittmann applies variations in surface energy and variations in swelling pressure in the ranges 0-40% RH and 40-100% RH respectively. For the purposes of this study, only those mechanisms which contribute to shrinkage behavior in relative humidity ranges exceeding 35-40% will be applied in the modeling section. For completeness of the discussion all mechanisms will be discussed further below.

The volumetric change in concrete has been partially attributed to the movement of water in gel and capillary pores. Cement paste that is subjected to a wet environment swells, whereas in drier conditions it shrinks. One mechanism that relates shrinkage to moisture movement is that of capillary tension (Please refer to Figure 2.4.1).
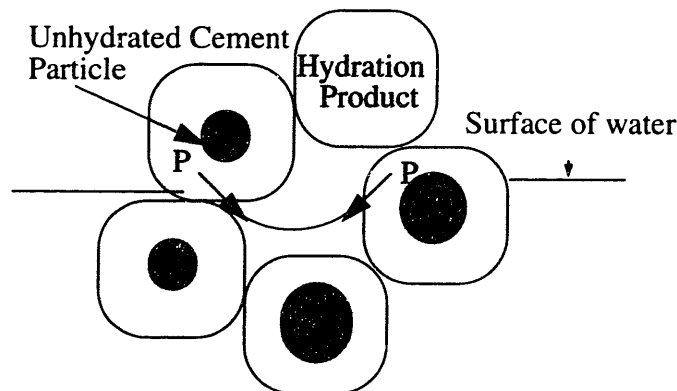
Figure 2.4.1. Representation of surface tension effects in the pore microstructure.

The vapor pressure of a liquid is defined as the pressure at which liquid and vapor coexist in equilibrium. This means that the total number of molecules leaving the liquid phase into the vapor phase equals the total number of molecules leaving the vapor phase and entering the liquid phase. When evaporation takes place in a liquid, the total number of molecules leaving the liquid phase exceeds the number reentering it from the vapor. The

29

relative vapor pressure of a liquid is typically defined as the ratio of pressure over the liquid in its current state, P, over the saturated vapor pressure at the same temperature, P_o. When the liquid of interest is water, many researchers refer to the vapor pressure expressed as a percentile as relative humidity, RH. In cement systems, if the pore walls are exposed to the vapor phase of water, the energy state is higher than the associated liquid vapor surface energy. The system always tends towards the lowest energy state, and so a curved meniscus forms spreading the liquid phase across the exposed solid phase. The tension in the liquid is related to the radius of the meniscus through the Laplace equation

$$\sigma' = -2\frac{\gamma_{LV}}{r} \qquad (2.4)$$

where the liquid tension is denoted by σ', the radius of curvature of the meniscus is r, and γ_{LV} is the liquid/vapor interfacial energy. The form of the Laplace equation presented is that for right cylindrical pores with equi-sized in- and out-of-plane radii of curvature. The liquid is in tension when the radius of curvature is negative (which occurs during evaporation of pore liquid) and the pore water wets the solid phase surface. The relation between the radius of curvature, r, of the meniscus and the corresponding vapor pressure P is given by Kelvin's equation

$$\ln\left(\frac{P}{P_o}\right) = \frac{2\gamma_{LV}}{RT\rho r} \qquad (2.5)$$

where P_o is the saturation vapor pressure, γ_{LV} is the liquid/vapor interfacial energy or surface tension, R is the universal gas constant, T is the temperature in degrees Kelvin, and ρ is the density of the liquid. The Kelvin equation is applicable for pores in the ranges ~5-5000 angstroms. For smaller pore sizes the concept of a meniscus breaks down, because the surface forces are so intense a meniscus cannot form. For larger pores sizes the Kelvin equation does not provide any useful information and BET techniques break down.

Returning to the expression, for a capillary pore experiencing no evaporation, the ratio $P/P_o = 1$, and the surface of the water is flat, i.e. the system is fully saturated. Subsequent decreases in the vapor pressure occur when evaporation starts and the radius of the meniscus becomes smaller until a critical point where it equals the radius of the pore. At that point it enters the pore and if further evaporation occurs the pore empties completely [Scherer 1992, Soroka 1979].

The relation helps describe why the large pores empty first and then progressively smaller pores as drying continues. Since drying rates are dependent on the pore sizes and distributions, this relation helps to explain, to a certain extent, why one would expect higher moisture loss as a function of increasing water-to-cement ratio early on.

The tensile stresses in the pore water are balanced by compressive stresses in the solid. These compressive stresses cause an elastic decrease in volume. The response of the solid network and subsequent elastic deformations are dependent on the skeletal rigidity. Therefore, for equi-distributed pore size distributions, pastes with higher elastic moduli will shrink less. This explains why pastes with lower water-to-cement ratios experience less shrinkage.

This mechanism can also explain why at early ages of drying there is a large amount of water lost with relatively little shrinkage. The large pores contribute little to shrinkage strains (see Laplace's equation above) and these are the pores that empty first. At later stages, the micropores become active and increased shrinkage is experienced with a decreased rate of moisture loss [Soroka 1979].

The forces experienced by the solid skeleton are related to the tensile force in the pore solution through the following expression:

$$f_c = \sigma' \times A_c \tag{2.6}$$

where f_c is the compressive force, σ' is the tensile force in the liquid, and A_c is the cross-sectional area of the water filled capillary pores. When a critical stage is reached during the drying process, a maximum value of shrinkage is obtained. Upon further drying some of the induced shrinkage strains should be recovered, and after complete drying full recovery must be expected if this mechanism holds. In general this behavior is not exhibited and so other mechanisms must be acting, because experimental results indicate that shrinkage continues until complete dehydration has taken place. The removal of water from interlayer CSH may account for the continued shrinkage strains observed.

The second major mechanism which affects drying shrinkage is attributed to the surface forces exerted by the colloidal particles. Surface tension experienced by these particles occurs due to the difference in electrostatic attraction of atoms or molecules at the surface versus the same type of atoms or molecules in the interior of the particle. The inte-

rior molecules are attracted/repulsed by their closest packed neighbors on all sides. Those on the surface have a complete plane where the attraction/repulsion of similar molecules does not occur, and the interaction between the solid surface and the gaseous interface is not in equilibrium. The surface contracts upon itself and so results in tensile forces. This 'surface tension' is defined as the force acting tangentially to the surface per unit length of surface. The units of surface tension are given as N/m. Energy must be applied to the system to increase the area of a surface. The units of surface energy are given as $ergs/cm^2$.

Returning to the form of the Laplace equation, but applying it now to the solid surface, the solid vapor interfacial energy, γ_{sv}, is related to the inverse of the radius of curvature of the particle. For simplified analysis, spherical particles are chosen with the relation then equal to

$$\sigma = \frac{2\gamma_{sv}}{r} \qquad (2.7)$$

For the colloidal size gel particles compressive forces can easily reach 250 N/mm^2. This is of sufficient magnitude to induce reduction in volume of the solid gel. Adsorption of water molecules on the surfaces of the gel reduce the interfacial tension and the gel expands elastically. A common expression relating changes in interfacial surface energies to shrinkage strains is [Soroka 1979]

$$\frac{\Delta l}{l} = \varepsilon_{sh} = k(\gamma - \gamma_o) \qquad (2.8)$$

where γ and γ_o are the solid-vapor interfacial energies at to different constant relative humidity environments.

This expression predicts a linear relationship between shrinkage strain and changes in solid-vapor interfacial energy. It is expected that this relationship will hold only for the adsorbed layers on the gel, and not for gels with excess moisture. As such it is only applicable to very dry specimens (stored in environments < 40%RH). For the purposes of this study, it will play a lesser role than a similar expression relating solid-liquid, liquid-vapor energies.

The third mechanism, swelling pressure is also commonly referred to as disjoining pressure. This pressure is generated when two gel particles are spaced close enough together that the number of adhered layers of water molecules typical of the given internal relative humidity are compressed. An easy way to picture this scenario is to imagine that

32

water adsorbed on a charged surface exhibits an ordered structure. When additional layers become adsorbed, the extent of order decreases further away from the solid surface. Typical ordered ranges for cement gels are five molecular layers, or 13 angstroms. Because of the ordered nature of this water, if two parallel plates are spaced slightly under the thickness of the adsorbed layers (~26 angstroms) a pressure is generated. The ordered water is capable of bearing 'load'. The chemical potential of this water is then at a higher state then free water and diffusion towards the lower chemical potential water may take place. Some researchers use this idea as one of the basic mechanisms for creep. Higher relative humidities result in greater numbers of adsorbed layers and hence increase swelling. Lowers relative humidities cause shrinkage. This is the primary mechanism involved in Powers model. Feldman and Serada discount this argument.

The final mechanism to be discussed is that of movement of interlayer water. Powers discounts the importance of this mechanism, while Feldman and Serada insist that this a governing mechanism for moisture movement at very low relative humidity environments, i.e. <35% RH). Movement of the interlayer water in the Feldman and Serada model is possible both outwards during drying and inwards during re-saturation. The other models presented consider the spacing between the CSH sheets fixed and once interlayer water leaves it cannot return. Hence the shrinkage is irreversible [Soroka 1979].

This concludes the discussion on the mechanisms which contribute to drying shrinkage. The most important one of interest in the range of environmental conditions applicable to this study is that of capillary tension. The next section presents a simplified explanation of how the shrinkage reducing admixture works. This information will then be applied and tested in the analytical modeling section.

2.5 Shrinkage Reducing Admixtures

Several new types of shrinkage reducing admixtures have been proposed both in Japan as well as in the United States [Ogawa et al., 1993, Fujiwara et al., 1994, Shah et al., 1992, Shah et al., 1997, Shoya et al., 1990, A, B, Tomita et al., 1986, Uchikawa 1994]. These admixtures are direct applications of the dominant mechanism described above. They are surfactants which reduce the solid-liquid, liquid-vapor interfacial surface energies in the

analysis of calculating shrinkage stresses applying the Laplace equation, the relative amount of expected decrease in shrinkage is directly related to the decrease in surface tension of regular pore solutions versus admixed pore solutions. Again, mix designs with higher water-to-cement ratios, water content, and cement content are expected to experience greater shrinkage strains. Yet the scaling effect is expected to work for mixes of similar designs.

2.6 Differential Shrinkage Strains

Differential shrinkage strains occur in structural members just after casting due to differences in the rates of drying of interior and exterior elements. If each element were allowed to shrink at its equivalent unrestrained shrinkage value at the given internal relative humidity (RH), continuity between the different layers of the member would be lost. Depending on the internal RH value, the cement or concrete sheet will shrink or swell at a different rate then for lower or higher RH values. Figure 2.6.1. graphically depicts curling deforma-

Non-uniform Drying   Unrestrained Shrinkage in Sheets   Internally Restrained Deformations
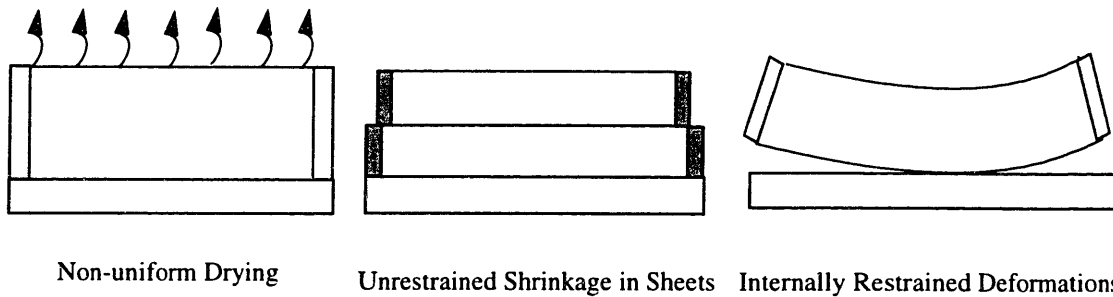
Figure 2.6.1. Differential shrinkage induced by non-uniform drying rates.

tions caused by convective drying from the top surface of a slab alone. The other edges are insulated from moisture movement and one-dimensional flow occurs. The curling deformations resulting from non-uniform moisture profiles are very sensitive to size effects. This happens because the rate of moisture movement from internal regions to a given surface is governed by capillary and diffusional flow. Diffusional flow governs soon after setting takes place. The solution to the one-dimensional flow of moisture in porous media is very non-linear containing and exponential term, so the resulting moisture profile changes dramatically with thickness of the slab (thickness is the characteristic length of the system). The analytical modeling section will present the full solution to the one-dimensional flow problem. The next section presents a brief overview of the assumptions used by pre-

vious researchers to solve the deformation problem.

2.7 General Plate Theory

The theory for calculating plate or slab responses due to external loads is well established. The early theoretical treatment of concrete slabs poured on grade, by Westergaard in 1926, modeled the slab on grade system as a simple plate resting on an elastic foundation (or Winkler foundation). He applied the following simplifying assumptions in order make the problem tractable:

- The slab is elastic, homogeneous, and isotropic with temperature independent material properties.
- Plane section prior to deformations remain plane after bending.
- Stresses and strains normal to the slab face are negligible and assumed to be zero.
- Deflections of the slab are small when compared to overall slab dimensions, (small strain theory).
- The slab is subjected to temperature variations through its' thickness which are independent of time. This temperature variation is constant on all planes parallel to the slabs upper and lower faces.
- Warping is not of sufficient magnitude to result in only partial support by the subgrade.

As he pointed out in his analysis, there are two critical time periods of interest for slabs poured on grade, just after casting and before opening the slab to live loads, and any time after the slab has been opened for general service. Prior to usage, the slab experiences volumetric changes due to changes in temperature and moisture content. If the changes are sufficiently large, the early post set strength of the slab may be exceeded and cracking will ensue. At later times two types of temperature and moisture variations are present, seasonal variations and daily cyclic changes. Irrespective to the effect studied, there are three areas of the slab of interest: the corners, the interior area, and the edges of the slab.

Results obtained from these assumptions have been substantiated with experimental results, but as reported by Leonards and Harr full support of the slab throughout its service life often does not occur. Poorly consolidated subgrades, pumping, and excessive mechanical loads may contribute to only partial support.

Also inducing curling deformations by using equivalent linear temperature gradients through the slab thickness can underestimate actual stress levels. Leonards and Harr pro-

ceeded to calculate curling deformations accounting for slab lift off with a finite difference computer scheme. Again for the sake of simplicity, temperature gradients were linearized and moisture gradient were not addressed. The authors did say that a similar approach could be applied for moisture content. Pickett calculated differential shrinkage strains assuming that shrinkage strains could be modeled following a diffusion like model and obtained fairly good results compared to laboratory experiments. He did not account for the rigidity of the subgrade or possible consolidation of the subgrade. As this type of information was not published in textbooks, because it was considered of secondary importance, many modern researchers have reworked this problem, but most with an emphasis on temperature effects. To the author's knowledge, no one has combined all the knowledge gained form these earliest of researchers and implemented their ideas in a usable computational model for the aid of practicing engineers. Also none of the previous researchers accounted for the effects of shrinkage reducing admixtures, and so the work presented in the analytical and computational modeling section are timely for the use of modern engineers.

2.8 Summary

Since the curling deformation of cement slabs cast on grade arise due to the changes in the moisture content through the slabs thickness, the response of individual layers at a given relative humidity may be superposed on the complete structure provided that linear elastic response governs. It is proposed that the drying shrinkage at different relative humidities can be determined from experimental tests and used in the analytical modeling section. Other parameters of interest are both the shape of the moisture profile and the change in the shape through time. To determine this kind of information very time consuming tests are required. Therefore the experimental methodology section will devote considerable time in the discussion of the development of a new testing technique.

This section presented a succinct literature review of drying shrinkage and some of the previous modeling work for curling deformations. Definitions of key ideas were discussed and detailed discussions of the governing mechanisms were presented. For the typical environmental conditions experienced in the Eastern United States, it is decided that the governing mechanism for drying shrinkage is capillary tension. The key assumptions

required for a simplified analysis of plate structures and drawbacks of some of these assumptions were also discussed. Linear elastic conditions with an isotropic material are the key assumptions. The transfer of mass and heat within the slab system for the conditions of interest are assumed uncoupled. Problems associated with slab lift off/partial support were discussed. This is important due to the large changes in measured stresses for this type of condition as opposed to a fully supported condition. Chapter 5 presents the analytical work associated with modeling these types of systems.

Chapter 3

Experimental Methodology

3.1 Drying Shrinkage Under Varied Environmental Conditions

3.1.1 Introduction

The objective of the drying shrinkage study is to obtain a fundamental understanding of how the shrinkage behavior of neat cement paste specimens are affected by varied constant relative humidities. This information is required to correlate how the curling deformations change with changes in moisture content through a slabs thickness. Also, the use of a newly developed shrinkage reducing admixture is studied to address its effects on shrinkage performance. Reductions in drying shrinkage strains as a result of the addition of this admixture is expected to result in changes in the moisture profile as well as curling behavior. This portion of the experimental methodology is divided into a description of materials used, mixing and casting procedures, and finally storage requirements of different specimens.

3.1.2 Materials and Mix Designs

A type I Portland cement was used throughout this and all the other studies.The generic chemical composition (weight percentage) is as follows: SiO_2 = 21.11; Al_2O_3 = 4.59; Fe_2O_3 = 3.30; CaO = 64.39; MgO = 2.86; SO_3=2.32; NaO_2 = 0.09; and K_2O = 0.54.

The study is interested in the changes of shrinkage behavior with changes in mix design, and time. Therefore, a total of twenty test mixes were designed and are outlined in Table 3.1. In the table the short hand notation used is: W represents water, C represents cement content, SF represents the addition of silica fume, and finally SRA represents the addition of the shrinkage reducing admixture. The addition of silica fume was included in the study to obtain a wide range in pore size distributions, as well as to test the affects of

the SRA on high performance mix designs. Also, the use of silica fume enhances durabil-

Mix Design	W/(C + SF)	% SRA	% SF
Ultra-high Strength (Not used Commercially)	0.25	0	0
High Strength	0.35	5	7.5
Typical Structural Strength	0.45		
Floor Systems	0.55		
Very Poor Quality - Low Strength	0.65		

Table 3.1: Mix designs used in drying shrinkage study.

ity of pastes by reducing the permeability of the mix by several orders of magnitude as compared to a regular neat cement paste. The five percent addition of SRA is by replacement of mixture water. The composition of the SRA is proprietary information and so is labeled by its generic chemical admixture name, SRA.

3.1.3 Casting Procedures and Storage Requirements

Three types of shrinkage specimens were designed: platelets, typical mortar samples filled with neat cement paste, and typical concrete shrinkage specimens, again filled with neat cement paste. The dimensions of the platelet specimens are 5.25 inches in length by one inch depth by one-quarter inch width. The small size was designed to reduce the length of drying time to reach equilibrium and for storage requirements. These specimens were

measured with a modified Humboldt comparometer depicted in Figure 3.1.1. Gauge points

Figure 3.1.1 The modified comparometer used to measure shrinkage strains for platelet specimens used in drying shrinkage study.

were screwed into the end-plates cast in the specimens. The end-plates were constructed from rectangular brass tubing with cap-end screws attached in the casting direction to assure adequate bond between the end-plate and the specimen. Figure 3.1.2 depicts the type of molds used to cast these specimens.

Platelet Mold for Drying Shrinkage Study

each platelet 0.25"x1"x5.25"

Top View

Front View   Side View
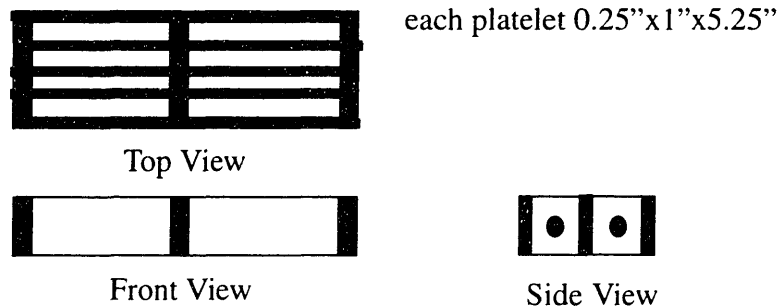
Figure 3.1.2 Mold used to cast platelet drying shrinkage specimens.

The typical size of mortar type specimens are one inch by one inch by eleven inches in length. Gauge points are cast into the samples for readings with a Humboldt Comparome-

ter. The typical size of a concrete shrinkage specimen is three by three by ten inches in length. These specimens also have embedded gauge points and measurements are also read with a Humboldt comparometer. Platelet specimens were cast in triplicates per environmental condition while standard mortar type beams were cast in duplicates.

Figure 3.1.3 depicts the standard comparometer and a typical paste specimen being measured. Figure 3.1.4 depicts the typical mortar mold used to cast these paste specimens.

Figure 3.1.3 Standard mortar comparometer and typical paste specimen used in drying shrinkage study.

Mortar Shrinkage Mold for Drying Shrinkage Study

Shrinkage Prism 1"x1"x11"

Top View

Front View

Side View
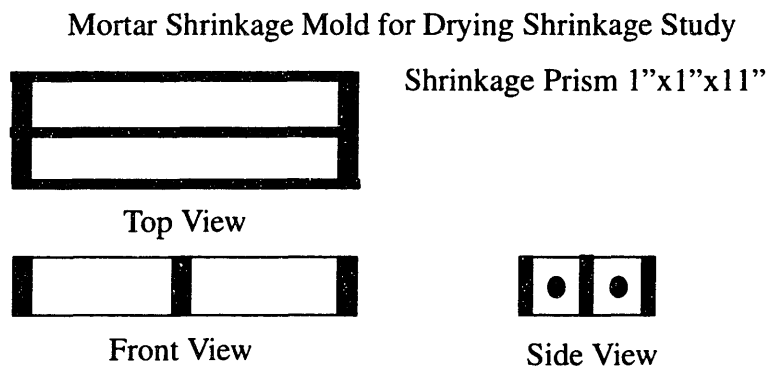
Figure 3.1.4 Mold for typical paste shrinkage prism.

The mixes were batched in a pan mixer for five minutes, with additional time for mixes that exhibited large clumps. One-half the water was placed in the mixer before half of the

41

solid material was added. Initial agitation of the half mix was allowed before the addition of any chemical admixtures and the rest of the materials. Some mixes that maintained lumps after dumping into a wheelbarrow, were further mixed by hand with a garden mashing tool till adequate homogeneity was obtained.

Typical ASTM standards require the partial filling of specimens followed by tamping to assure consistency through the thickness of specimens. However, due to the nature of the paste mixes, specimens were filled in thirds and then vibrated for 30-60 seconds depending on the fluidity of the mix. The small platelet specimens were filled using a plastic 50 cc syringe. All specimens were screeded off in a similar manner. The specimens were covered with plastic sheeting and allowed to cure for one day prior to stripping. The high water-to-cementitous material ratio mixes were allowed to cure for two days to assure adequate rigidity prior to stripping. Typical mortar and concrete type specimens were stripped, painted with a urethane coatings on the ends with gauge points, soaked in a saturated lime solution for thirty minutes and then initial readings of both weight and length were taken. The platelet shrinkage specimens had to be painted on the thin edges with a urethane coating to assure one-dimensional flow from the wide faces. Next they were drilled and end gauge points were attached to the brass tubing end pieces. The specimens were then weighed and initial length measurements were performed following modified ASTM C 157.

After initial measurements of weight and length were take of the mortar and concrete type cement paste specimens, they were stored in a room maintained at 50% RH and 72 °F. The platelet specimens were stored in small environmental chambers constructed of high density polyethylene (HDPE) tubs containing saturated salt solutions to obtain specific relative humidity environments at 72 °F. Table 3.2 lists the types of saturated salt solutions used for the environmental chambers. To ensure adequate dispersion and mixing of internal relative humidity for each chamber, small fans were mounted on the chamber walls and kept on at all times. Specimens were stored on drying racks maintained six-seven inches above the level of the saturated salt solutions, except for the 100% RH specimens,

which were immersed in a sealed container filled with laboratory water. Measurements of

Substance dissolved and solid phase	Temperature °F	% Humidity
Laboratory water	72	100
Zinc sulfate	72	90
Sodium thiosulfate penta-hydrate	72	78
Sodium nitrite	72	66
Zinc nitrate	72	42

Table 3.2: List of saturated salt solutions used in environmental chambers.

change in length and mass were taken at 1, 7, 14, 21, 28, 35, 42, 56, 70, and 90 days for all shrinkage specimens. The results from this portion of the study are discussed in Chapter 4.

3.2 Mechanical Properties

3.2.1 Introduction

The objective of this portion of the study was to determine the evolution of mechanical properties with maturation time. The mechanical properties measured: compressive strength and compressive modulus of elasticity, are used in the modeling portion of the study to predict stress behavior of curling specimens.

3.2.2 Materials, Casting Procedures, and Storage Requirements

The mechanical properties measured were compressive strength and compressive modulus of elasticity. The same mix designs, materials, and casting procedures were used as outlined in the drying shrinkage study above. The compressive strength tests were conducted at 7, 14, 28, 56, and 90 days following ASTM 39-94 guidelines. Modulus of elasticity tests were conducted at 7, 14, 28, 56, and 90 days. All specimens were stripped after one day and then placed with in a laboratory room maintained at 100% RH and 72 °F until the time of their testing. The compressive tests used triplicate 3x6 cylinder specimens while the compressive modulus tests used duplicate 4x8 cylinder specimens at each testing age. The results are further discussed in Chapter 4.

3.3 Curling Deformations

3.3.1 Introduction

The objective of this portion of the experimental methodology section is to quantitatively describe the curling behavior of neat cement paste specimens cast on infinitely hard sub-grades. This information is used to correlate modeling predictions with measured curling response. It is expected that the addition of shrinkage reducing admixtures will change the behavior of the curling specimens.

3.3.2 Materials

The same materials and mix designs described in the drying shrinkage portion of this section were used for the curling deformation study. A total of twenty different test mixes were prepared and tested.

3.3.3 Casting Procedures and Storage Requirements

Each curling specimen had nominal dimensions of 42 inches in length by 2.5 inches in width by one-half inch in thickness, see Figure 3.3.1 for typical mold. The molds were

Molds for Curling Study

Curling Prism 0.5" x 2.5"x 42"

Top View

Front View   Side View
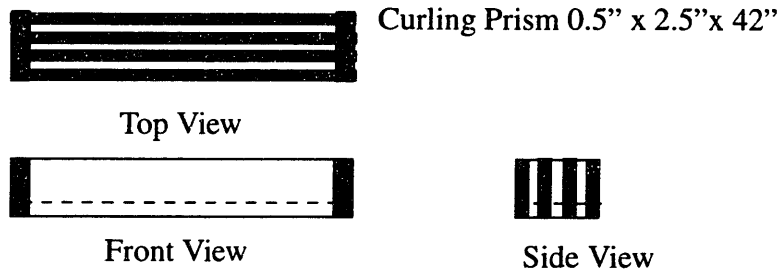
Figure 3.3.1 Typical curling specimen mold.

constructed of 46 inch long by 3.5 inch deep by either one-half or three-quarters of an inch wide PVC sheets. The 3/4 of an inch sheets were monolithic, while the intermediate 1/2 of an inch sheets were routed to the dimensions mentioned above. Several of these sandwiched plates could be placed together and clamped. This mold design was very useful for quick construction, de-molding and cleaning. Duplicate specimens were cast for each test mix, and the same mixing and curing conditions were followed as described in the drying shrinkage study for paste - mortar and concrete type specimens. That is molds were filled in thirds and then vibrated for 30-60 seconds. Then each mold was screeded, covered by

plastic sheets, and left for one or two days in the molds in the laboratory depending on the mix design. Upon stripping, each specimen was painted on five sides with a water based urethane coating and marked at the gauge points for measurement of the curling profile. The direction of bleeding was parallel to the top surface and may change the drying rates of the slabs somewhat. The curling specimens were then transferred to the same storage room as the drying shrinkage specimens (maintained at 50% RH and 72 °F). Curling deformations are determined by lining the curling specimen up against a 46 inch by 2.5 inch by 2.5 inch aluminum square tube and measuring displacements using an electronic caliper. Figure 3.3.2 depicts a typical curling specimen secured to the measuring beam with the electronic calipers used to determine out of plane deflections. Measurements of curling deformations were taken at 1, 3, 7, 14, 21, 28, 35, 42, 56, 70, and 90 days.

Figure 3.3.2 Curling measurement beam with typical specimen and electronic calipers.

3.4 Microstructural Analysis

3.4.1 Introduction

The objective of the microstructural study is to determine the effects of varying constituent percentages in mix designs on the pore size distribution of mixes. Drying shrinkage, curling deformations, and mass transport in cementitious composites are dependent on the pore sizes and distributions, and appropriate correlating factors need to be developed. A total of twenty test mixes are used. Results and discussions are presented in Chapter 4.

3.4.2 Materials

The same materials and mix designs described in the drying shrinkage portion of this section were used for the microstructural analysis study. A total of twenty different test mixes were prepared and tested.

3.4.3 Casting Procedures and Storage Requirements

Because the mortar and concrete type shrinkage specimens, as well as, the curling specimens were stored in a 50% RH, 72°F environment, the tested platelet specimens were also stored in the same environment. These specimens were cast following the same procedures described in the drying shrinkage study, and actually were a subset of those specimens. They were stored for 90 days prior to mercury poresimetry testing. The results from these tests are discussed in detail in Chapter 4

3.5 Moisture Profile Study

3.5.1 Introduction

In order to quantify the curling behavior of cementitious slabs subjected to varying drying rates from multiple regions on the slab, a very detailed and accurate measuring technique is required to describe the changes in moisture content as a function of mix design, and maturation. Conventional probe hygrometers fail to describe the non-uniformity of the moisture profile due to accuracy limitations [Terrill et al., 1986]. These types of probes ascertain relative humidity in large void structures post cored or preformed in the slab. Terrill et al. have demonstrated that information obtained using these types of probes are susceptible to large errors, because the internal relative humidity in these large macrovoids does not correlate well with total internal moisture content.

Other researchers have tried sectional analysis, that is sectioning a sample and baking off any residual moisture to obtain the moisture profile. While this technique has been proven to be accurate, it is very labor intensive. So there is a need for an accurate, efficient, testing technique to nondestructively ascertain moisture content as a function of mix design, maturity, and depth for slab systems.

Therefore, this section presents detailed information on the development of a new testing technique to quantitatively determine moisture content in structural members subjected to varying drying environments. First the necessary background information requisite to understanding the technique is presented and then the details pertaining to the testing procedure will be discussed

3.5.2 Background Information on Electrochemical Impedance Spectroscopy

Recent research applying electrochemical impedance spectroscopy (EIS) techniques to cementitious composites has yielded a wealth of information concerning developing microstructure, hydration reaction rates, and damage propagation under static loading conditions [Christensen et al., 1992, Gu et al., 1992, Gu et al., 1993 A, B, C, McCarter et al., 1988, McCarter et al., 1990, Xie et al., 1993, Xie et al., 1994, Xu et al., 1993]. EIS techniques are also widely used in corrosion studies. The basis of the technique stems from the response of an alternating current applied across a pair of electrodes separated by an electrolyte and/or dielectric material. Depending on the frequency range of the applied sweep, detailed information concerning both electrode kinetics and bulk material response may be obtained [Christensen et al., 1992, Gu et al., 1992, Gu et al., 1993 A, B, C]. The electrode/cement contribution to the impedance response is important at lower frequencies, whereas bulk material response dominates at higher frequencies [Gu et al., 1992, Gu et al., 1993 A, B, C].

Impedance is a complex quantity composed of resistance, capacitive, and inductive elements. For cementitious composites, inductive elements are not used in modeling system response. The a-c impedance is the analog of resistance for d-c circuits. Applying d-c circuit theory, the resistance is defined by Ohm's Law:

$$R = \frac{V}{I} \tag{3.1}$$

and for a-c circuit theory the impedance is defined by:

$$Z = \frac{E}{I} \tag{3.2}$$

where E represents the applied voltage measured in Volts, I is the current measured in Amps, R is the resistance measured in Ohms, and Z is the impedance in units of Ohms. Both current and voltage can be decomposed into real and imaginary components and expressed vectorially. The impedance is then expressed as the quotient of the voltage and current.

$$Z = \frac{(E' + jE'')}{(I' + jI'')} = Z' + jZ'' \tag{3.3}$$

The modulus of the impedance is defined as:

$$|Z| = \sqrt{(Z' + jZ'')(Z' - jZ'')} .$$ (3.4)

The analysis of EIS results is conducted using equivalent electrical circuit models. Each element in the model circuit must have physical meaning derived from either properties of the system or microstructure. Figure 3.5.1 is a typical equivalent circuit used to describe a simple cement paste electrode system [Gu et al., 1992]. McCarter et al. [1988,
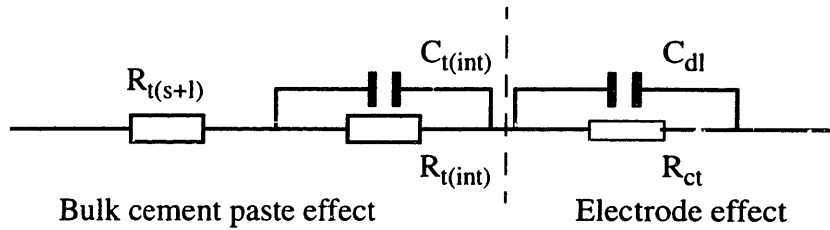
Figure 3.5.1. Simplified equivalent circuit for one layer of cement paste.

1990], outlined the necessary steps required to develop an equivalent circuit model for cementitious systems to ensure physical significance of circuit elements, and Gu et al., applied similar reasoning to develop an equivalent circuit model capable of relating detailed information about the cement system microscopic properties.

The two most common ways of representing impedance data graphically are through Nyquist and Bode plots. The complex component of the impedance is plotted versus the real component of impedance in a Nyquist plot (See Figure 3.5.2). For high frequency
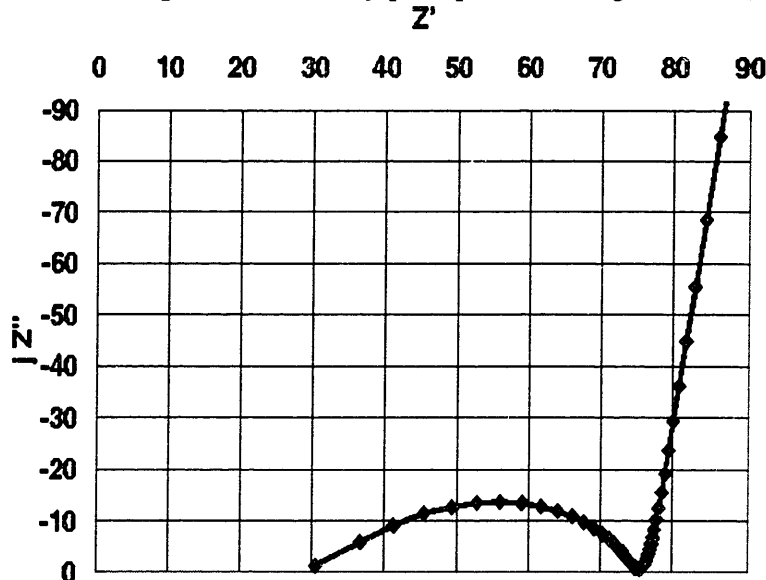
Figure 3.5.2. A sample Nyquist plot of a cement paste cylindrical specimen.

ranges, 10E+04 to 15E+07, the Nyquist plot for typical cementitious composites displays a depressed semi-circle. The impedance response for an ideal system composed of simple combinations of resistance and capacitive elements in series and/or in parallel will form a perfect semi-circle in the Nyquist plot (See Figure 3.5.3). Gu et al., have attributed the non-ideal behavior to a "spread in relaxation times" of the ions adsorbed on the solid-liquid interface, surface roughness, and the uneven distribution of current across the interfaces [Gu et al., 1993]. To account for the non-ideal behavior a frequency dependent element is introduced in the equivalent circuit model used to predict bulk material changes as a function of environmental conditions and time.

Bulk cement effect   Electrode effect

$-jZ''$

ω

Z'

$R_{t(s+l)}$ $R_{t(s+l)} + R_{t(int)}$ $R_{t(int)} + R_{ct}$
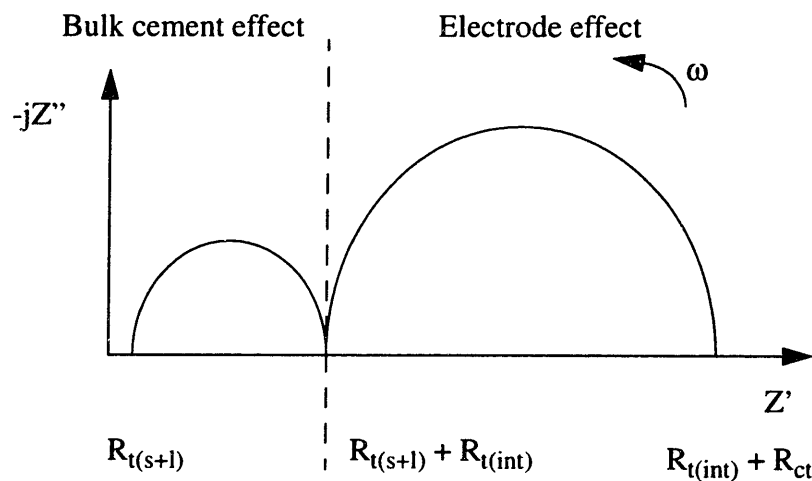
Figure 3.5.3. Nyquist plot of the complex impedance response of the equivalent circuit model.

The important parameters obtained from the Nyquist plot associated with maturity of microstructure are the diameter of the high frequency arc, the depression angle, and the projected intercepts of the arc with the real component of impedance. Each of these quantities must be carefully extracted from the data plots, and some finesse with handling the data is required.

Bode diagrams plot modulus and phase angle versus the logarithm of frequency (See Figure 3.5.4). The real component of the impedance is due to resistive elements which are in phase with the applied current, therefore the phase angle for these types of elements is near $0°$. The phase angle of a perfect capacitor is $-90°$. For systems with combinations of resistive and capacitive elements the phase angle varies between the two bounds. In the above figure, it is readily apparent that either modulus or phase angle at a given frequency

range can accurately differentiate differences in the response of cementitious materials subjected to different environmental conditions. It is because of the intuitive sense associated with the phase angle that makes it a logical choice for indicator of moisture content.
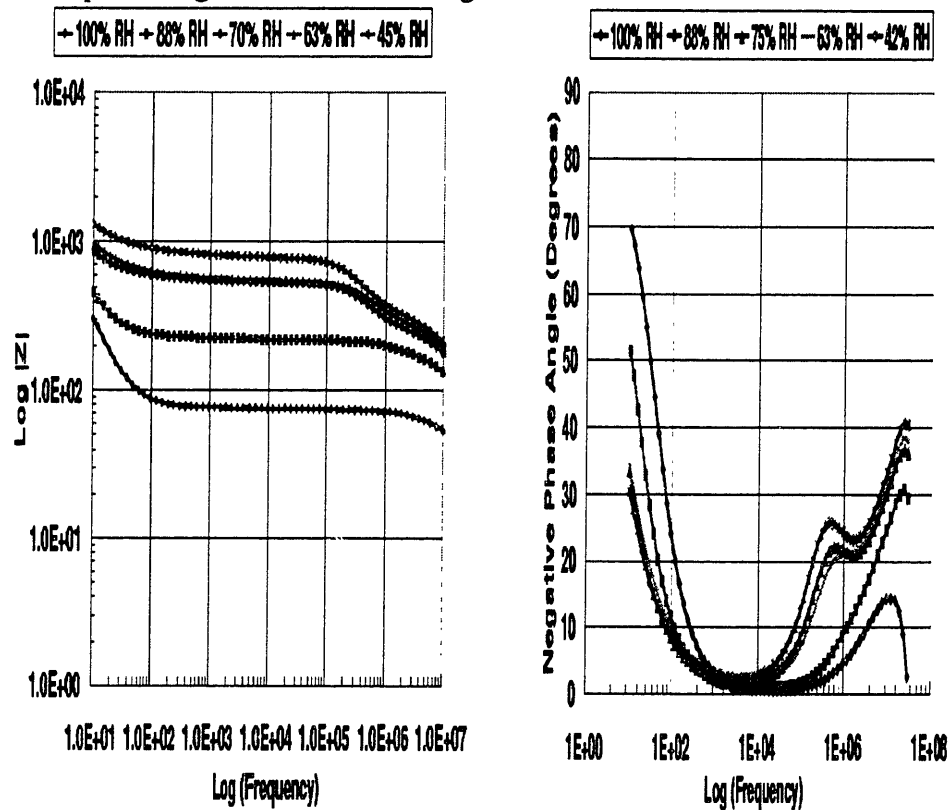
Figure 3.5.4. Bode plot demonstrating typical response for cement specimens stored in different constant environmental conditions.

When cement specimens are first mixed, the constituents are in a water-colloidal suspension and the electrochemical response is best represented as a dielectric electrolyte dispersed between the two electrodes. The sample is considered fully saturated. An equivalent circuit model of this system would best be represented by a series of resistors and the high frequency response depicted in a Nyquist plot is not semi-circular in shape. As the hydration reactions proceed and the water is consumed, the microstructure starts to develop interfaces between the hydration products and the unhydrated cement. Water is also lost after initial curing due to evaporation and subsequent drying. Therefore, the once fully saturated material develops a porous network and becomes unsaturated as drying proceeds. There are three types of water present in the porous network: chemically adsorbed, physically adsorbed, and free water. Depending on the pore size distribution of the specimen, each type of water will affect the determination of the moisture content of

50

the sample. The two competing sources of moisture loss in the material are hydration and drying.

Terrill et al., conducted a study on ascertaining the moisture profile of rectangular specimens using crack initiators and relative humidity probes, and determined that the relative humidity probes are unable to accurately ascertain changes in moisture content in gel pores and may be only applicable to meso-to-macro porous systems [Terrill et al., 1986]. The advantage of using a.c. electrochemical measurement techniques is the fact that these types of measurements are very sensitive to moisture content in any of the available forms/ types.

A small perturbing a.c. signal is applied across the set of electrodes and the salt ions in the pore water solution respond by fluctuating in response to the field until they reach their relaxation time which is the time required to fluctuate in phase with the applied field at the given frequency. The relaxation time is dependent on the source of water responding, i.e., free water has the fastest response while chemically adsorbed water has the slowest response. As described earlier, the spread in relaxation times of the material is depicted in the Nyquist plot as a depression of the semi-circle below the real component of the impedance. Since the real component of the impedance is composed of the resistance's of elements in the porous network and the electrolytic material, the phase angle of these components are small near $0°$. Therefore for the fully saturated case, in the earliest time times after mixing there is no formation of a high frequency arc. Later as pores start to empty and interfaces start to develop the high frequency response evolve. When a pore is completely empty of water it acts as a leaky capacitor and maintains a phase angle close to $-90°$. Therefore by plotting phase angle as a function of depth for the profile specimens one is able to ascertain a qualitative moisture profile.

The purpose of the electrochemical impedance experiments are to ascertain specific parameters from the Bode or Nyquist plots which may serve as key indicators of moisture content of a specimen without the need to develop sophisticated equivalent circuit models. Often times several different equivalent circuit models may describe the same experimental information well. Detailed understanding of the mechanisms and microstructure of the system and user expertise are required to generate meaningful circuits. A simplified test is desired for the lay person. The developed test will demonstrate the ability of the electro-

chemical impedance spectroscopy results in predicting changes in the moisture gradients in neat cement paste samples.

3.5.3 Materials

A Type I portland cement was used for all experimental specimens. The same form of silica fume was used in this study as was used in the drying shrinkage study.

3.5.4 Specimen Preparation, Casting Procedures, and Storage Requirements

Two types of specimens were developed for the EIS moisture profile experiments. The first specimen type was composed of a pair of concentric cylinder electrodes embedded in high density polyethylene (HDPE). This specimen is modeled after the specimens used by Christensen et al. [Christensen et al., 1992]. The two electrodes are composed of type 304 stainless steel. The inner diameter of the outside electrode is 3/4 of an inch and the outside diameter of the inner electrode is 0.0625 inches. The length of the electrodes is 3/4 of an inch. Figure 3.5.5 depicts a typical concentric cylinder specimen. Paste mixes are batched

Concentric Cylinder Specimen
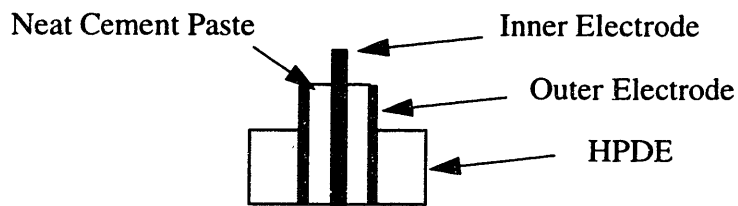
Figure 3.5.5 A typical concentric cylinder specimen.

in a Hobart mixer until the paste develops a uniform consistency. The freshly mixed paste is then injected into the mold using a plastic 50 cc syringe. The molds are vibrated for 30-60 seconds at a high frequency low amplitude. These specimens are then stored in different constant relative humidity environments.

The second set of molds, the moisture profile molds, are constructed of four inch by four inch by 1/2 of an inch, four inch by four inch by one inch, and four inch by four inch by two inch HDPE plates. A two inch cylinder was bored through the center of each mold and then evenly spaced paired holes for the electrodes were drilled in a counterclockwise manner on each face of the HDPE, see Figure 3.5.6. This was done to ensure that there was minimal interference between electrode pairs at any given height. The electrodes were

made from 19 gauge type 304 stainless steel tubing. The electrode lengths were 1.6 inches

Top View

Front View
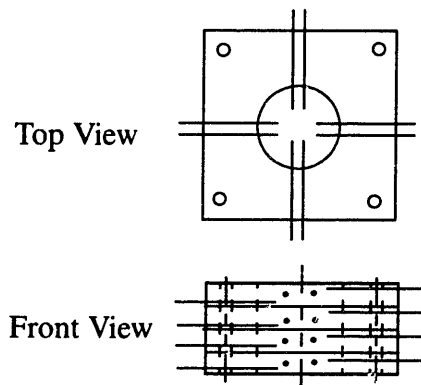
Figure 3.5.6 Typical two inch EIS profile mold.

and the length of the electrode exposed to the cement paste was 0.4 inches. The one inch specimens contained six pairs of electrodes, the two inch specimens contained twelve pairs of electrodes, and the 1/2 inch specimens contained three pairs of electrodes.

In order to ascertain moisture content within specimens, the concentric cylinder specimens were filled with paste, cured one day, and then stored in four different environmental chambers at 72° F and the following relative humidities 100, 88, 75, 63, and 42. The environmental chambers were constructed of HDPE containers containing saturated salt solutions to establish the required relative humidity environments. Electrochemical and mass loss measurements were taken at 1, 3, 7, 14, 21, 28, 35, 42, 56, 70, and 90 days. The results from these tests are used to correlate the water content in a specimen as a function of time. The moisture profile specimens are filled with the same mix designs as the concentric cylinder specimens and tested at the same ages. These specimens are stored in a 50% RH environment at 72°F.

The impedance data was collected using a Solatron 1260 frequency response analyzer. Measurements were taken logarithmically in a frequency range from 30 MHz to 10 Hz with ten readings per decade. A signal amplitude of 0.1 of a volt was used throughout the sweep.

3.5.5 Summary

This section presented information on why conventional methods to determine moisture

content as a function of slab depth are either inefficient or inaccurate. To address this important problem, a new testing technique applying electrochemical impedance spectroscopy techniques is described. First the background information on electrochemical impedance spectroscopy was discussed and then the experimental methodology was presented. The results obtained using this technique are discussed in Chapter 4.

3.6 Summary

All of the tests required to fully describe how curling deformations occur in cement slabs cast on grade were described, as well as, those tests which will provide information concerning differences in behavioral response due to the addition of a drying shrinkage reducing admixture. As moisture leaves the system, the non-uniform moisture profile develops and individual layers of cement paste experience different drying shrinkage strains. If compatibility between layers is enforced curling deformations occur. The first test series varies water-to-cementitious material ratios and the presence of the shrinkage reducing admixture to test affects on long term drying shrinkage performance. This information will then provide the necessary correlation between constant relative humidity environment and drying shrinkage so that the drying shrinkage strain field may be constructed. Mass loss behavior is also studied to determine diffusivities of specimens at different ambient relative humidity environments.

Next mechanical properties are obtained to feed into the model. Then curling specimens are developed and tested to determine actual changes in magnitudes of deformations between the SRA admixed and reference mixes. Microstructural studies are carried out on mature 90 day old specimens to determine whether the addition of the SRA changes the pore structure of neat paste specimens. This information is also used to determine theoretical shrinkage strains based upon the Kelvin and Laplace equations.

The last study is conducted to determine how di-electric response of maturing cementitious systems changes due to the addition of the shrinkage reducing admixture and moisture loss from a single face. Various types of specimens are used to obtain correlations between specific constant relative humidity environments and moisture loss. The size effect is studied by varying the exposed surface area to volume ratios for the three different thicknesses studied. The use of the electrochemical impedance spectroscopy technique is expected to provide a very efficient manner to determine moisture changes in cement systems. It is hoped that this testing technique can then be modified for use in the field. The next chapter presents the results obtained from these test series. Finally, the results will be used in conjunction with the analytical developments to predict curling deformations in time for various mix designs.

Chapter 4

Experimental Results

4.1 Drying Shrinkage

4.1.1 Introduction

As stated earlier in the experimental methodology section, the objective of the drying shrinkage study is to obtain information about the affects of different constant relative humidity environments on the shrinkage performance of a number of mix designs that change the rate of development of the microstructure and the pore sizes and distributions. In the literature review portion of this text, the key factors affecting drying shrinkage were outlined. A new chemical admixture developed to reduce drying shrinkage strains is tested and very dramatic results are obtained for the higher water-to-cementitious ratio mixes while mixed results are obtained for the high strength low water-to-cementitious ratio mixes. A total of twenty design mixes were tested, and the results from these tests are further discussed below.

This section of the thesis is split into two separate sections. The first discusses the drying shrinkage behavior of the three different types of mix designs: high, intermediate, and low water-to-cementitious ratio mix designs. The design mixes were chosen based upon the types of mixes typically used for different types of structural systems. The lowest and highest mixes are not usually used in practice, but were included for completeness of trends. The second section relays information pertaining to mass loss behavior of the drying shrinkage platelet specimens. As discussed in the experimental methodology section, the platelet specimens, a subset from each mix, were subjected to different constant environmental conditions. Both the drying shrinkage and moisture loss information will be useful in ascertaining drying rates as a function of mix design and will be incorporated into the modeling section.

4.1.2 Drying Shrinkage Performance of High Water-to-Cementitious Ratio Mixes

The high water-to-cementitious (W/C) ratio mixes are defined as those mixes with a W/C

ratio greater than or equal to 0.55. The W/C = 0.55 ratios may be used for floor systems that require high workability and/or finishability. These mix designs often provide moderate strength and permeabilities compared to the intermediate W/C ratios. The W/C = 0.65 ratios were included in the study for completeness of trends. Both the W/C = 0.55 and 0.65 mixes are expected to experience the largest mass losses and drying shrinkage strains.

Figure 4.1.1 depicts the response of the W/C = 0.55 reference paste mix to different constant relative humidity environments. As expected the largest shrinkage strains occur
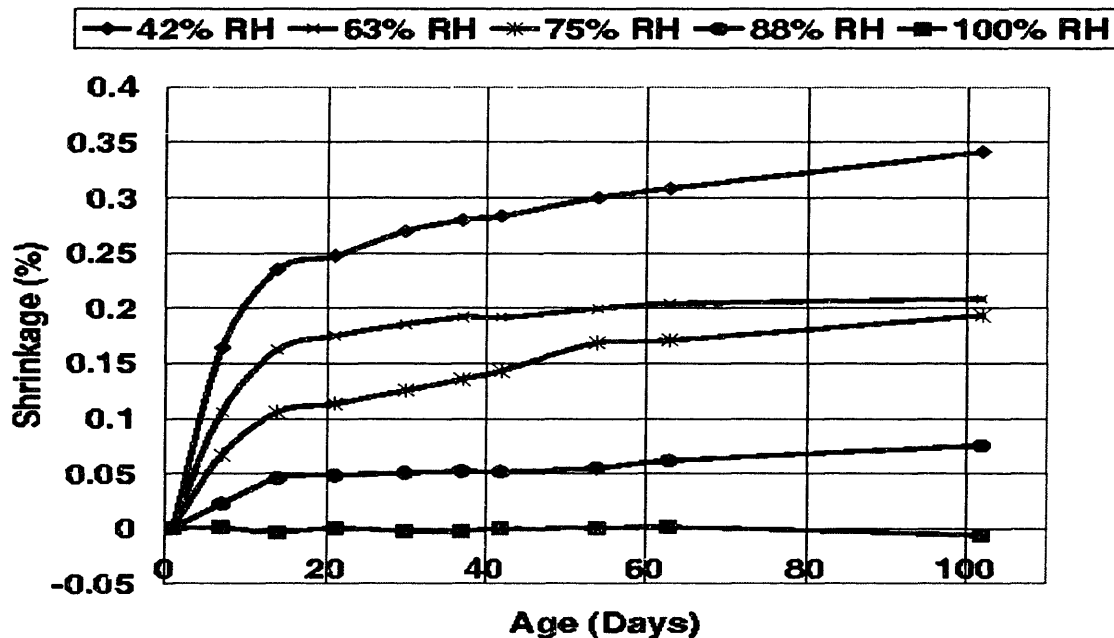
Figure 4.1.1 The drying shrinkage performance of the reference W/C = 0.55 paste mix.

in the harshest drying environment, 42% RH. The magnitude of swelling is very small for the fully saturated condition. At 102 days the specimens continue to experience changes in shrinkage strains, but at significantly reduced rates for the higher relative humidity environments. The 42% RH environment specimens experience the highest shrinkage strains with a magnitude at 102 days of 0.34%. The distribution of magnitudes between the different environments is relatively wide spread, with the difference between the 63% RH and the 75% RH the lowest. One problem noted during the course of the experimental program was the variability of relative humidity with temperature. The 75% and 63% RH environmental conditions were the two most sensitive of all the saturated salt solutions. These two mixes had to be monitored closely for drift in RH values and adjusted accordingly. Therefore, the information obtained from these two conditions will be scrutinized carefully

57

before drawing final conclusions concerning the applicability of the analytical model in Chapter 5.

Figure 4.1.2 depicts the companion mix with a 5% replacement by weight of mixture water with the drying shrinkage reducing admixture. Similar trends occur in terms of
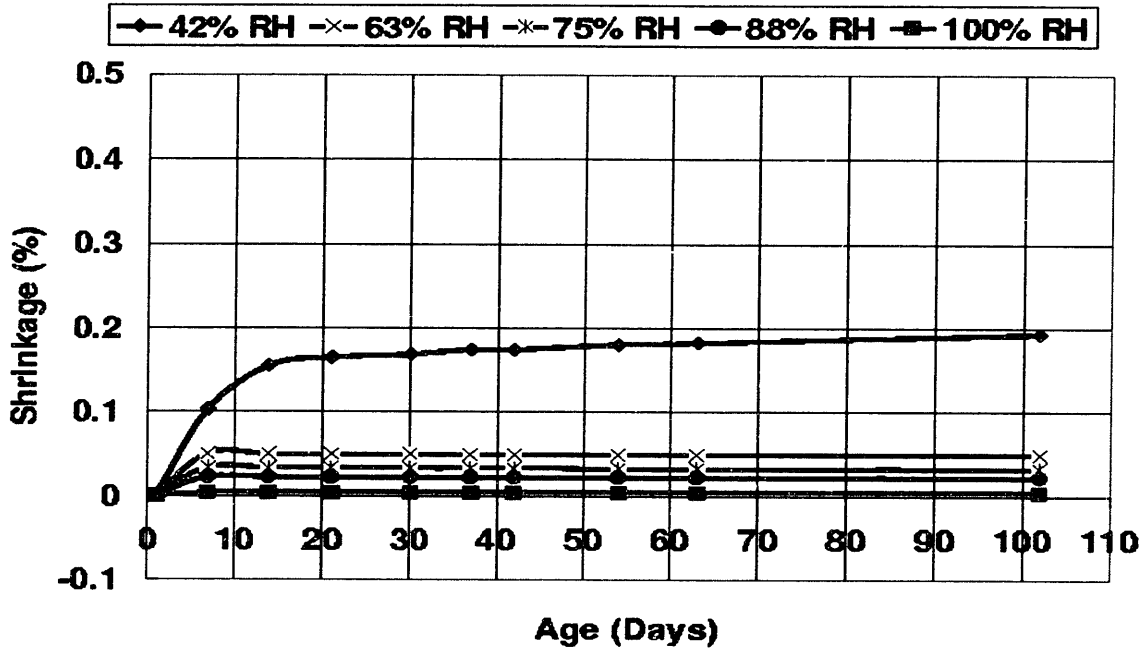
Figure 4.1.2 The drying shrinkage performance of the W/C = 0.55 with a 5% replacement of mixture water by weight with the SRA design mix.

increasing shrinkage strains with decreasing relative humidity, but the magnitudes of the shrinkage strains have decreased considerably. It appears as if these specimens have reached an equilibrium state since there are only very small changes in shrinkage with time after 28 days. The exception is the 42% RH environmental condition, which still shows a considerable decrease in shrinkage rate compared to the reference design mix. The differences in shrinkage between the 100%, 88%, 75%, and the 63% environmental conditions have decreased and are separated considerably from the 42% RH test speci-mens. The shrinkage reduction between the two types of mixes is lowest for the 42% RH condition, 43.5% at 102 days, and is 76.3%, 83.0%, and 70.2%% for the 63% RH, 75% RH, and 88% RH respectively. The differences in 7 day magnitudes are approximately 40%, 52.4%, 50%, and -1.3% respectively from lowest RH to highest RH shrinking envi-ronments. Figure 4.1.3 depicts the change in shrinkage behavior of the W/C = 0.55 design

mix with a 7.5% addition of silica fume. Note the dramatic increase in drying shrinkage
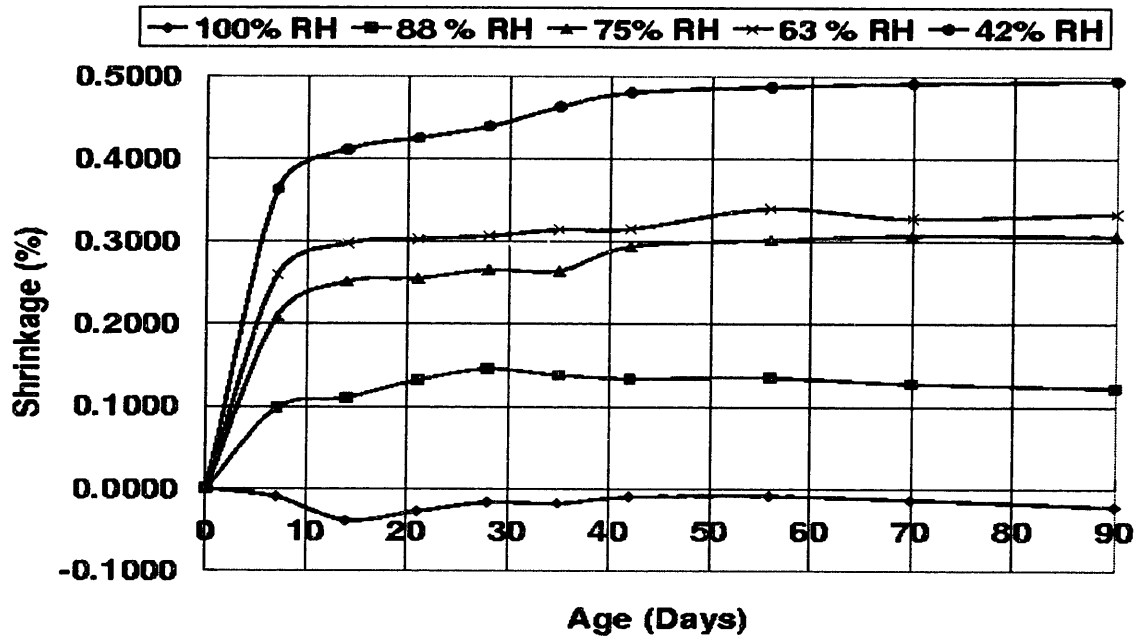
Figure 4.1.3 The drying shrinkage performance of the W/C = 0.55 with a 7.5%
replacement of cement by weight with silica fume design mix.

with the addition of the pozzolan admixture. The average magnitude of drying shrinkage
for the 42% RH specimens at 90 days is 0.494%. There is little difference between the
intermediate environments of 75% RH and 63% RH with magnitudes about 0.34% and
0.3% respectively. This follows the same pattern established with the reference paste mix.
The increases in the magnitudes between the pozzolan admixed mix design with the refer-
ence mix design are +44.4%, +59.8%, +58.5%, and +62.33% respectively for the 42 - 88%
RH specimens. These specimens appear to have reached their equilibrium shrinkage val-
ues, since the change in slope of shrinkage versus time is slight. This type of behavior was
expected because pozzolan admixed mixes typically experience large increased shrinkage
rates early on due to the increased hydration reaction rates. Also the magnitudes of the
shrinkage experienced are expected to be larger than the reference mix following the cap-
illary tension theory because of the refined pore structure. This shall be further discussed
in the microstructural analysis portion in Section 4.4.

As depicted in Figure 4.1.4, there is a considerable reduction in drying shrinkage for
the 5% SRA admixed design mix compared to the complementary pozzolan admixed
design mix. The improvement in performance by reducing the magnitudes of drying
shrinkage strains are: 51.2%, 42.0%, 32.8%, and 24.4% respectively for the 42 - 88% RH

environments at 90 days. It is surprising that the 63% RH and the 75% RH shrinkage curves intersect several times and reach approximately the same equilibrium value. The
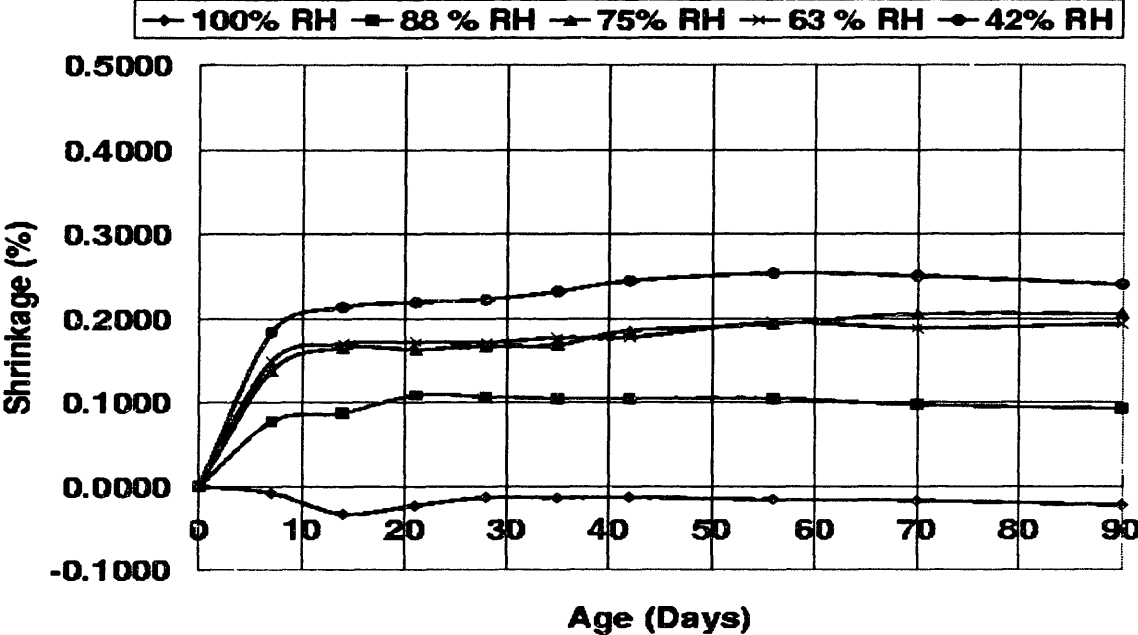
Figure 4.1.4 The shrinkage performance of the W/C = 0.55 with both a 7.5% replacement by weight of cement with silica fume and a 5% replacement by mixture water of the SRA design mix.

pore size distributions for this two mixes may be similar enough that at the given ambient environmental conditions the internal moisture contents are very similar and hence the shrinkage behavior is also similar. Another interesting trend is the reduction in efficiency at higher relative humidity environments. This is contrary to the behavior of the reference versus 5% admixed SRA design mixes. Moist environments should enhance the final magnitudes of hydration, thus refining the pore structure of samples. The final equilibrium moisture content then dictates which pores are actively inducing shrinkage stresses on the skeletal matrix. Since there are so many active variables, it is hard to tell based upon this single set of tests which trend is appropriate.

Figure 4.1.5 depicts the shrinkage behavior of the four W/C=0.55 mixes at the harshest drying environment, 42% RH. The SRA admixed mixes clearly improve shrinkage performance. The trend followed in terms of increasing drying shrinkage with age is: the 7.5% silica fume admixed test series, the reference paste series, the 7.5% silica fume and 5% SRA admixed series, and then the 5% SRA admixed series. The 7.5% silica fume design

60

mix experiences the largest drying shrinkage strains as expected due to its refined pore structure. The reference paste mix experiences the next largest shrinkages, while the com-
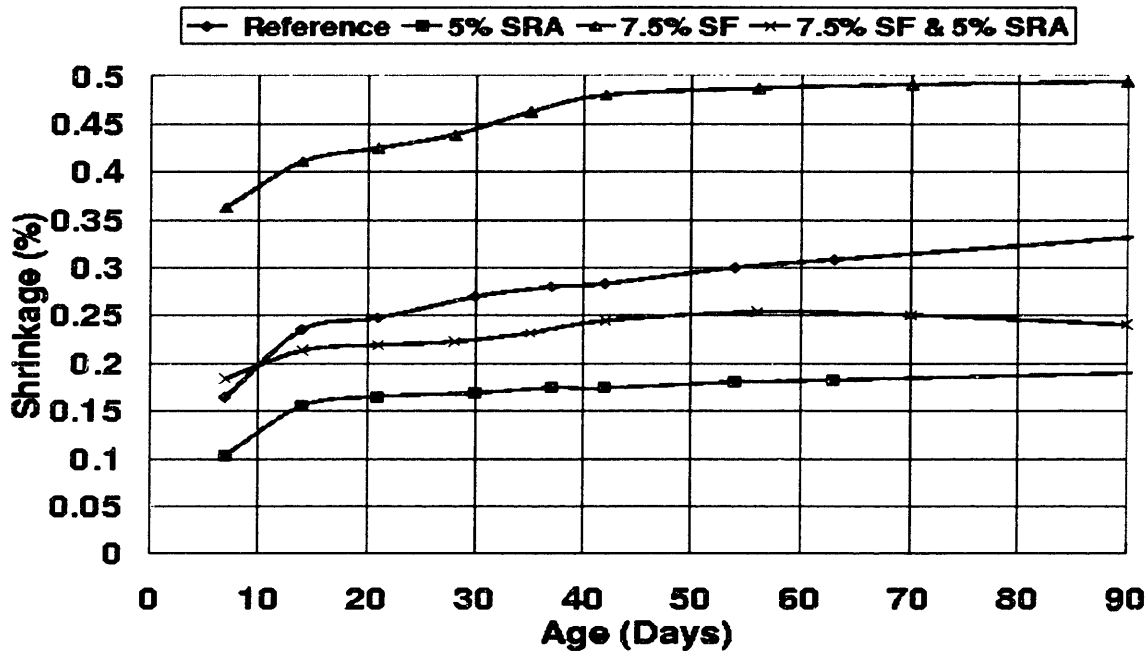
Figure 4.1.5 The drying shrinkage performance of the W/C = 0.55 mixes at 42% RH.

bined admixed 7.5% silica fume and 5% SRA design mix is intermediate between the reference and the paste with 5% SRA test mix. The question of the affect of admixing the SRA on developing microstructure is discussed in the microstructural analysis section. However, if the microstructure is relatively similar for the reference and SRA admixed mixes, it is purely the reduction in surface tension that can account for the improved performance. This information is useful for designers who may require higher strengths and lower permeability mix designs and choose to place a pozzolan admixed floor system with the addition of the SRA.

The W/C = 0.65 mixes provided similar results, with the highest shrinkage strains in the order: pozzolan admixed, reference paste, pozzolan admixed with 5% SRA, and finally paste admixed with 5% SRA. Figure 4.1.6 depicts the results of shrinkage performance in

the harshest shrinkage environment, 42% RH. The magnitude of drying shrinkage of the
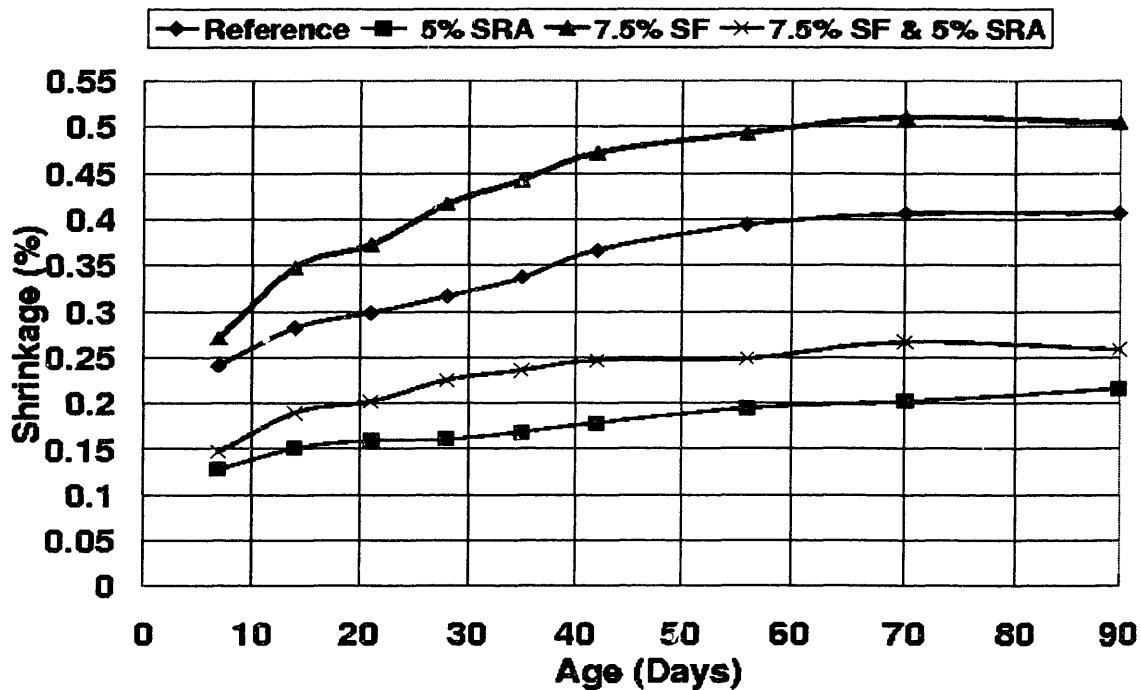
Figure 4.1.6 The shrinkage performance of W/C = 0.65 mixes at 42% RH.

four mixes at 90 days are: 0.535%, 0.407%, 0.255%, and 0.216% respectively listed in the same order as given above with increased shrinkage of 31.4% for the 7.5% pozzolan admixed mix design, and reduced drying shrinkages by 38% for the 7.5% admixed pozzolan with 5% SRA mix design and 47% for the admixed 5% SRA replacement by mixture water mix design. The drying shrinkage data for all the high water-to-cementitious material ratio mix designs attached in Appendix I.

4.1.3 Drying Shrinkage Performance of Intermediate Water-to-Cementitious Ratio Mixes

The intermediate water-to-cementitious material ratio mixes are defined as those mixes with a W/C ratio greater than or equal to 0.35 and less than or equal to 0.45. The W/C = 0.45 ratios are often used for floor systems that require early strength development. The W/C = 0.35 ratios mixes are usually not used for most floor systems, but may be used in the design of panel systems or other structural elements that require higher compressive strengths and lower permeabilities. These test mixes are expected to experience smaller drying shrinkage strains than those experienced by the higher water-to-cementitious mate-

rial ratios. Figure 4.1.7 presents the shrinkage performance of the W/C = 0.45 reference
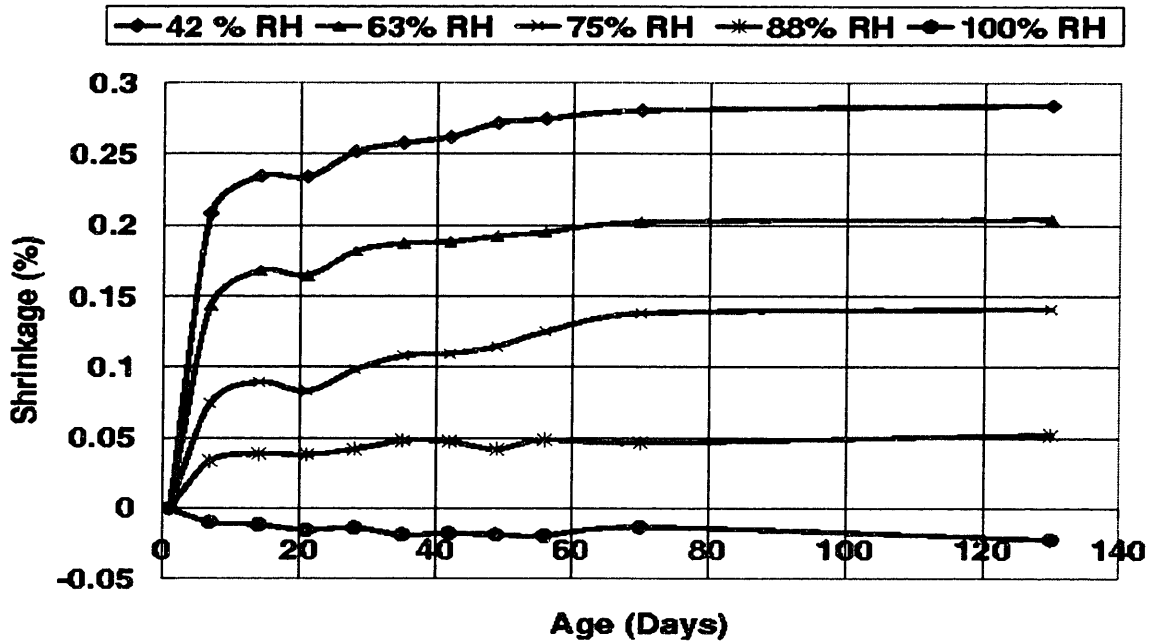
Figure 4.1.7 The shrinkage performance of the W/C = 0.45 reference paste mix
subjected to different constant environmental conditions.

paste mix design as a function of different constant environmental conditions. The same

trends established earlier apply, with swelling occurring for the fully saturated specimens

and increasing shrinkage strains with decreasing relative humidity environments. The

other three design mixes also exhibit the same behavior with varying magnitudes of drying

shrinkage for each constant environmental condition. The trend of highest shrinkage strain

to lowest also is followed as discussed above for each mix design. The differences in dry-

ing shrinkage magnitudes at the harshest environment are: +48.6%, -12.1%, and -33.0%

with respect to the reference mix at 90 days. Note the small variations in the measured

shrinkage strains with age. At 21 days the reference paste mix experiences a drop in

shrinkage which implies that the saturated salt solutions were above the required constant

relative humidity range desired. Also, the 75% RH series appears to have stabilized at two

different points which could have occurred if the environmental chamber drifted slightly

lower in relative humidity. These observations will be addressed further in the drying

shrinkage modeling discussion in Chapter 5.
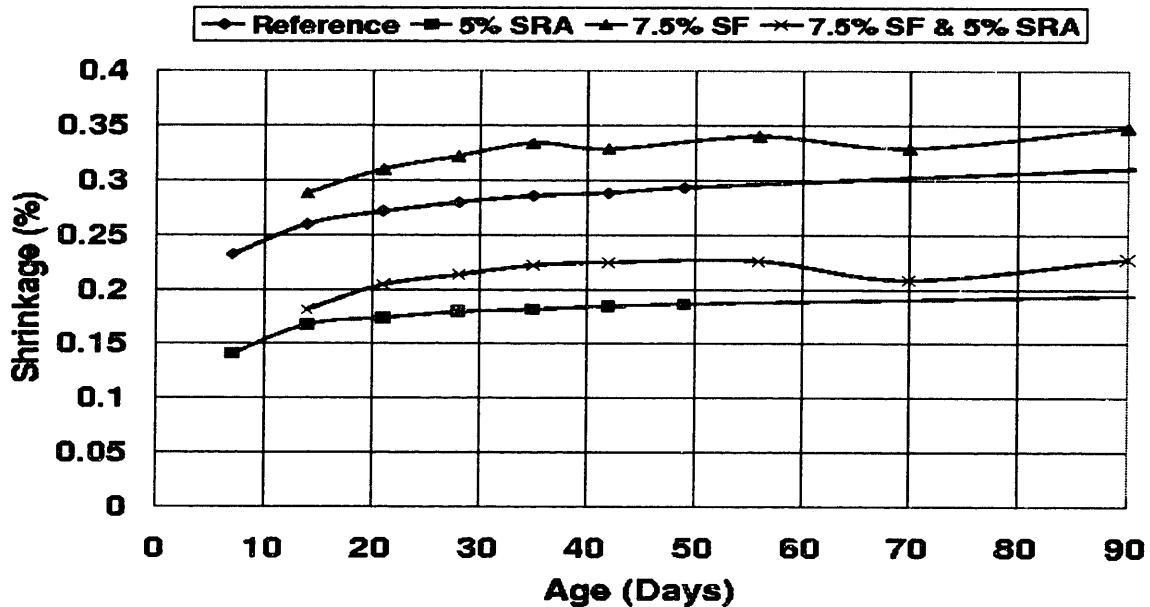
Figure 4.1.8 The shrinkage performance of the W/C = 0.35 mixes at 42% RH.

Figure 4.1.8 shows the trends of drying shrinkage for the harshest environment for the four W/C = 0.35 mix designs. Again trends follow similarly to the all previously discussed mix designs. However the magnitudes of the percentage difference in drying shrinkage compared to the reference paste have dropped considerably: +11%, -27.5%, and -37.8% respectively at 90 days. Again drawing on capillary tension theory, the governing effects on drying shrinkage performance are rigidity of the skeletal matrix, the surface tension of the pore solution, and the tensile strength of the pore walls. The smaller W/C ratio mixes are providing higher matrix rigidities at earlier ages, and so the reduction in efficiency of the shrinkage reducing admixture is not surprising. Further discussions are presented in the microstructural analysis section. The shrinkage data for the W/C=0.35 and 0.45 mix designs are attached in Appendix I.

4.1.4 Drying Shrinkage Performance of Low Water-to-Cementitious Ratio Mixes

The mix designs with a W/C = 0.25 are usually not used for most practical design considerations and were included in the study for completeness of trends. Due the very low water contents of these mixes, very low mass loss is expected. Figure 4.1.9 depicts the behavior of drying shrinkage performance of the four mix designs subjected to the harshest environmental condition, 42% RH. However the trends typically followed have now changed. The silica fume admixed mixes, with and without the SRA, experience less shrinkage than the

reference and the 5% admixed SRA mixes. The magnitudes of shrinkage reduction are: -
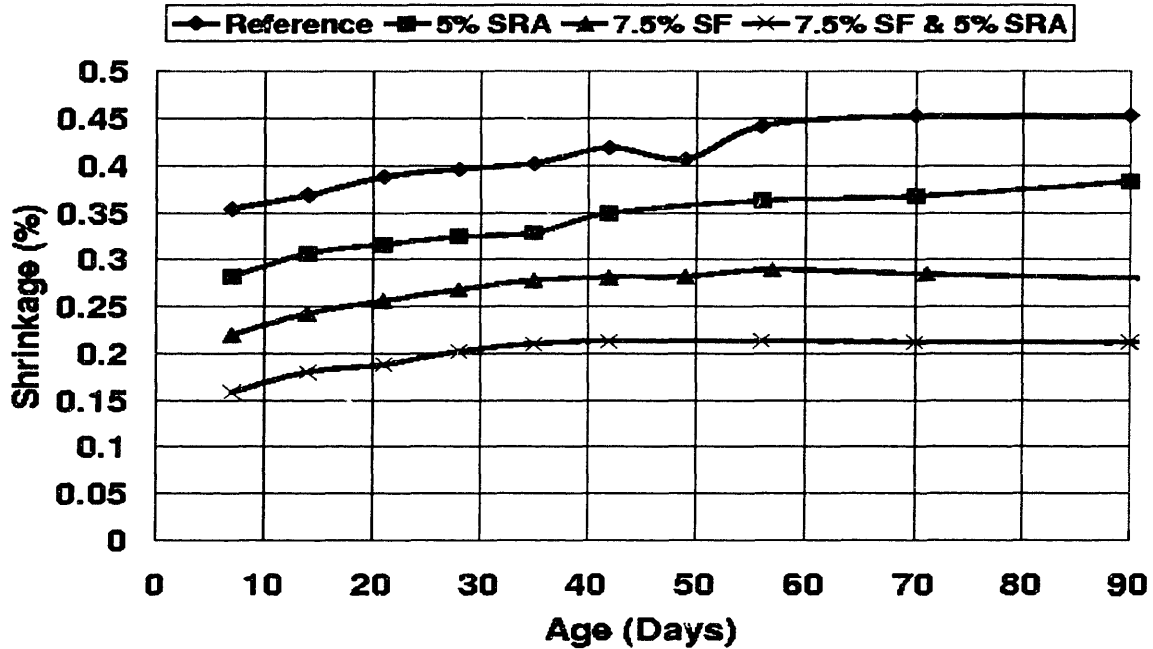
Figure 4.1.9 The shrinkage performance of the W/C = 0.25 mixes at 42% RH.

39.9%, -15.5%, and -53.6% respectively at 90 days with respect to the reference paste mix. The same trends of increasing shrinkage strain with decreasing relative humidity are followed.

One possible explanation for the behavior is that the silica fume mixes have much finer pore size distributions and thus their diffusivities are much lower than the reference and 5% SRA admixed design mixes, hence they lose water at slower rates. This allows for a greater degree of hydration to occur. Provided that the early hydration reaction thermal stresses produced were smaller than the strength of the bulk paste matrix, thermal microcracking will not have occurred and hence the matrix is rigid enough to resist any deformations due to capillary forces. These ideas will be tested and discussed further in the mass loss portion of the discussion in the next section. The shrinkage values for these test mixes are included in Appendix I.

Finally, Figures 4.1.10 through 4.1.13 present the drying shrinkage performance of all the test mixes at the harshest test environment, 42% RH. Note the interesting result that
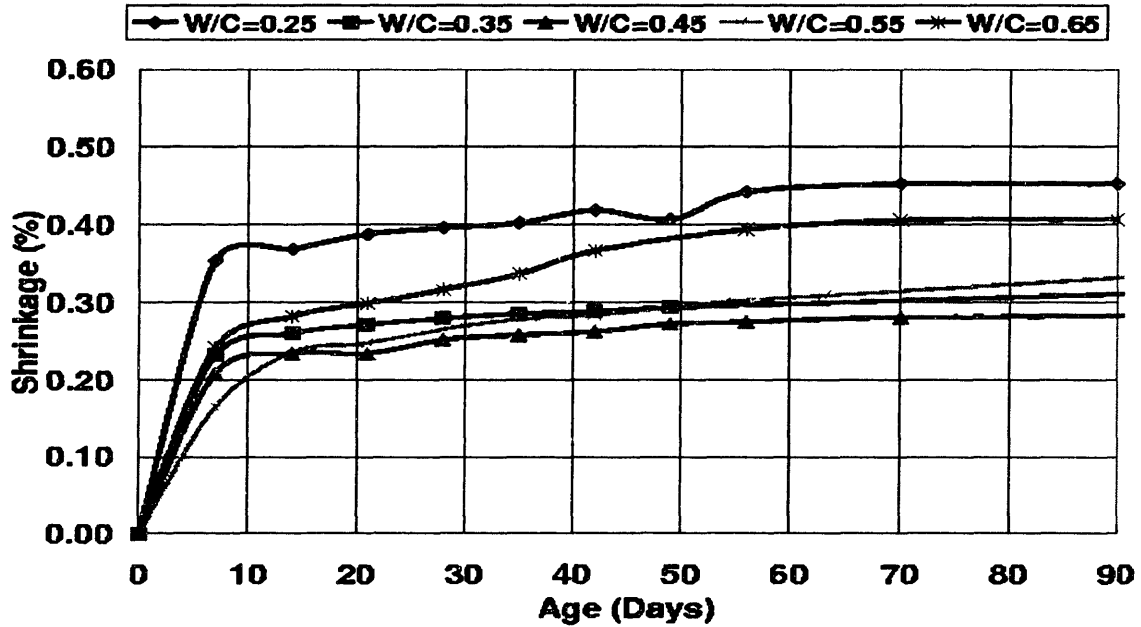
Figure 4.1.10 The shrinkage performance of all paste reference mixes at 42% RH.

the highest shrinkage strains are experienced by the W/C = 0.25 test mixes. At first the results may seem contrary to what one would expect, but for the test mix designs the cement contents of each mix were not held constant. Drying shrinkage is not only dependent on water-to-cementitious material ratio but also cement content, therefore a direct comparison of shrinkage results may not be appropriate. The results are applicable to mixes designed with very similar cement factors and thus still provide useful information with which to correlate the performance of the analytical mode. The spread in shrinkage strains is not very large for the W/C = 0.35, 0.45, and 0.55 mixes. The W/C = 0.25 and 0.35 contain the highest cement contents and therefore it is not surprising that they experience large shrinkage strains. Also, since the W/C = 0.65 mix loses the most water, it is not surprising that it shrinks the second largest of all mixes.
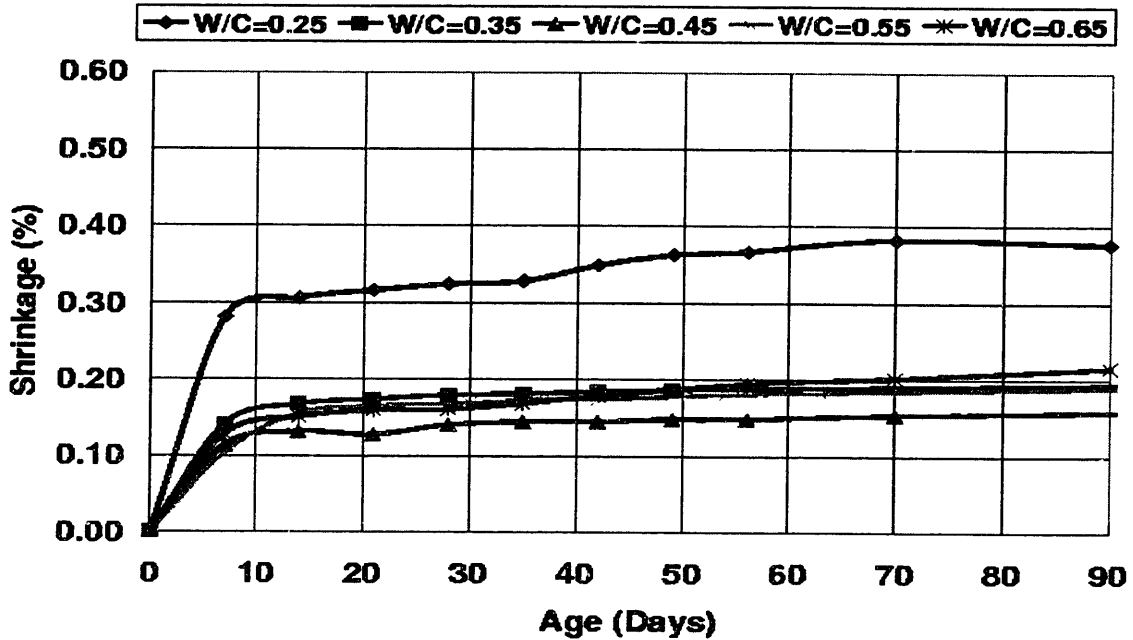
Figure 4.1.11 The shrinkage performance of all the paste plus 5% SRA
admixed mixes at 42% RH.

Figure 4.1.11 shows an interesting clustering of shrinkage strains for the all mixes

excluding the W/C = 0.25. The admixed 7.5% silica fume reference mixes depicted in
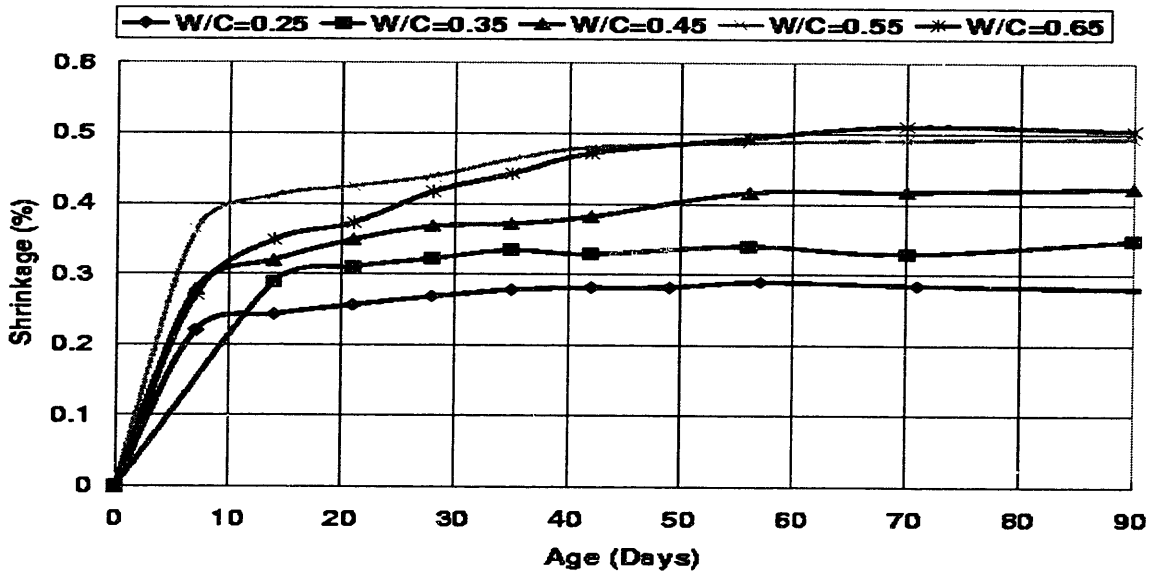
Figure 4.1.12 The shrinkage performance of all 7.5% admixed silica fume paste
mixes at 42% RH.

These mixes experience a very interesting pattern. Shrinkage increases with increasing

water-to-cementitious material ratio. This is opposite to what occurred in the reference

paste mix. Figure 4.1.12 are spread further apart. Figure 4.1.13 depicts the admixed 7.5% silica fume with the 5% SRA. These mixes all experience very similar long term shrinkage strains. Again the distribution of curves is with the same pattern established for the previous SRA admixed mixes.
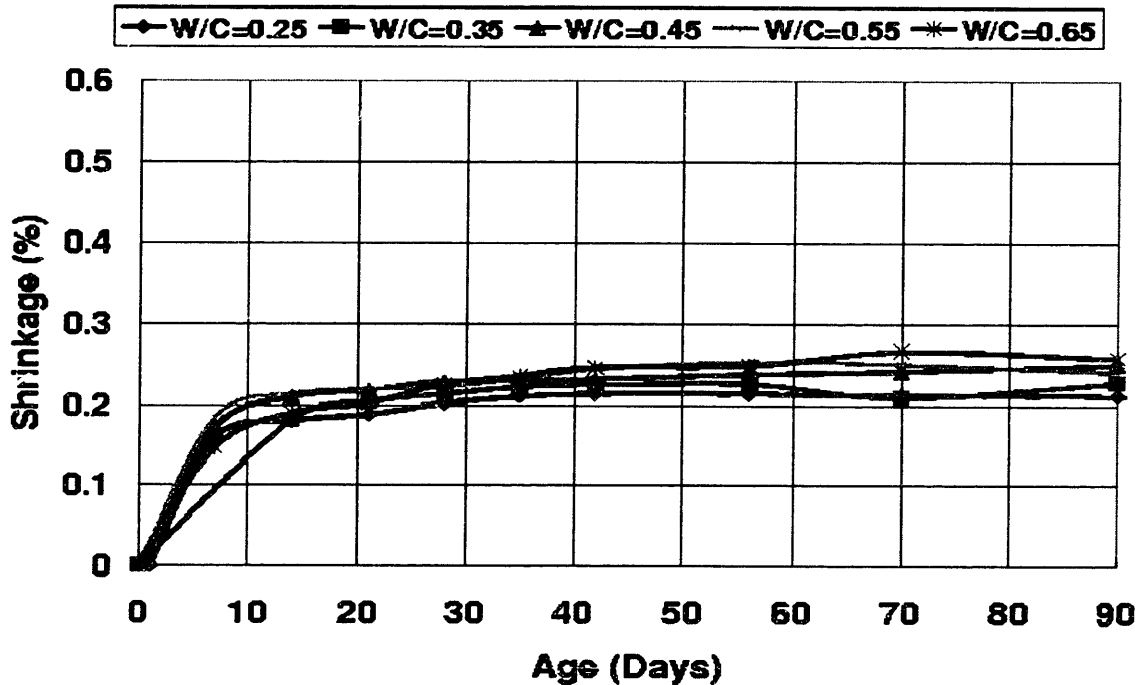
Figure 4.1.13 The shrinkage performance of all the 7.5% silica fume plus 5% SRA admixed mixes at 42% RH.

It is interesting to note that the 5% SRA admixed test series with a W/C = 0.25 performs very differently then the 7.5% silica fume admixed with 5% SRA with a W/C = 0.25. In Figure 4.1.11 the W/C = 0.25 test series appears almost like an outlying curve compared to the similar response of the other mixes. The same behavior does not occur for the complementary silica fume admixed SRA test series in Figure 4.1.13. Possible explanations for the changes in the behavior may become apparent after the mass loss behavior and microstructural analysis sections.

4.1.5 Moisture Loss of High Water-to-Cementitious Ratio Mixes

The meaning of high water-to-cementitious material ratio has been defined earlier. Based upon the shrinkage performance that these mixes experienced when a subset of specimens are subjected to different constant relative humidity environments, it is expected that they

shall experience the greatest mass losses through time. Figure 4.1.14 depicts the average
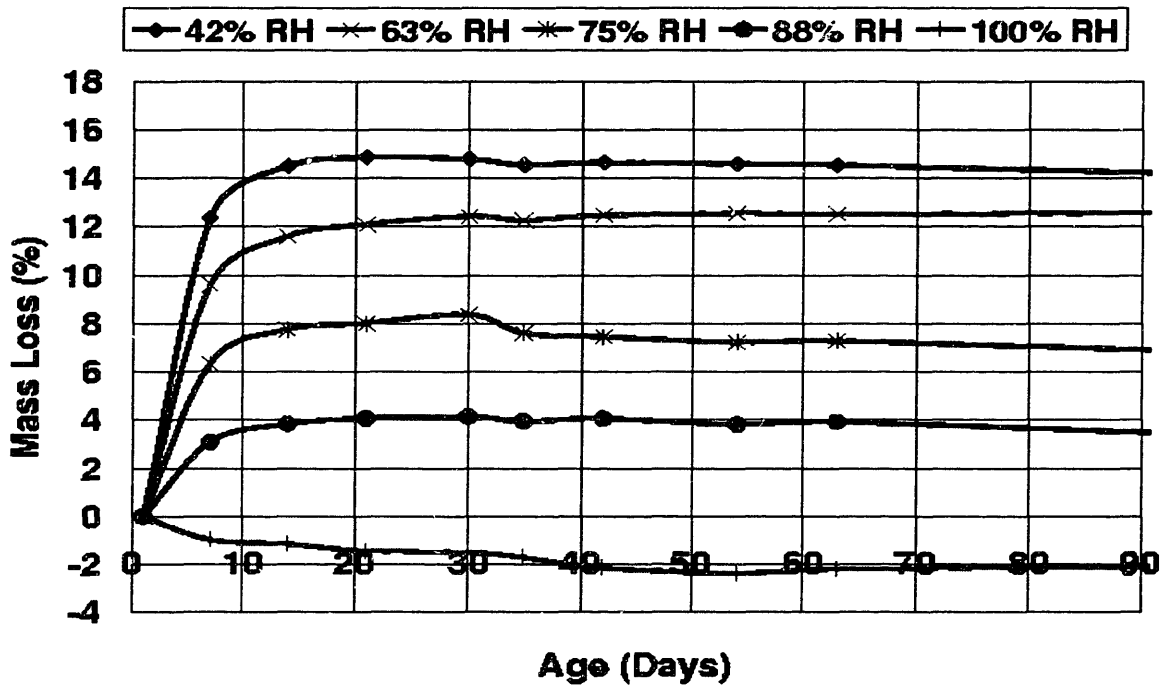
Figure 4.1.14 The average mass loss behavior of the W/C = 0.55 reference paste platelet specimens subjected to different constant relative humidity environments.

changes in mass loss behavior of the W/C = 0.55 reference paste mix. As expected the harshest drying environment causes the most moisture to leave the system. However, after the first 21 days there is very little change in mass loss. The exception is the 75% RH environmental condition which appears to have a slight discontinuity at 35 days and may represent a slight drift in relative humidity. Also, following the trend established for shrinkage, the amount of water lost is proportional to the ambient environmental condition, increased mass loss for decreased relative humidity. This trend is followed by all the other mixes with the same W/C ratio but with varying chemical admixture contents. The magnitudes of moisture lost follows the trend: the silica fume and 5% SRA admixed mix, the silica fume admixed reference mix, the 5% SRA admixed mix and then the paste reference.

Figure 4.1.15 depicts the moisture loss behavior of the 5% SRA admixed paste mix. Despite the fact that the SRA mixes shrink less than their complementary reference mixes, they lose more moisture. If the pore structure were identical respectively, then the reduc-

tion in surface tension is the only possible explanation for both the reduced shrinkage strains experienced.
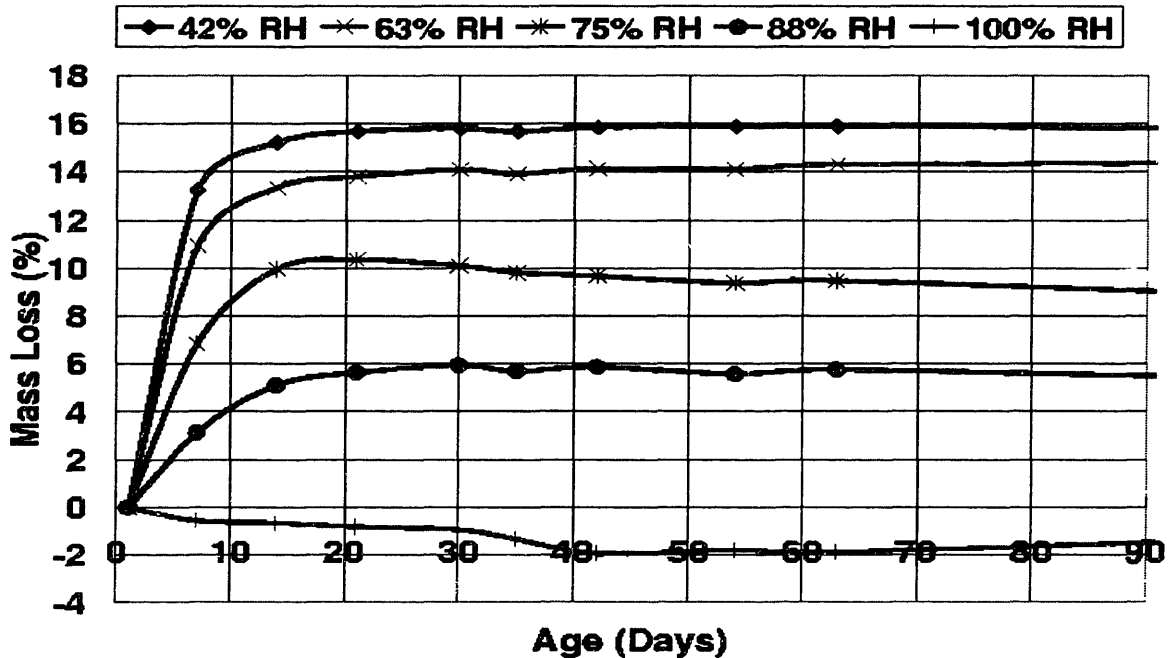
Figure 4.1.15 The average mass loss behavior of the W/C = 0.55 5% SRA admixed paste platelets subjected to different constant relative humidity environments.

However, the ease with which the moisture leaves the system remains unexplained. In the microstructural analysis section it becomes apparent that the pore structure for this particular mix is coarsened due to the addition of the SRA and hence one would expect that there would be greater moisture loss.

Observe that as discussed above there is greater moisture loss for these specimens compared to the complementary reference paste specimens. There is little difference in water absorption, but the reference mix does absorb more water at different periods of time.

The W/C = 0.65 mixes experience greater moisture losses then the W/C = 0.55 mixes with a few exceptions which may be due to the environmental relative humidity drift. This behavior is expected due to the coarser microstructure developed for the higher water-to-cementitious material ratio mixes. Figure 4.1.16 compares the behavior of the silica fume mixes at 42% RH.

It is interesting to note that the relative amounts of moisture absorbed for the specimens immersed in water are less for the lower water-to-cementitious ratio mix and for the

silica fume mixes. A possible explanation is that the smaller pores are less permeable and hence takes longer to absorb water from the external system if the governing transport phenomena is diffusion or effusion. However if the mechanism is capillary suction, then the reduced surface tension inhibits the height to which the liquid may penetrate.

Figure 4.1.16 depicts the moisture loss behavior of all the W/C = 0.65 test mixes at 42% RH. There is a considerable difference between the 7.5% silica fume with a 5% SRA
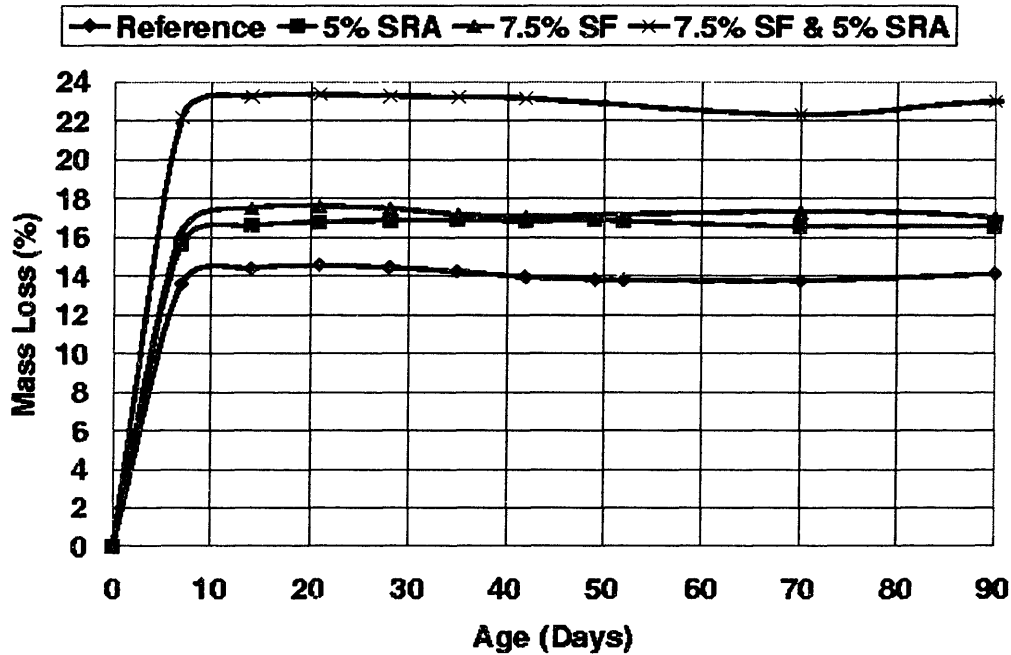
Figure 4.1.16 The behavior of the silica fume admixed test series subjected to the 42% RH environmental condition.

replacement by mixture water test series with the other test series. As expected it is greater than the associated silica fume reference mix, but the magnitude seems a little too much. If the initial condition of the environmental chamber was below the prescribed 42% RH environmental condition at the time that the specimens from this mix was placed into the chamber, then excess irreversible moisture loss could have occurred and skewed the results. It is interesting that the associated shrinkage values for these specimens seem very reasonable when compared to companion specimens from the other mixes. Special attention is paid to this behavior in the analytical modeling section to assure that the experimental results are not skewed.

Note that for the SRA admixed test series, the amount of water absorbed is consistently less than for the complementary reference mixes. Figure 4.1.17 shows this behavior for the W/C = 0.65 mix at 7, 28, and 90 days.
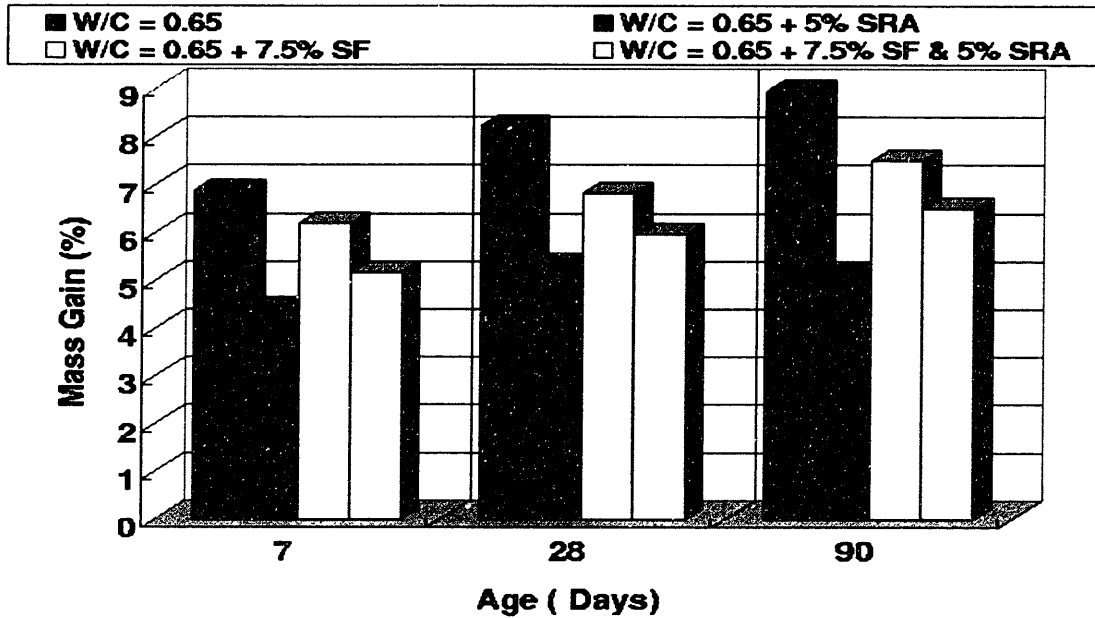
Figure 4.1.17 The mass gain behavior of the W/C = 0.65 mixes at various ages in a fully saturated environment.

4.1.6 Moisture Loss of Intermediate Water-to-Cementitious Ratio Mixes

The microstructure of the W/C = 0.45 mix is much finer than the higher water-to-cementitious mixes, and hence it is expected that the amount of moisture lost should be smaller. Figure 4.1.18 depicts the mass loss behavior of the reference paste mix as a function of several different constant relative humidity environments. The trend of increasing moisture loss with decreasing relative humidity drying environment is followed by all four test mixes in this series. Note that there appears to be consistent drift in both the mass loss and shrinkage.
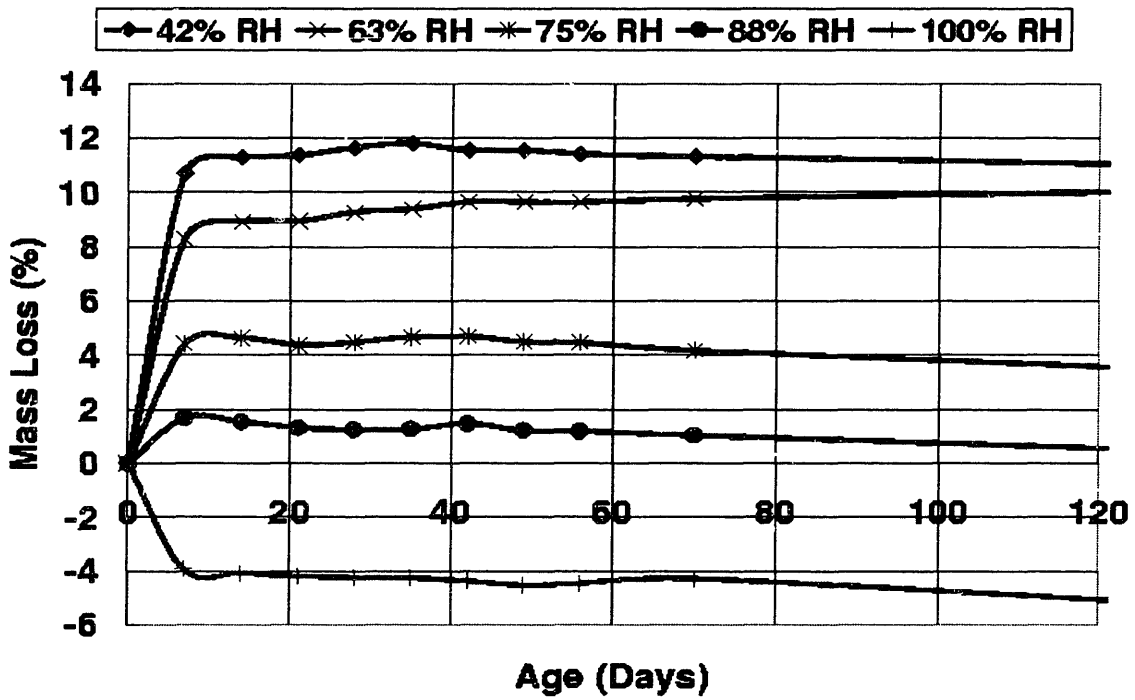
Figure 4.1.18 The mass loss behavior of the reference paste W/C = 0.45 mix at various constant relative humidity environments.
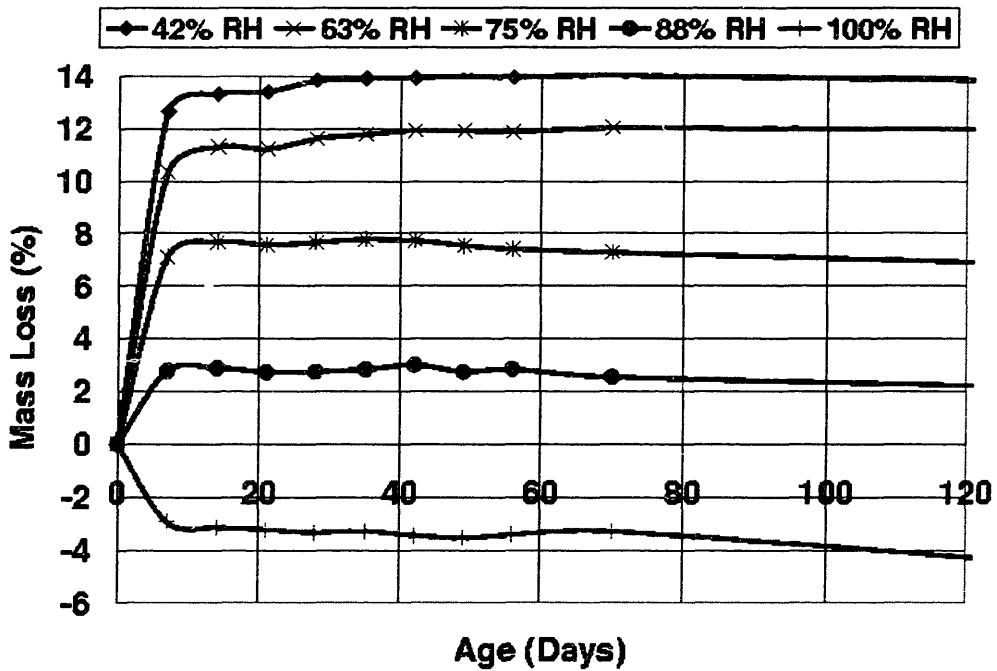
Figure 4.1.19 The mass loss behavior of the W/C = 0.45, 5% SRA admixed mix at several different constant relative humidity environments.

behavior of the reference paste and the 5% replacement by mixture water of SRA mixes at the 75% RH and the 88% RH environmental conditions. The mass loss behavior of the 5% SRA mix is depicted in Figure 4.1.19.

The W/C = 0.35 mixes lose less moisture than the W/C = 0.45 complementary mixes as expected. The spread in mass loss data decreases between SRA admixed and reference mixes. This may be occurring due to the finer pore structure. As the pore walls get closer together, they are able to exert greater surface forces. If the surface forces are sufficiently large, then the thickness of the adsorbed water layers increases and additional free water becomes loosely bound. The movement of water from the pore system is due to both vapor diffusion and capillary suction forces. The diffusion of pore water in very fine pores is very slow, and if the capillary forces cause no or little moisture movement then the accompanying mass loss trends similar to what we have determined. These hypotheses shall be tested in the microstructural analysis section where detailed information about the microstructure of these mixes are determined. A further discussion is also made in the analytical modeling section in Chapter 5.

Figure 4.1.20 depicts the typical behavior of the W/C = 0.35 mixes at the harshest environmental condition, 42% RH. The mass loss data for these test series are included in Appendix I.
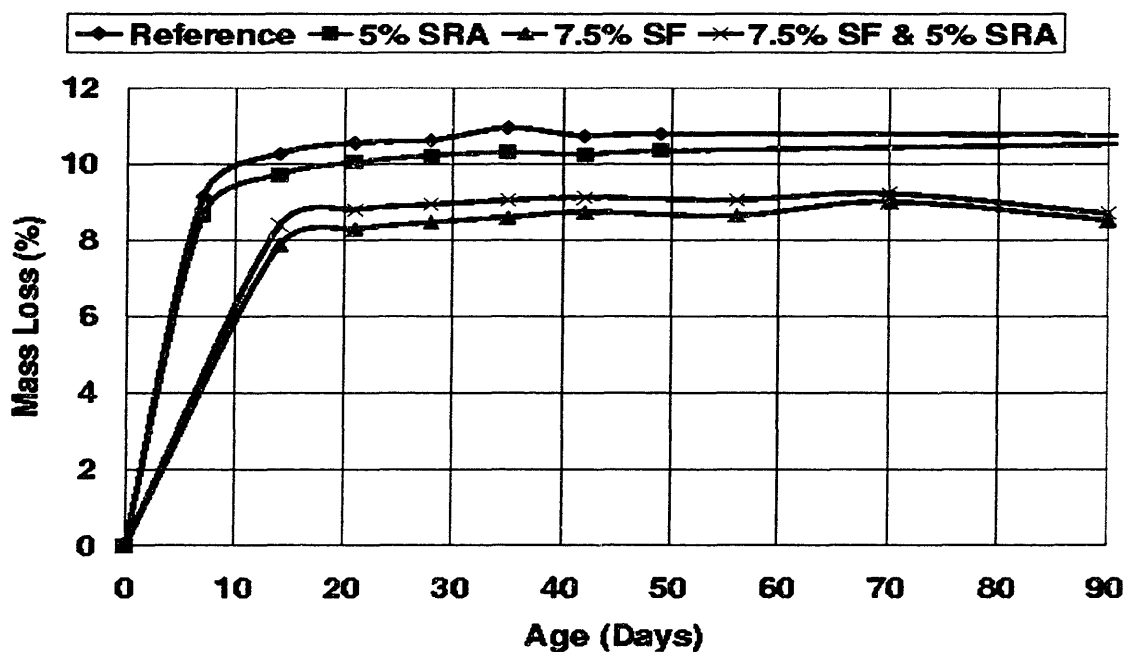
Figure 4.1.20 Typical mass loss behavior for the W/C = 0.35 test mixes, 42% RH.

4.1.7 Moisture Loss from Low Water-to-Cementitious Ratio Mixes

These test series have the finest pore structures of all the test mixes therefore their permeabilities are very low. The uptake of water must occur at a very slow rate, as well as the drying behavior. Since this mix is at such a low water-to-cementitious ratio, it is expected that the specimens shall be subjected to internal self desiccation. Therefore a key mode of moisture loss is through internal hydration which may be of the same order of magnitude as the moisture loss due to drying. This is important to note for the modeling section. Figure 4.1.21 depicts the behavior of the reference paste W/C = 0.25 platelets subjected to different constant relative humidity environments. It is apparent that the same trends followed by the other mixes are also followed here, greater mass loss at lower relative humidity environments.

Figure 4.1.22 depicts the trends for all the W/C = 0.25 test mixes at 42% RH. Note that the uptake of water from the fully saturated case is larger than the associated W/C = 0.35 mixes due to greater differences between internal and external conditions. So despite the lowered permeability, the driving force for absorption is large enough to ensure greater moisture absorption. Similar trends are followed for the silica fume admixed test series. Mass loss behavior of the reference, the 5% SRA admixed, the 7.5% silica fume admixed, and the 7.5% silica fume with 5% SRA mixes are depicted in Figures 4.1.23 through 4.1.26. In Figure 4.1.23, the W/C = 0.65 and W/C = 0.55 curves intersect one another 14 days and then the W/C = 0.55 mix loses more moisture from that time onward. The other three series follow the regular pattern of moisture loss with mix design. It is very interesting that the W/C = 0.25 mix loses the least water but experiences the largest shrinkage strains. Again the explanation proffered is that this mix had the highest cement content of all the mixes, and the lowest water content. So it should have a large propensity to shrink and lose little water. It had very little water to begin with.
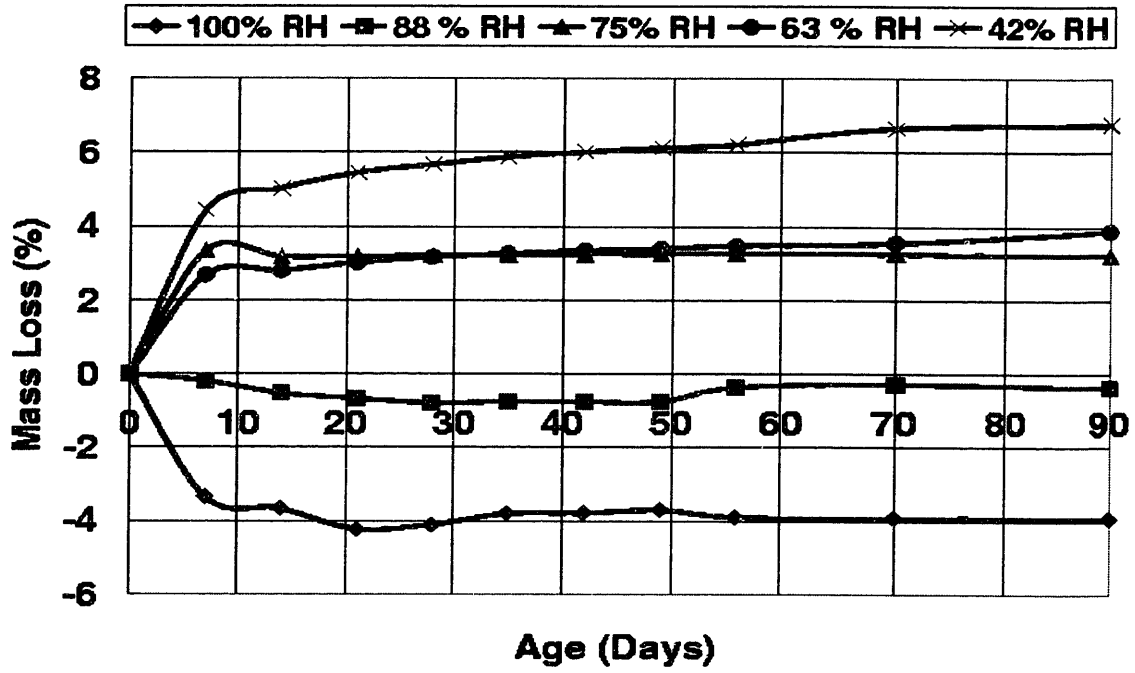
Figure 4.1.21 The mass loss behavior of the reference paste W/C = 0.25 mix.
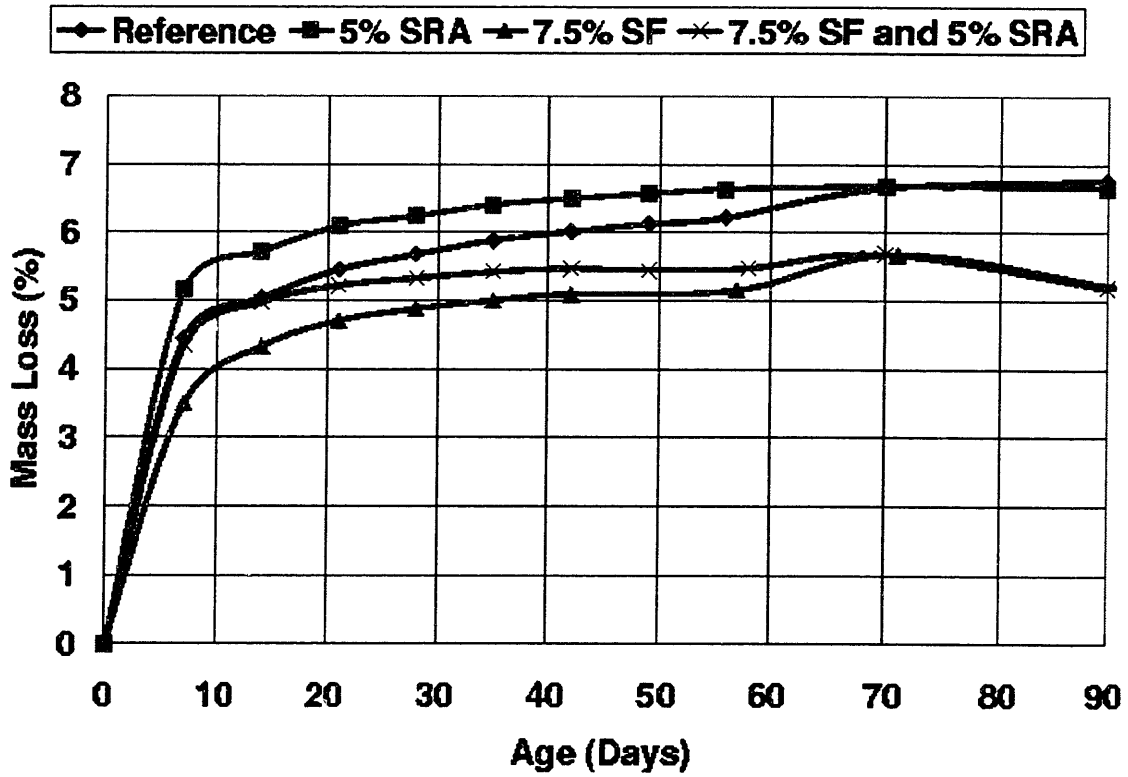
Figure 4.1.22 The mass loss behavior of all W/C = 0.25 mixes at 42% RH environment.

Figure 4.1.24 follows the regular pattern expected from the shrinkage results. That is greater mass loss with reduced ambient relative humidity condition. It is interesting to note the relatively large separation between the magnitudes of moisture loss for these mixes when the shrinkage strains were very closely clustered except for the W/C = 0.25 mix. The shrinkage strains almost progressed in reverse order: 0.45, 0.65, 0.55, 0.35, 0.25, from lowest shrinkage to highest. The mass loss behavior of the 7.5% silica fume admixed series is somewhat out of order: 0.35, 0.45, 0.25, 0.55, and 0.65. The shrinkage pattern followed is: W/C = 0.25, 0.35, 0.45, 0.55, 0.65, with the W/C = 0.55 mix crossing the W/C = 0.65 mix at 50 days. The pattern of W/C ratio with moisture loss and shrinkage is followed fairly well with this mix. Figure 4.1.25 follows the trend exactly, which corresponds also with the shrinkage data. The moisture loss data for these test mixes are attached in Appendix I.
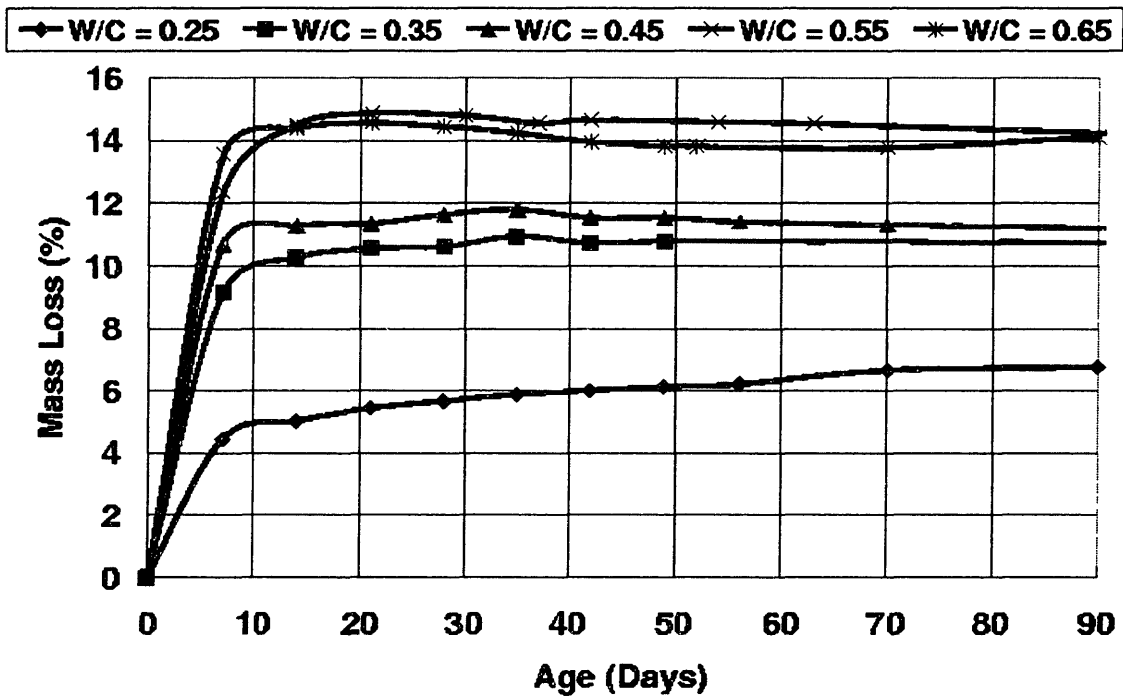
Figure 4.1.23 The mass loss behavior of the reference paste mixes for all W/C ratios at 42% RH.
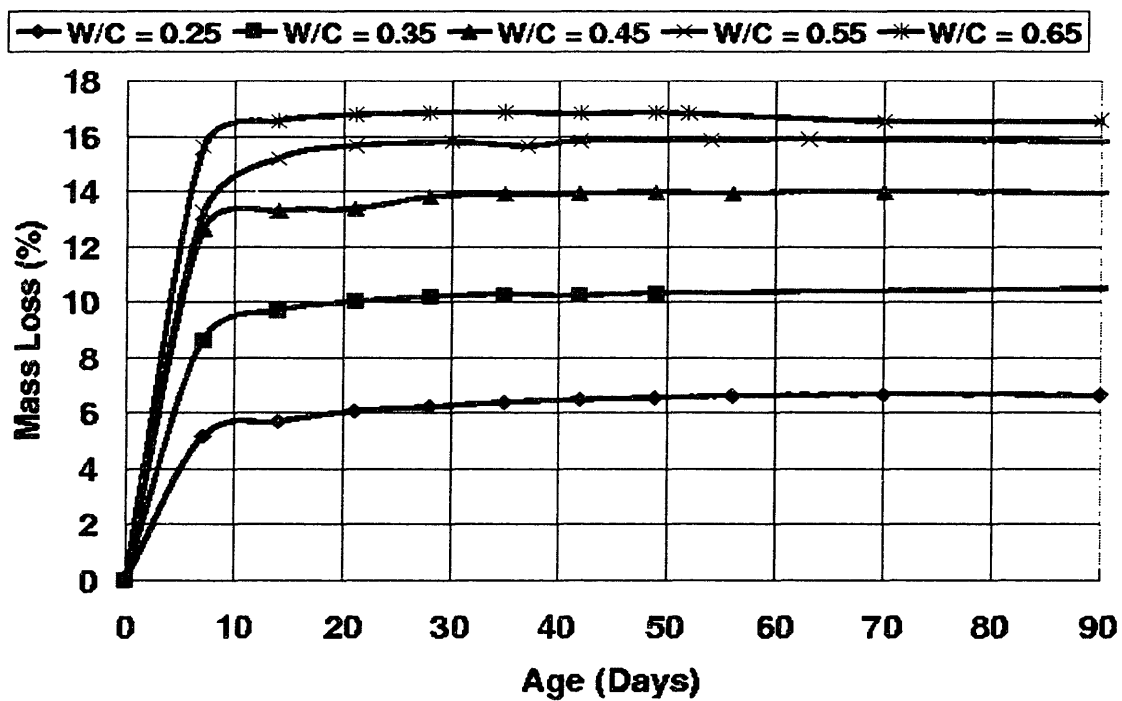
Figure 4.1.24 The mass loss behavior of all 5% SRA admixed mixes at 42% RH.
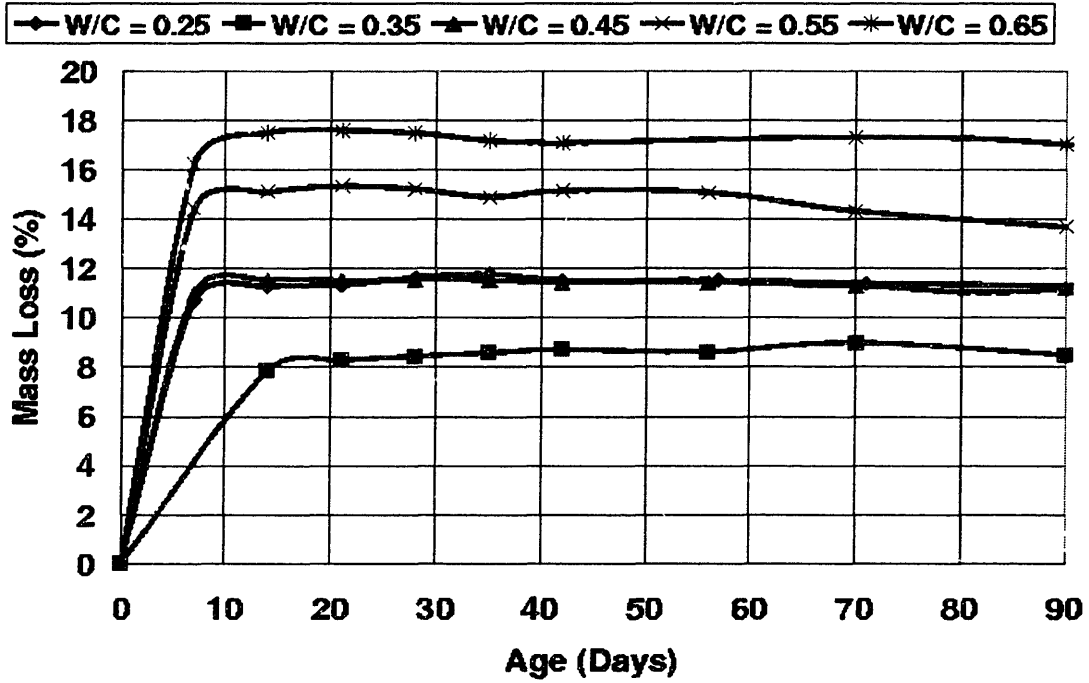
Figure 4.1.25 The mass loss behavior of all 7.5% silica fume mixes at 42% RH.
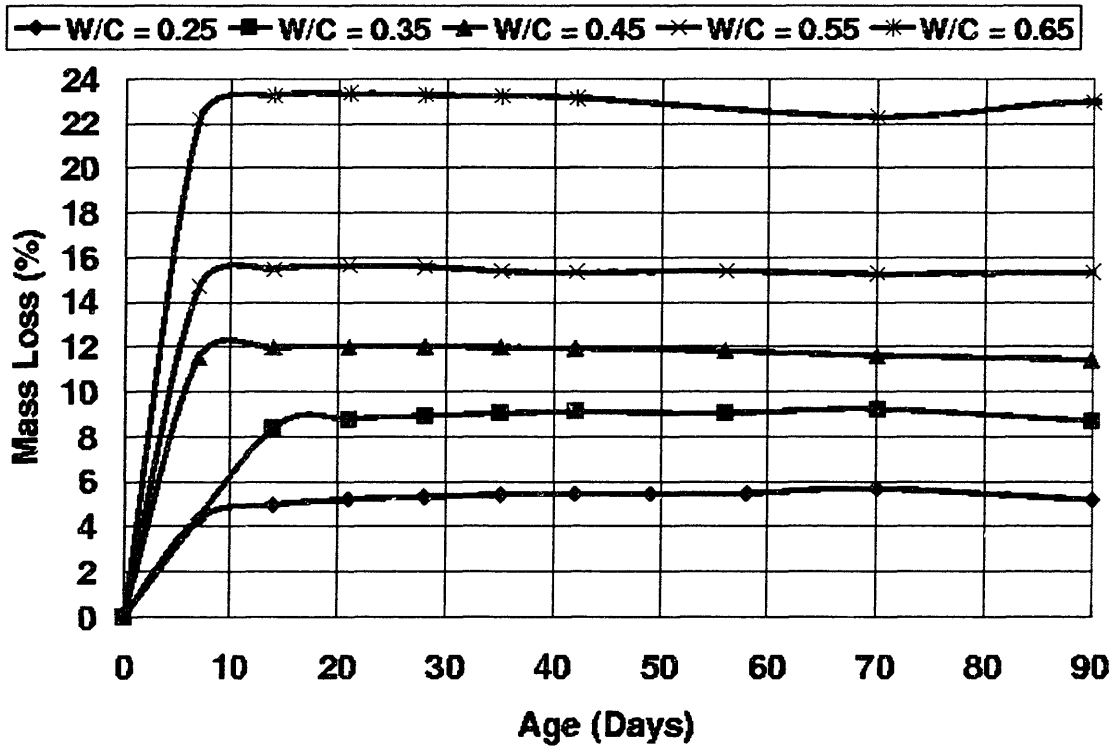
Figure 4.1.26 The mass loss behavior of all 7.5% silica fume with 5% SRA mixes at 42%RH.

4.2 Mechanical Properties

4.2.1 Introduction

The objective of the mechanical property tests is to determine how the addition of the SRA as well as changes in the mix design affect the evolution of mechanical properties in time. The properties required to accurately model the curling behavior of cement slabs are: the compressive strength and the compressive modulus. The tests are conducted using adapted ASTM procedures, and the results and discussion of trends follow.

4.2.2 Compressive Strength

As discussed in the experimental methodology section, 3x6 cylinder specimens were used to characterize changes in compressive strength behavior with maturation time. However, the 3x6 test cylinder data obtained from testing was extremely erratic. Some possible causes of the erratic behavior established for the larger 3x6 cylinder specimens are: the creation of large air voids due to poor consolidation, pour lines caused by partial setting of separate layers, irregular bleed pathways, as well as drying and thermal shrinkage strains that cause severe microcracking. After 14 days, the differential strains established in the cylinders due to internal restraint and tension near the surface are sufficient to cause severe cracking that then penetrates into the cylinder causing it to further degrade.

So in order to obtain the required property, standard mortar cube specimens were used instead of the 3x6 cylinders, but filled neat cement paste. These specimens are much better suited for this particular test because of the greatly reduced volume to surface area ratio. The appropriate ASTM standard for mortar cube testing was modified for the paste specimens and followed.

The early age results obtained from the cube specimens contained a much smaller spread in the averaged data. Figure 4.2.1 shows the evolution of compressive strengths for the
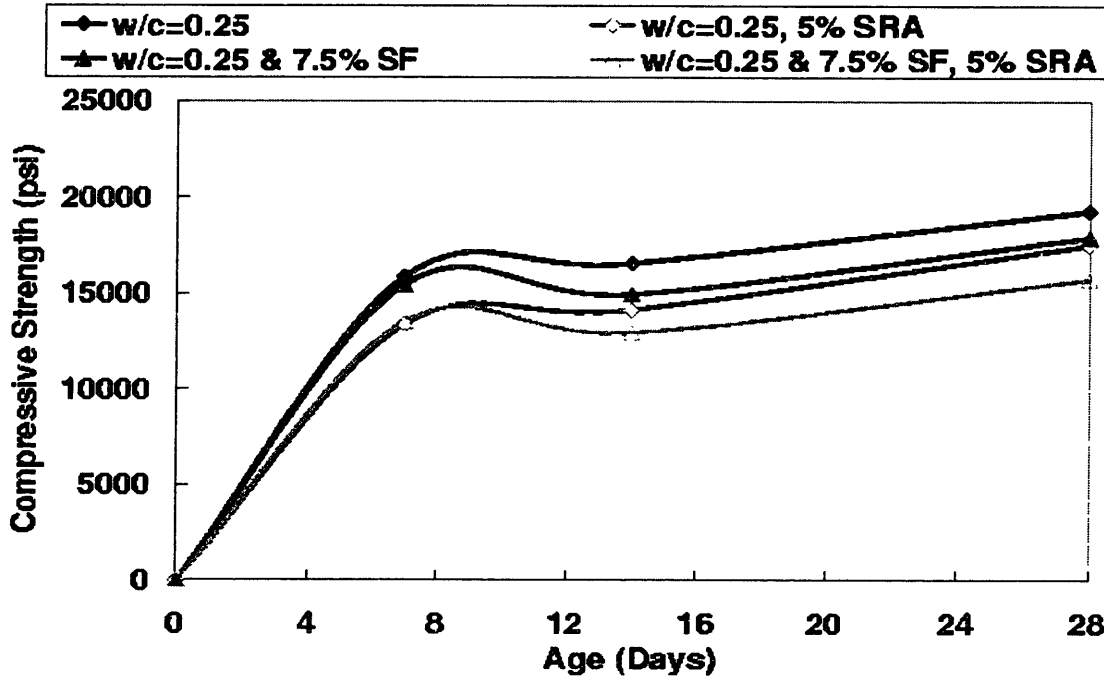
Figure 4.2.1 The averaged compressive strength behavior for the W/C = 0.25 mixes.

W/C = 0.25 mixes. Note the consistent drop in strength at 14 days for the silica fume admixed mixes. This type of behavior is fairly common. The early strength development is followed by a short dormant period. The strength then grows again usually after 21 - 35 days and increases dramatically between 56 - 90 days. The reference paste and reference paste plus silica fume mixes are consistently stronger than the SRA admixed test mixes at this water-to-cementitious ratio. This trend is not followed for the higher water-to-cementitious material ratio test mixes.

Figures 4.2.2 and 4.2.3 depict the changes in compressive strength behavior for the cube mixes at all the various water-to-cementitious material ratios at 7 and 28 days respectively. The W/C = 0.25, 0.35, and 0.45 reference mixes at seven days are stronger than the complementary SRA admixed test mixes. However, the 5% SRA admixed W/C = 0.55 and 0.65 mixes are stronger than the reference mixes at the same age. For early age strength a reduction in drying shrinkage at the lower water-to-cementitious material ratios may

enhance the compressive strength performance while playing a lesser role at the higher

water-to-cementitious material ratios.

▋w/c=0.25	▋w/c=0.25, 5% SRA	▋w/c=0.25 & 7.5% SF	▋w/c=0.25 & 7.5% SF, 5% SRA
▋w/c=0.35	▋w/c=0.35, 5% SRA	▋w/c=0.35 & 7.5% SF	▋w/c=0.35 & 7.5% SF, 5% SRA
▋w/c=0.45	▋w/c=0.45, 5% SRA	▋w/c=0.45 & 7.5% SF	▋w/c=0.45 & 7.5% SF, 5% SRA
▋w/c=0.55	▋w/c=0.55, 5% SRA	▋w/c=0.55 & 7.5% SF	▋w/c=0.55 & 7.5% SF, 5% SRA
▋w/c=0.65	▋w/c=0.65, 5% SRA	▋w/c=0.65 & 7.5% SF	▋w/c=0.65 & 7.5% SF, 5% SRA
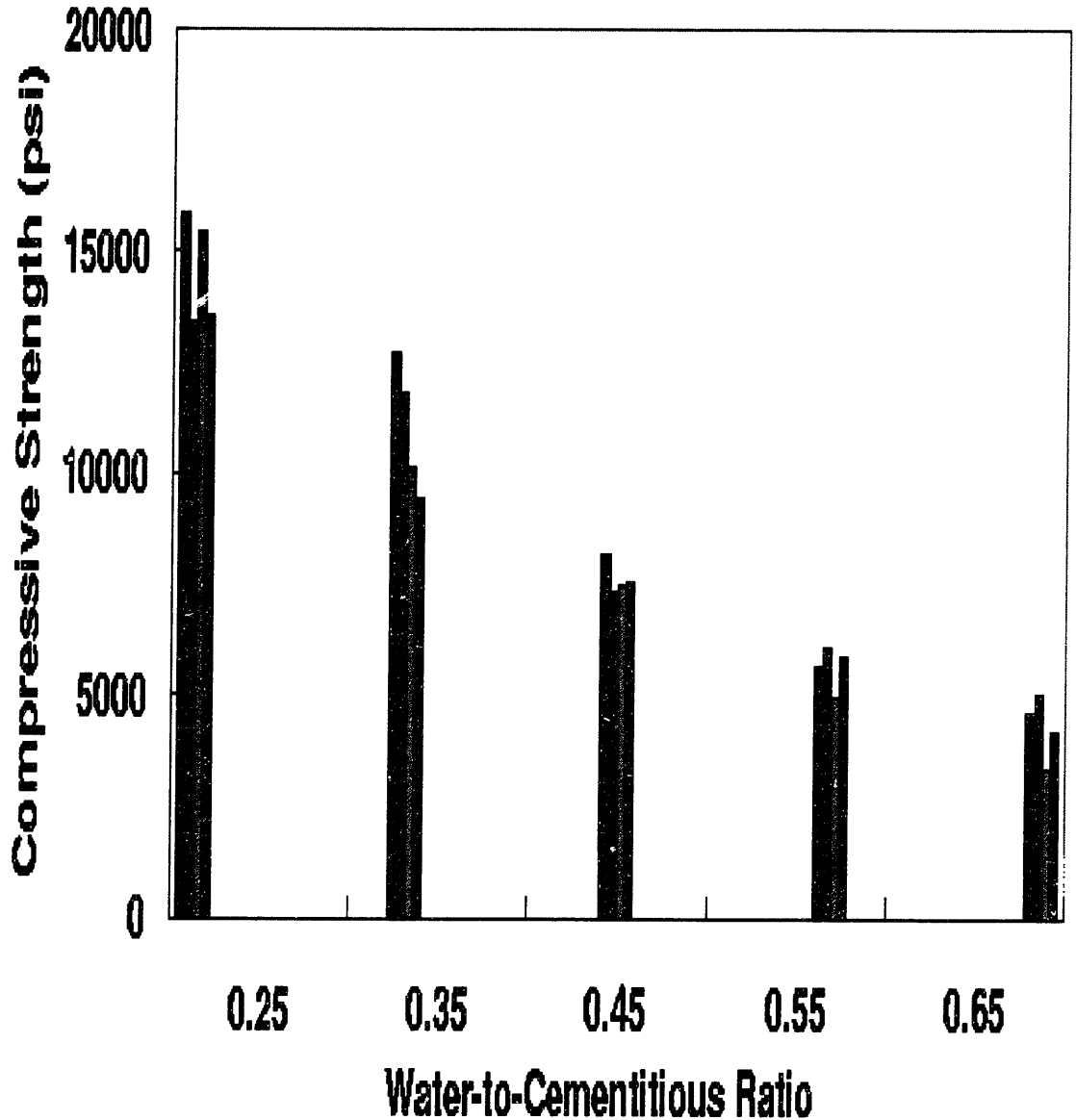
Figure 4.2.2 The averaged compressive strength for the W/C = 0.25 cube specimens
at 7 days.

■w/c=0.25	ᴵ⃞w/c=0.25, 5% SRA	■w/c=0.25 & 7.5% SF	■w/c=0.25 & 7.5% SF, 5% SRA
■w/c=0.35	ᴵ⃞w/c=0.35, 5% SRA	■w/c=0.35 & 7.5% SF	■w/c=0.35 & 7.5% SF, 5% SRA
■w/c=0.45	ᴵ⃞w/c=0.45, 5% SRA	■w/c=0.45 & 7.5% SF	■w/c=0.45 & 7.5% SF, 5% SRA
■w/c=0.55	■w/c=0.55, 5% SRA	■w/c=0.55 & 7.5% SF	■w/c=0.55 & 7.5% SF, 5% SRA
■w/c=0.65	■w/c=0.65, 5% SRA	■w/c=0.65 & 7.5% SF	■w/c=0.65 & 7.5% SF, 5% SRA
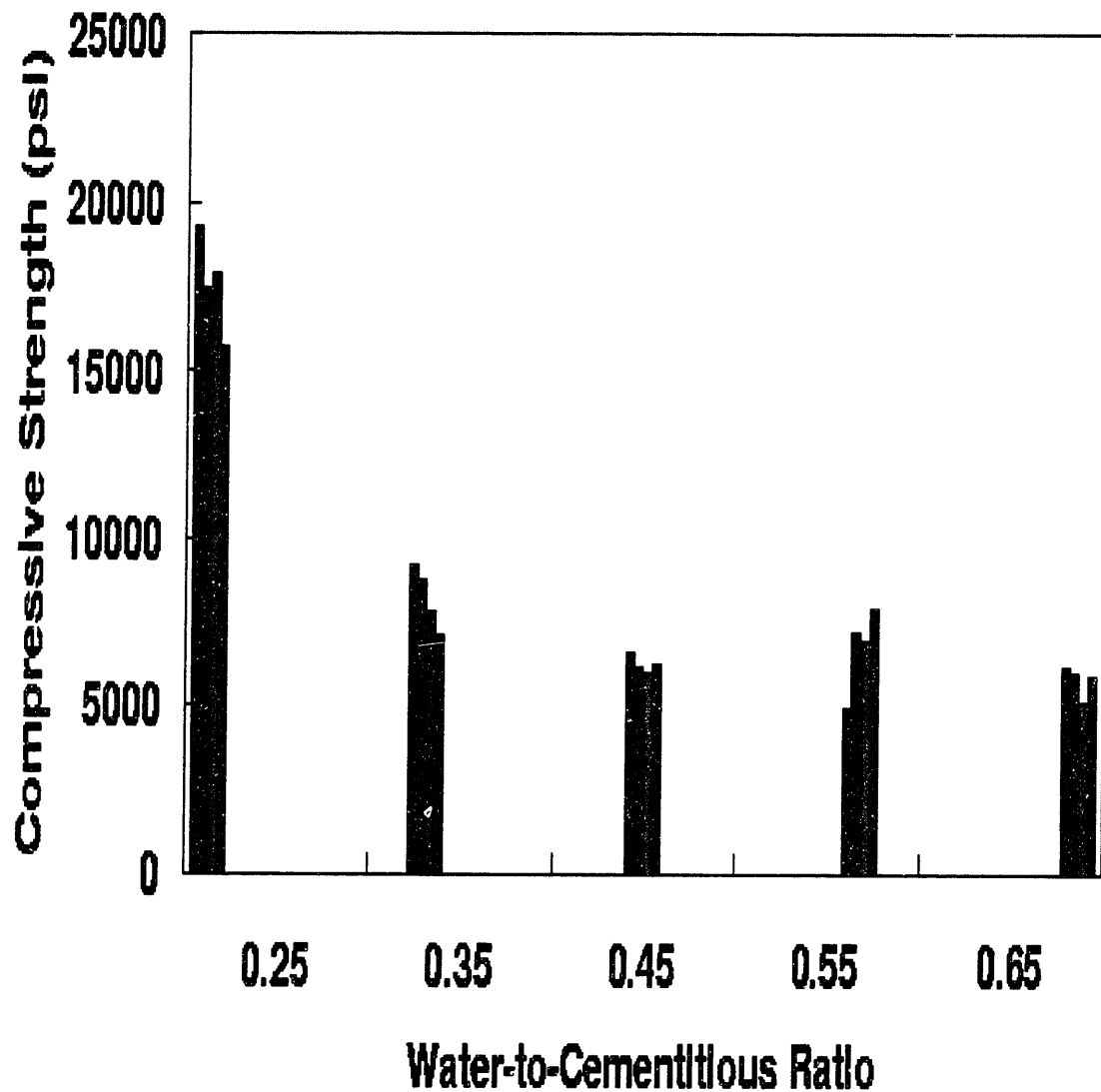
Figure 4.2.3 The averaged compressive strength behavior of all mix design
cube specimens at 28 days.

It was also noticed that when the mixing was taken place, the 5% SRA admixed mixes had

higher workabilities. Measurements were not taken on a flow table, the workability was

determined by the ease of flow through the 50 cc syringe used to fill platelet molds. The presence of large air voids and/or flow lines may have been reduced.

Again, Figure 4.2.3 shows the 28 day behavior of all test mixes. Some of the mixes experienced reductions in compressive strength at this age: W/C = 0.35 and 0.45. These mixes experienced high shrinkage strains at this age and these large strains may have caused the reductions in strength. The W/C = 0.25, 0.55, and 0.65 mixes gained strength as expected. The same trends in terms of mix type and higher strength values established at 7 days is followed. The average compressive strengths of all the test mixes determined by cube specimens up to 28 days are included in Appendix I. Simple logarithmic regressions were performed on all mixes and these formulas will be used to establish changes in behavior through time in the modeling section of this report.

4.2.3 Compressive Modulus of Elasticity

As described in the experimental methodology section, 4x8 cylinders were used to establish the evolution of compressive modulus of elasticity in time. Figures 4.2.4 and 4.2.5 depict the changes in the compressive modulus of elasticity between mix designs at 7 and 28 days respectively. In both graphs the modulus information for the W/C = 0.35 paste with and without the addition of 5% SRA by replacement of mixture water are not included. These tests series were not included due to the malfunction of the testing rig at both these ages. As expected the compressive modulus increases with a decrease in water-to-cementitious material ratio. The finer pore structure increases the rigidity of the paste matrix. The exception to this trend occurs for the W/C = 0.55 mix. The addition of the SRA has a variable effect at 7 days with increases in modulus for the W/C = 0.35 paste, 0.45 paste plus 7.5% silica fume, and the 0.65 paste plus 7.5% silica fume. The other mixes have higher compressive moduli for the reference mixes.

■w/c=0.25	□w/c=0.25, 5% SRA	■w/c=0.25 & 7.5% SF	□w/c=0.25 & 7.5% SF, 5% SRA
□w/c=0.35	□w/c=0.35, 5% SRA	■w/c=0.35 & 7.5% SF	▣w/c=0.35 & 7.5% SF, 5% SRA
■w/c=0.45	□w/c=0.45, 5% SRA	■w/c=0.45 & 7.5% SF	▣w/c=0.45 & 7.5% SF, 5% SRA
■w/c=0.55	□w/c=0.55, 5% SRA	■w/c=0.55 & 7.5% SF	▣w/c=0.55 & 7.5% SF, 5% SRA
■w/c=0.65	□w/c=0.65, 5% SRA	■w/c=0.65 & 7.5% SF	▣w/c=0.65 & 7.5% SF, 5% SRA
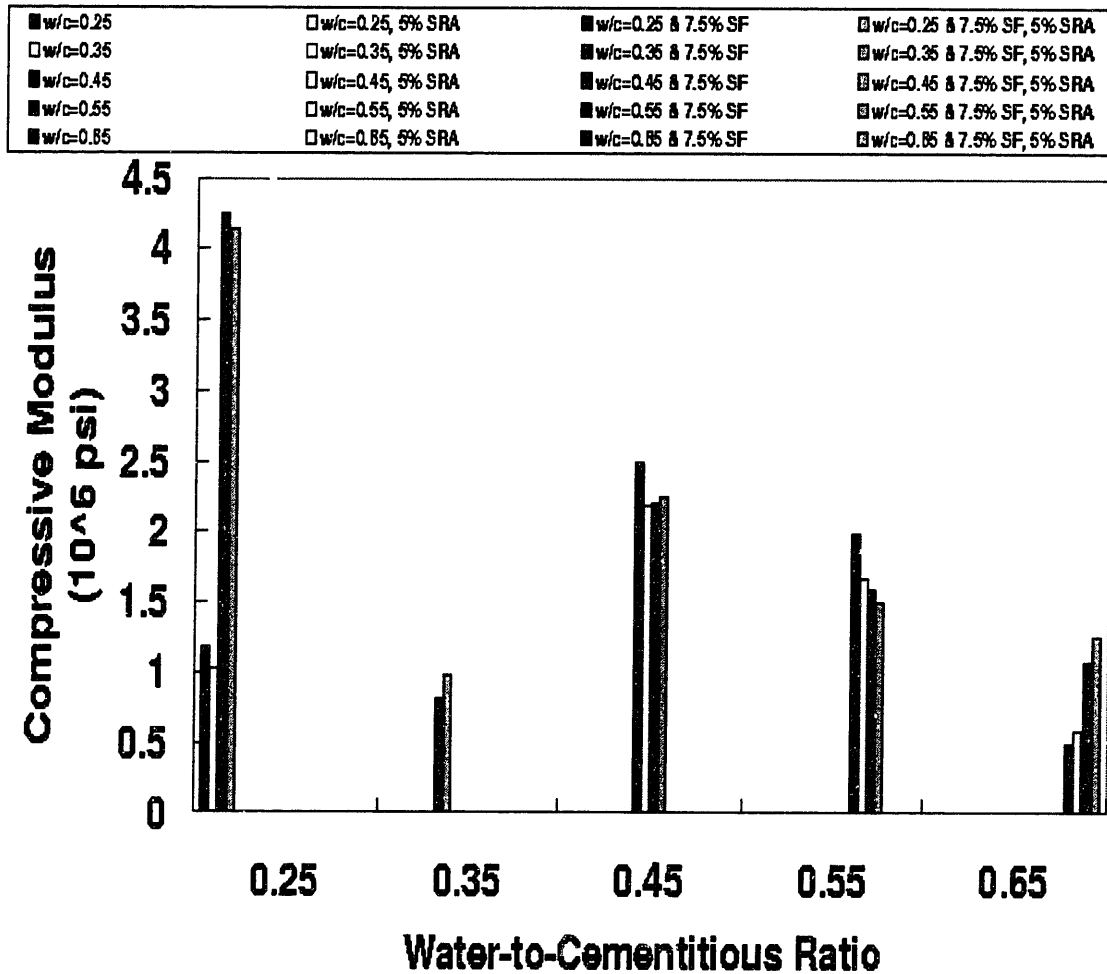
Figure 4.2.4 The compressive modulus of elasticity of the various mixes at 7 days.

Changes in the behavior at 28 days follow: increased moduli for all the W/C = 0.25, 0.35, 0.45, the reference paste 0.55, and 0.65 test mixes. Again compressive modulus increases with decreasing water-to-cementitious material ratio with the exceptions of the W/C = 0.35 mixes and the reference and SRA admixed W/C = 0.25 mixes. This may be due to the internal microcracking due to the self-desiccation. All magnitudes increase at 28 days compared to the 7 day values as expected. Based upon the information presented, the addition of 5% SRA has a variable but slightly positive effect on the compressive modulus of elasticity. Higher moduli imply that higher stresses are needed at the same strain to produce cracking. The compressive moduli data are included in Appendix I. Simple logarithmic regressions were performed on all mixes and these formulas will be used to establish

changes in behavior through time. This information is used in the modeling section to determine the stresses produced from curling deformations at a given relative humidity environment and moisture content.

■w/c=0.25	□w/c=0.25, 5% SRA	▓w/c=0.25 & 7.5% SF	▤w/c=0.25 & 7.5% SF, 5% SRA
□w/c=0.35	□w/c=0.35, 5% SRA	▓w/c=0.35 & 7.5% SF	▤w/c=0.35 & 7.5% SF, 5% SRA
■w/c=0.45	□w/c=0.45, 5% SRA	▓w/c=0.45 & 7.5% SF	▤w/c=0.45 & 7.5% SF, 5% SRA
■w/c=0.55	■w/c=0.55, 5% SRA	▓w/c=0.55 & 7.5% SF	▤w/c=0.55 & 7.5% SF, 5% SRA
■w/c=0.85	□w/c=0.85, 5% SRA	▓w/c=0.85 & 7.5% SF	▤w/c=0.85 & 7.5% SF, 5% SRA
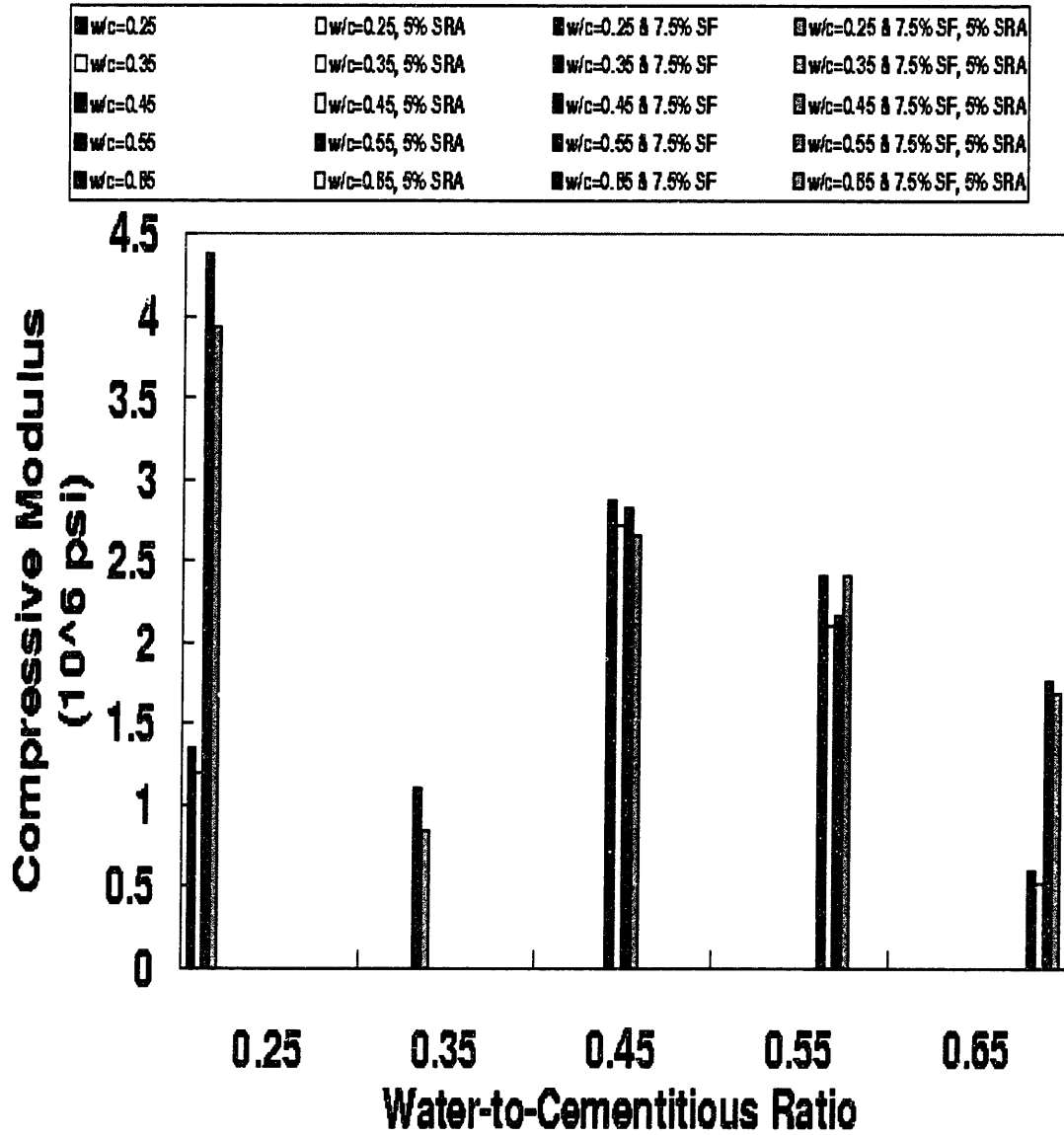
Figure 4.2.5 The compressive modulus of elasticity determined at 28 days.

4.3 Curling Deformation Study

4.3.1 Introduction

A total of twenty test mixes were tested in the curling deformation study to determine changes in curling behavior with time resulting from changes in mix design and the pres-

86

ence of the SRA. Each test mix had duplicate specimens which were measured at the times described in the experimental methodology section and the averaged results are discussed and presented below. This information shall be used to correlate and verify findings presented in Chapter 5 about analytical and computational modeling of curling deformations due to changes induced in moisture content through a specimens depth by the addition of the SRA.

4.3.2 High Water-to-Cementitious Material Ratios

These test mixes experienced the highest reductions in curling deformations with the use of the SRA. Figure 4.3.1 shows a typical prolifigram of the W/C = 0.65 reference paste mix at various ages. All the test series experience some curling due to the one dimensional loss of moisture through the top surface of the cement plates. The magnitudes of curling at the ages shown: 0, 7, 28, 56, 70, and 90, are all increasing in magnitude, however very early age data indicates that the degree of curl fluctuates with early age. Again the curling deformations were measured by placing the specimen on it side against a rectangular piece of aluminum tubing and then restraining it with elastic bands at either end. A pair of electronic calipers were then used to measure the out-of-plane deformations. The experimental methodology section has a picture of the measuring procedure. Some of the earlier ages experience greater curling deformations than the 28 day curling deformation.
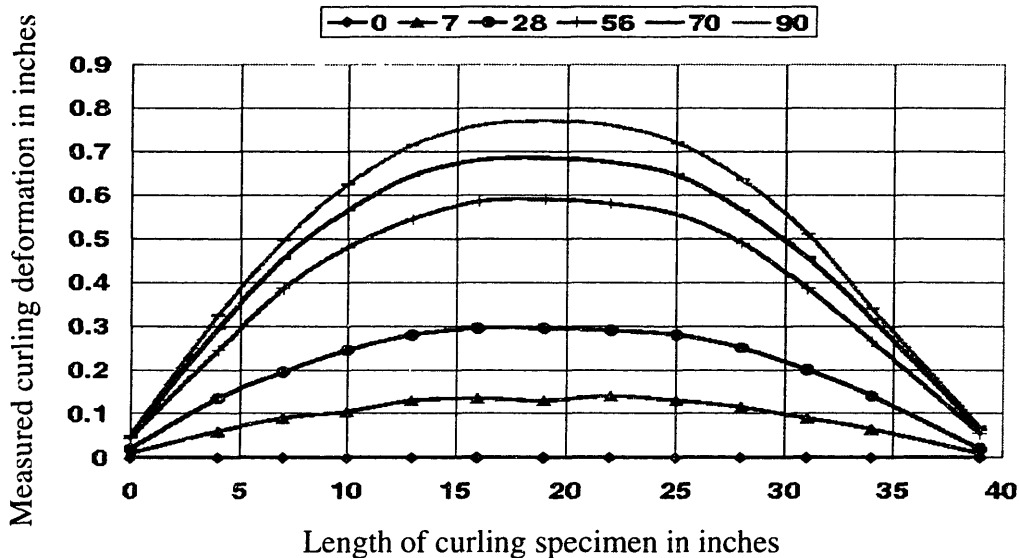
Figure 4.3.1 Prolifigram of reference paste W/C = 0.65 mix at various ages.

This may be due to the nonuniform manner in which hydration proceeds, i.e. greater hydration in the interior portion of the specimen and less hydration at the surface. Also some additional testing information indicates that a perfect seal was not obtained, which may cause drying fronts from both edges and the bottom surface. At some point in time the movement of moisture equilibrates such that moisture is lost again in a one dimensional manner from the top surface. Another possible explanation is that early age creep occurs relieving the curl stresses and then when additional moisture is lost the creep response is overcome.

Figure 4.3.2 shows the center-line deflection reductions at four different ages ranging from 7 - 90 days. The silica fume admixed series experienced the largest curling deformations and the greatest reductions due to the addition of the SRA. The slope of the curve becomes negative after 28 days, when the largest curling reductions occurred. The same shape of curve occurs for the reference paste and the 5% SRA admixed series. At 90 days there is
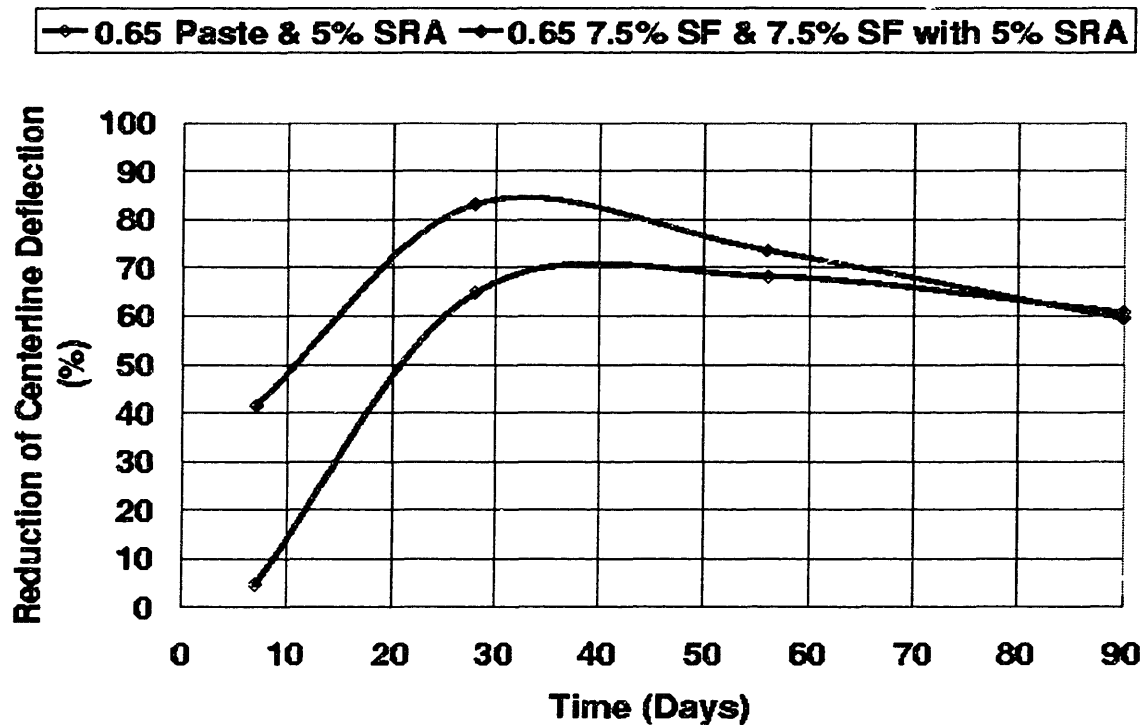
Figure 4.3.2 Comparison of center-line deflection reductions for the reference and the silica fume admixed series, W/C = 0.65.

comparable reductions in curling deformations for the two types of mixes: paste, and silica fume admixed. Please note that although the reductions in curling decrease somewhat with age there is still a considerable difference in curl between the SRA and reference mixes.

Figure 4.3.3 depicts the same behavior for the W/C = 0.55 test series. Again the greatest difference in center-line curling deflection occurs for the silica fume admixed series. At 90 days there is comparable reductions between the paste and silica fume series. There is a dramatic change in the slope of the silica fume mix difference curve at 56 days. A possible
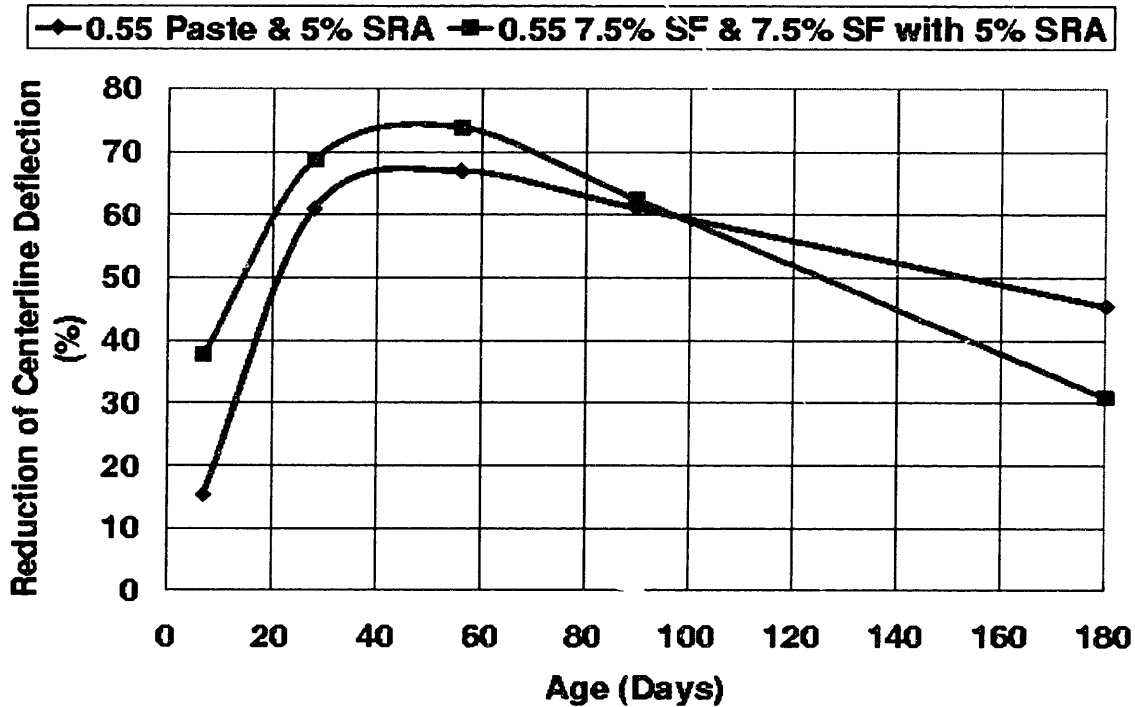
Figure 4.3.3 Curling reductions experienced by the W/C = 0.55 test series.

explanation is that the creep relaxation is greater for the silica fume mixes. All specimens were cast using identical procedures and stored in the same environment, therefore the difference in behavior must be attributed to the internal redistribution of moisture from points of high stress to region of lower stress. The relaxation experienced by the SRA admixed mixes is much less than that experienced by the reference mixes. This could occur because the chemical composition of the pore solution changes dramatically for the SRA admixed mixes. When drying occurs, the organic polymer in solution of the SRA comes out of solution and establishes a higher concentration near the drying front. The solubility index of the SRA is approximately 17%. If the redistribution of moisture occurs in this region, then the viscosity of the pore solution changes and we must expect that the creep response will change. Further research into this area should be addressed. A summary of the center-line curling data is attached in Appendix I.

4.3.3 Intermediate Water-to-Cementitious Material Ratios

Similar results are exhibited by the W/C = 0.45 test series as those experienced by the higher water-to-cementitious material ratio mixes. Figure 4.3.4 shows the curling center-line deflections of the reference paste and silica fume mixes as well as the SRA admixed mixes between the ages of 7 and 180 days. At earlier ages the reference paste mix experi-
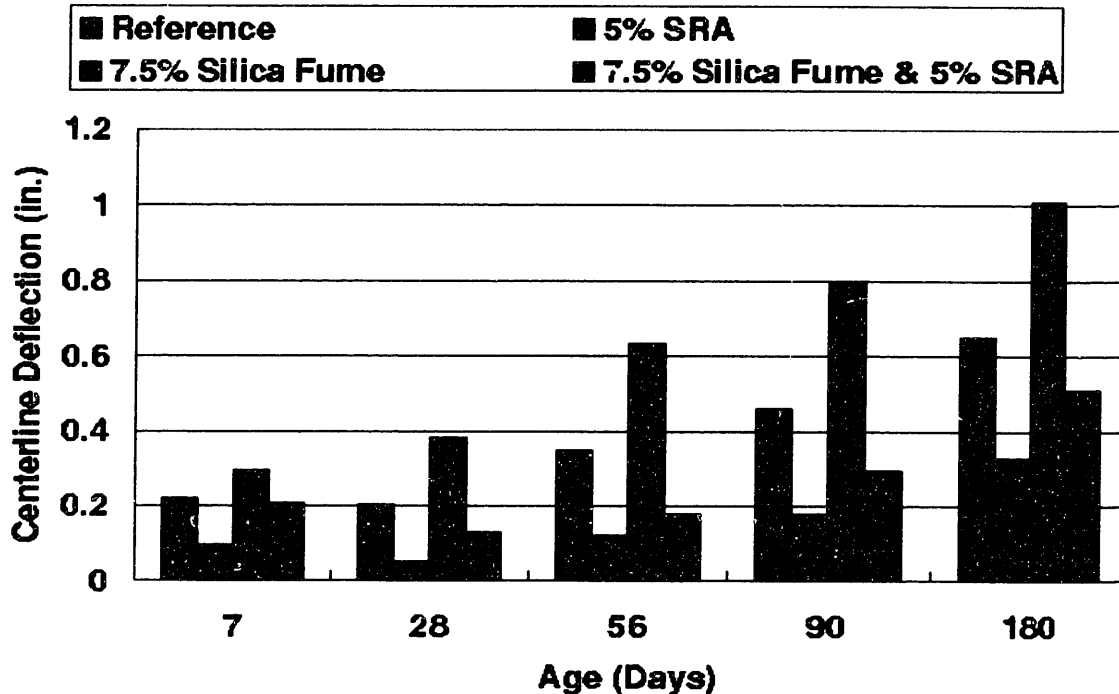
Figure 4.3.4 Center line curling deflections of W/C = 0.45 test mixes
between 7 and 180 days.

ences the largest reductions in curling deformations compared to the silica fume admixed mixes. This trend is opposite of that established for higher water-to-cementitious material ratios which consistently experienced larger curling reductions for the silica fume mixes. Note that at 180 days there are comparable reductions for both type of mixes. Between 56 - 180 days the greatest benefits are experienced by the silica fume admixed mixes. Again creep is occurring at a greater magnitude for the reference mixes which explains the reductions in effectiveness of the SRA admixed mixes.

Figure 4.3.5 depicts the reductions in curling deformations experienced by the W/C = 0.45 testing series with and without the SRA. Note the radically changed behavior

for the paste series. The optimum benefit for that mix is experienced at 28 days, and is

—◆—0.45 Paste & 5% SRA —■—0.45 7.5% SF & 7.5% SF with 5% SRA
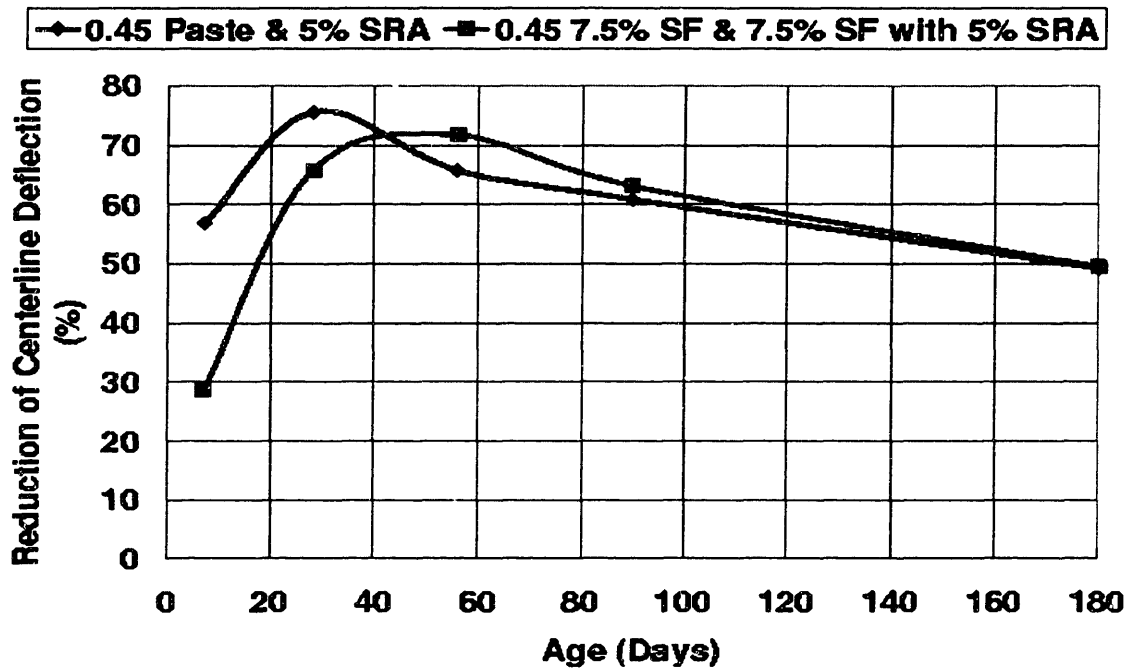
Figure 4.3.5 Reductions in curling center-line deflections of the W/C = 0.35 mixes.

larger in magnitude than the silica fume mixes. The silica fume mixes lag the paste mix until 42 days at which time they experience greater benefit from the presence of the SRA. Comparable reductions occur at 42 and 180 days between both mix types. Again note that the relative difference in curling reductions serves only as a basis of comparison between the silica fume and reference test series due to the addition of the SRA. The actual magnitudes of curl for these specimens are smaller than those experienced by the higher water-to-cementitious ratios and the reductions in efficiency are consequently scaled.

Figure 4.3.6 depicts the reductions in curling deformations experienced by the W/C = 0.35 mixes. Note the dramatic change in behavior exhibited by this mix design. The silica fume mixes experience a very early peak performance, and then become increasingly less well behaved until 56 days. Then the same type of behavior occurs, a dropping off of effectiveness of the SRA. Both mixes experience comparable reductions in curling at 28 and 165 days. Note that at 180 days all specimens are experiencing the same amount of curling

91

deformation. Again the magnitudes of these curling deformations are much smaller then the higher water-to-cementitious material ratio mixes.

Figure 4.3.6 The reductions in curling deformations experienced by the
W/C = 0.35 mixes.

The summary of the center-line deflection values for the various mixes are attached in Appendix I.

4.3.4 Low Water-to-Cementitous Ratios

The W/C = 0.25 test series behaves considerably different than the higher water-to-cementitious ratios. Similar to the W/C = 0.35 silica fume mix, the largest reductions experienced occur early on at 7 days. Figure 4.3.7 shows the different behavior experienced by these test mixes. The negative values correspond to greater curling deformations for the SRA admixed test series. The 7.5% silica fume admixed mixes perform better than the reference mixes. The self desiccation of water in these mixes cause considerable internal consumption of moisture, which may produce more uniform hydration reaction products

through the plate thickness. If the microstructure becomes sufficiently rigid to resist mois-
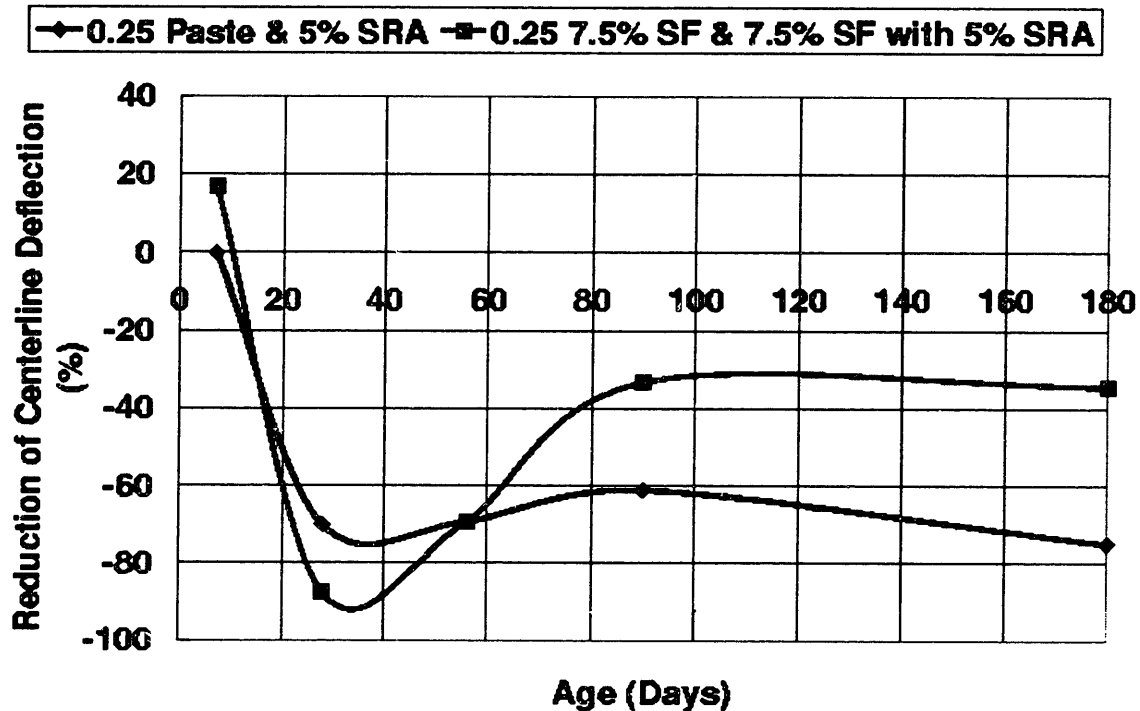
Figure 4.3.7 Reductions in curling center-line deflections for the W/C = 0.25 mixes.

ture induced deformations, then smaller overall curling deformations are expected. What may be producing the increased non-uniformity in moisture content, and hence greater curling deformations in the SRA admixed series is the nonuniform distribution of polymer coming out of solution. The added differential in concentration may be sufficient to produce unwanted flow of moisture. This possibility is under further investigation and will not be reported in this report. The summarized center-line deflection data for these test series are included in Appendix I.

4.4 Microstructural Analysis

4.4.1 Introduction

The purpose of the microstructural analysis is to determine the effects of changing mix design and the addition of an SRA on the pore size distributions of matured hardened cement paste samples. A total of twenty mixes are tested, using the Mercury Intrusion Poresimetry techniques. Finer pore structures are expected with lowered water-to-cementitious material ratios. The addition of the pozzolan additive will further reduce the pore

structure. By applying the simplified capillary tension theory, we propose to explain quantitatively the reductions in shrinkage experienced by the SRA admixed mixes.

4.4.2 High Water-to-Cementitious Ratios

Figure 4.4.1 depicts the normalized cumulative pore size distribution for the W/C = 0.65 reference paste and 5% SRA admixed test series. The normalized curve was determined
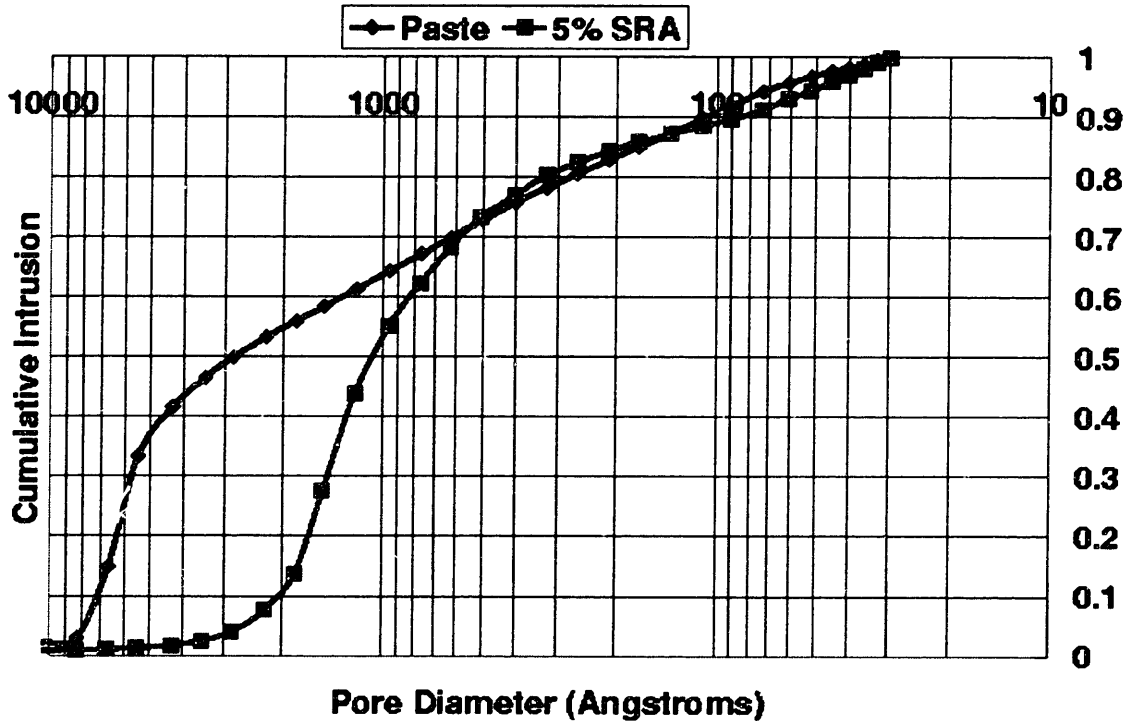
Figure 4.4.1 Normalized cumulative distribution of pore sizes for the W/C = 0.65 reference and 5% SRA admixed test series.

by dividing the intruded volume at a given pore diameter size by the total intruded volume. The most significant differences between the two mixes occur for pores with diameters greater than 1800 angstroms. The reference mix is much coarser than the SRA admixed test series. As will be discussed later in this section, the pore range which exerts the largest influence on drying shrinkage is within 2 - 1000 angstroms. The larger pores contribute less to shrinkage strains than the smaller pores. Based upon this hypothesis, the reference mix should shrink less than the complementary SRA admixed mix. It does not because the SRA admixed test series has a dramatically reduced surface tension which effectively shifts the 5% SRA curve to the left and hence these specimens experience smaller shrinkage strains. This of course is verified by the drying shrinkage data presented earlier.

94

Figure 4.4.2 shows the normalized cumulative pore distribution for the 7.5% silica fume and the 7.5% silica fume plus a 5% replacement of mixture water with the SRA test
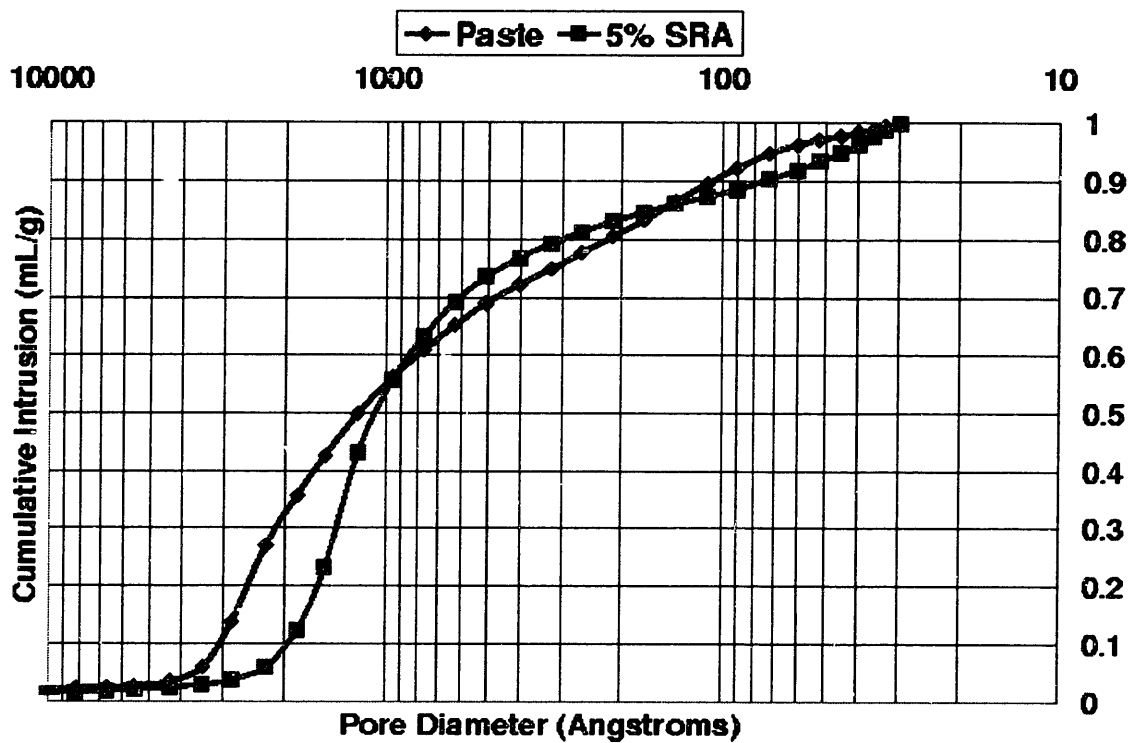
Figure 4.4.2 The normalized cumulative distribution of pores for the W/C = 0.65 silica fume admixed test series with and without the SRA.

mixes. The difference between the two curves is much smaller than the difference between the paste mixes, therefore the reduction in shrinkage should be greater. This occurs because the effective distribution is shifted by a constant amount, i.e. the ratio of surface tensions in the pore solutions for the two mixes. The silica fume mixes are almost exactly the same, therefore the shift will result in pores of much greater diameters becoming active thereby reducing the experienced shrinkage strains. For pore sizes greater than 1000 angstroms the reference silica fume mix is coarser. This follows the same trend established for the reference paste mix.

The steepness of the 5% SRA curve at approximately 1800 angstroms indicates that a large proportion of the pores are active at that diameter provided that by applying Kelvin's equation the moisture content of the matrix is in that pore range. The reference silica fume mix is active over a larger pore range since the curve is less steep. This will be further discussed later in this section.

95

Figure 4.4.3 depicts the normalized cumulative distribution of the W/C = 0.55 reference paste and the paste plus a 5% replacement of mixture water by the SRA. Unlike the W/C = 0.65 mixes discussed above, the microstructure is coarser for the SRA admixed test mix. However the magnitudes of the separation between the two mixes is similar.
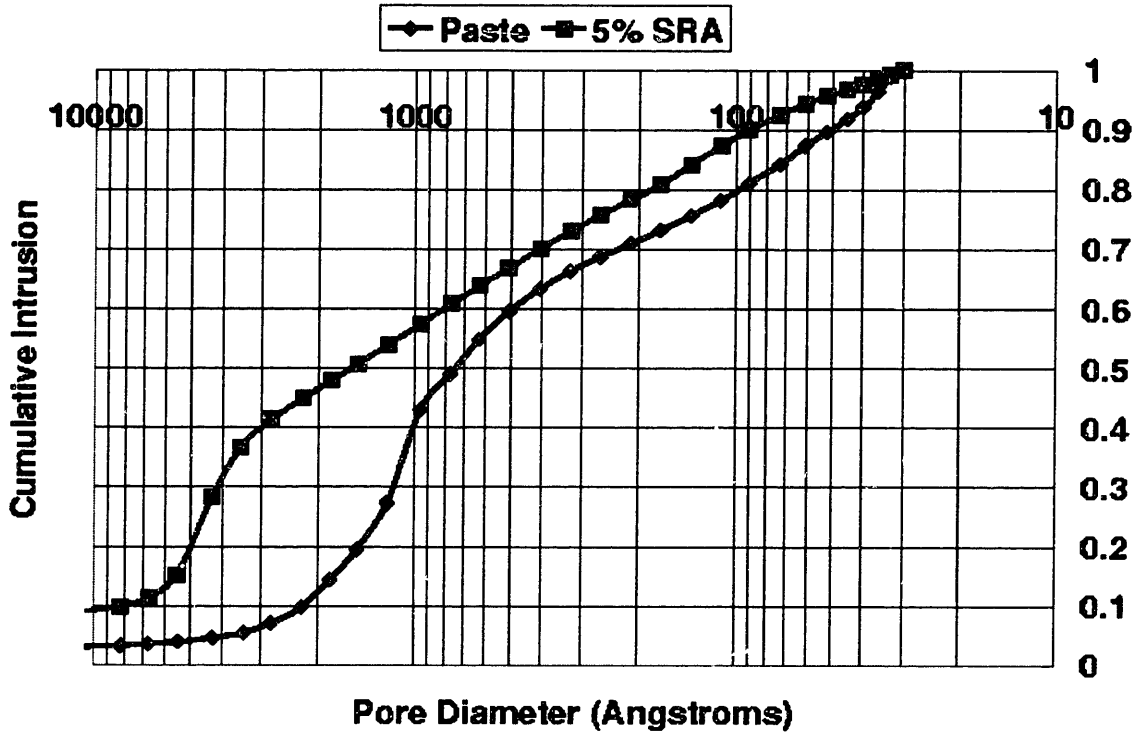
Figure 4.4.3 The normalized pore distributions of the W/C = 0.55 reference paste and the paste plus a 5% replacement of mixture water with the SRA mixes.

As expected the overall distribution is finer than the paste W/C = 0.65 mix. The behavior of a sharp distinction at a particular pore size is also switched, i.e. the paste is centered around 1400 angstroms while the SRA curve is around 4700 angstroms. It is interesting to note that the fineness of the silica fume admixed W/C = 0.65 mix is comparable to the W/C = 0.55 mix. This should imply similar shrinkage characteristics provided that the compressive moduli of elasticity are similar.

The 7.5% silica fume mixes are depicted in Figure 4.4.4. They are finer than the paste series as expected, with the largest portion of pores clustered about 1000 angstroms.
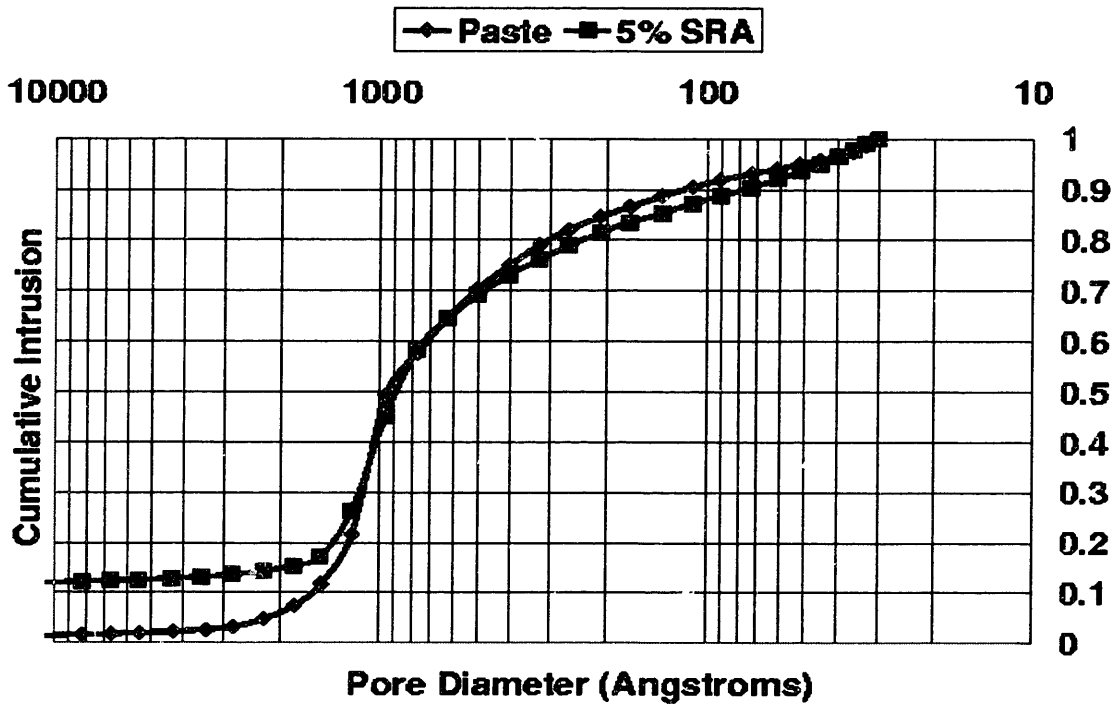
Figure 4.4.4 The normalized cumulative distribution of pores for the W/C = 0.55 silica fume admixed test series with and without the SRA.

Therefore these mixes should experience larger shrinkage strains than the associated paste mixes. This was verified with the shrinkage data from the drying shrinkage study. Note how the two curves almost lie one on top of the other for the finer pore sizes. This follows the same trend established for the higher water-to-cementitious material ratio above. However, like the reference paste mix, for the larger pores the SRA admixed test series is coarser. If a sample contains a moisture content in that range, it should experience much smaller shrinkage strains. This also was verified in the drying shrinkage study discussed above.

4.4.3 Intermediate Water-to-Cementitious Material Ratios

Figure 4.4.6 depicts the affect that the SRA has on the microstructure of the W/C = 0.45 paste and paste plus a 5% replacement by mixture water with the SRA test mixes. Similar
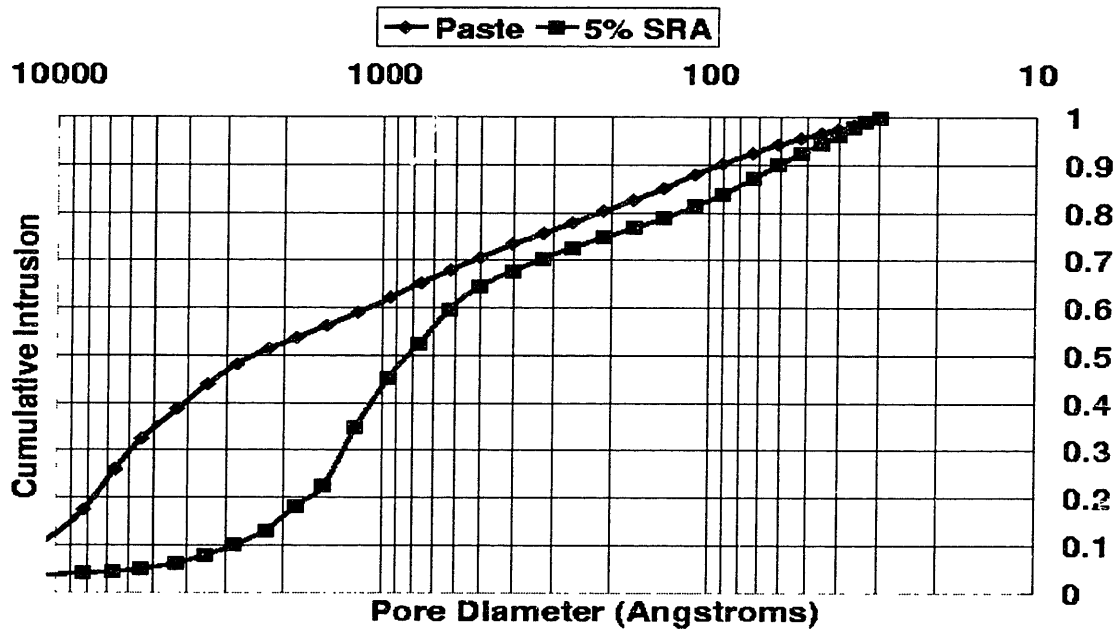
Figure 4.4.6 The normalized distribution of pores for the W/C = 0.45 paste mixes with and without the SRA.

to the W/C = 0.65 paste mixes, the paste mix is coarser than the SRA admixed mix. Again the behavior of reduced slope of the reference versus SRA admixed curve occurs. The SRA test series is clustered about approximately 1000 angstroms, while the paste mix is clustered about 3700 angstroms. These mixes should exhibit similar shrinkage strains as those experienced by the W/C = 0.55 paste plus a 7.5% replacement of cement with silica fume mixes. Here however there is a much larger spread of pore sizes so the effect is greatly determined by specimen moisture content. Also the effective distribution for the SRA mix will be closer spaced to the paste mix than for the W/C = 0.55 paste plus a 7.5% replacement of cement with silica fume mixes so the reductions in shrinkage should be less dramatic.

Figure 4.4.7 shows the behavior of the W/C = 0.45 test mixes with a 7.5% replacement of cement by silica fume with and without the SRA. As expected the pore structure is
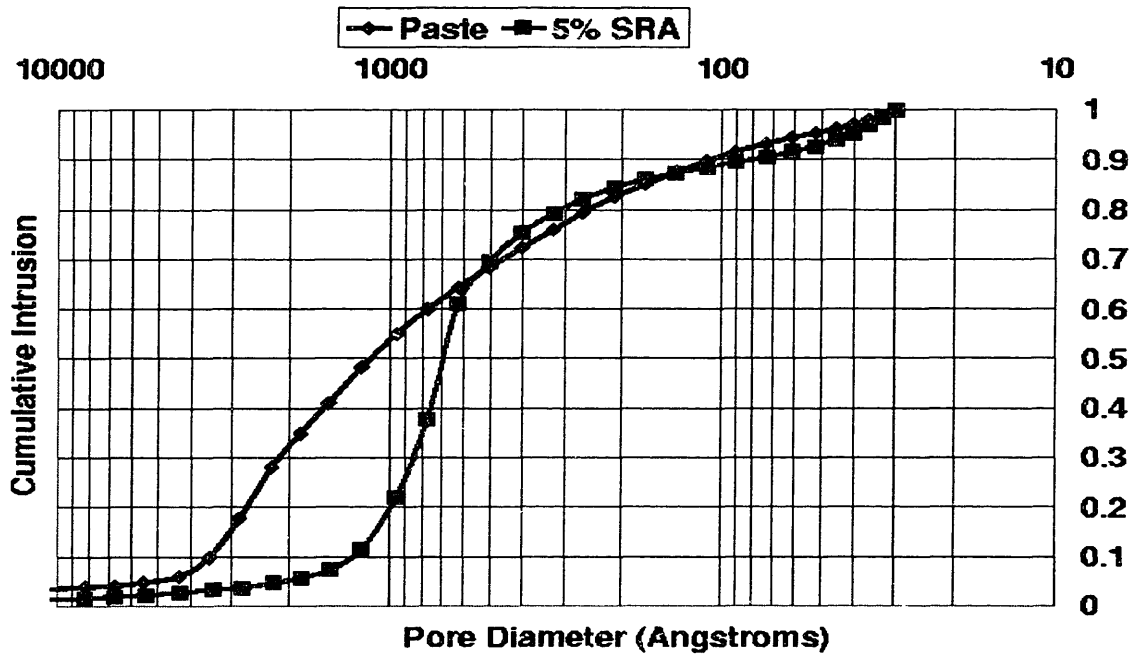
Figure 4.4.7 The normalized cumulative distribution of pores for the W/C = 0.45 paste plus 7.5% silica fume with and without the SRA mixes.

refined with a similar spread between the reference silica fume and SRA mixes. This pattern indicates that the reductions in drying shrinkage should be less than for the W/C = 0.55 mixes. Note the overlap in pore structure for pores smaller than 600 angstroms. This type of behavior is consistent with all the previous mixes. For the ultra-fine pores, at least those measurable with the MIP technique, there seems to be little difference between the two type of mixes.

Figure 4.4.8 shows the changes in pore structure caused by the addition of the SRA for the W/C = 0.35 paste mixes. The paste mix is coarser than the SRA admixed mix in the pore ranges which contribute most to drying shrinkage strains. When the "effective" distri-

bution is plotted one surmises that the effectiveness of the SRA will decrease. This behavior is verified with information obtained in the drying shrinkage study discussed above.
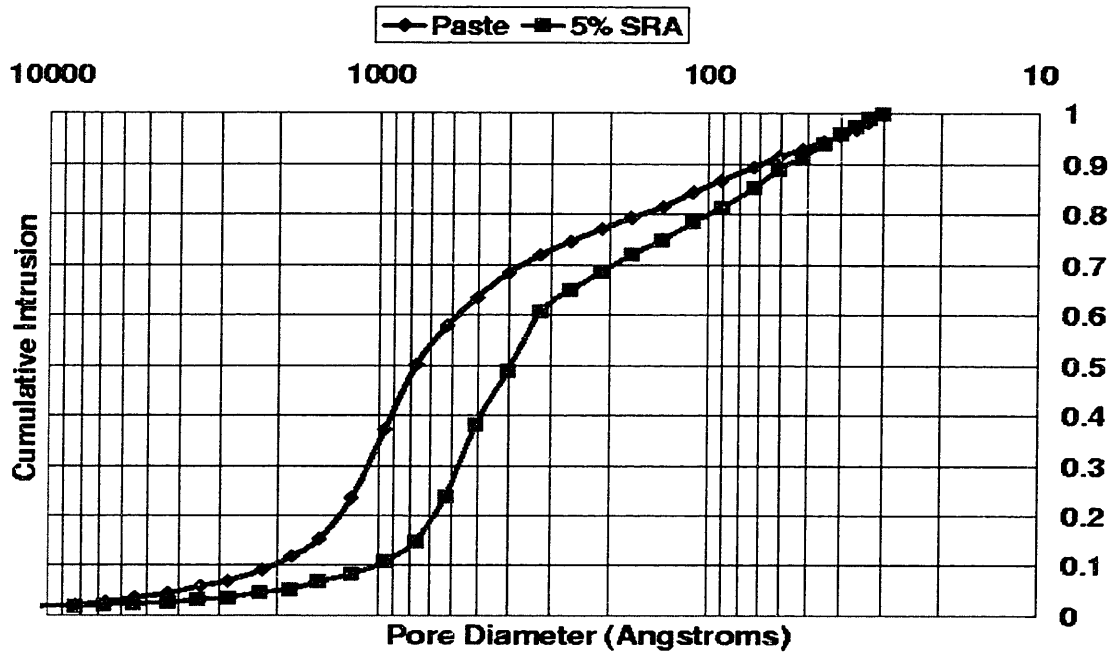
Figure 4.4.8 The normalized cumulative distribution of pores for the W/C = 0.35 paste mixes with and without the SRA.
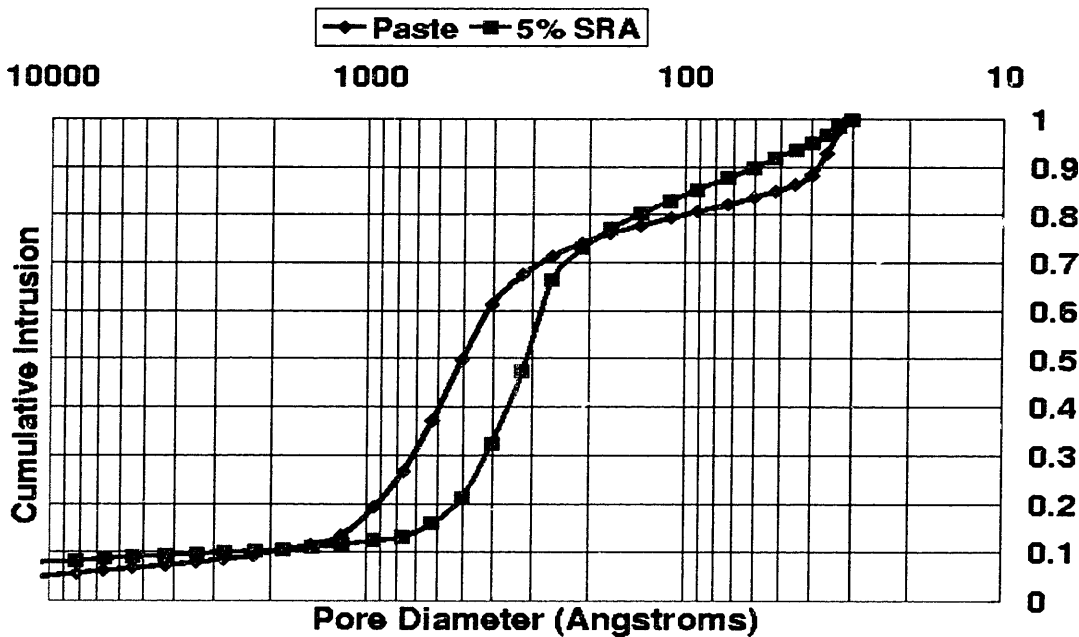
Figure 4.4.9 The normalized cumulative distribution of pores for the W/C = 0.35 silica fume mixes with and without the SRA.

100

Note the dramatic decrease in pore sizes for these mixes. The SRA mix is clustered about 500 angstroms while the paste is clustered about 900 angstroms. Again moisture content will play an important role in terms of the efficiency of the SRA.

Figure 4.4.9 depicts the affects on microstructure of adding the SRA to the silica fume mixes. As with the reference paste mix the reference silica fume mix is coarser than the SRA admixed mix. The points about which a large proportion of pores cluster for the two mixes are: 600 and 400 angstroms for the silica fume paste and silica fume SRA admixed mixes respectively. The trend of very little difference between the two types of mixes on pore structure for silica fume mixes has changed, in that there is a more pronounced difference between these two mixes. This indicates that depending on the moisture content in the matrix, different degrees on reduction are expected. Again this type of behavior was verified in the drying shrinkage study.

4.4.4 Low Water-to-Cementitious Ratios
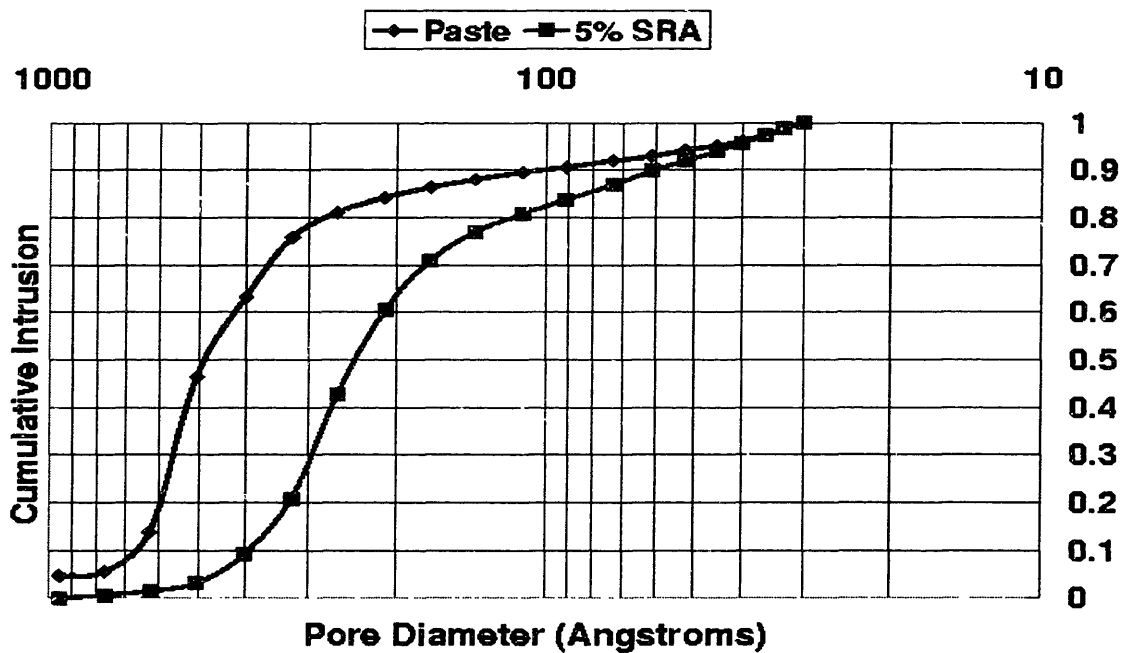
Figure 4.4.10 The normalized cumulative pore distributions of the W/C = 0.25 reference paste and 5% SRA admixed mixes.

The final test series consisted of paste and silica fume mixes with and without the SRA at a W/C = 0.25. These mixes contain very fine pores. Figure 4.4.10 depicts the affects that the SRA has on the pore structure of the paste mixes. Again the reference paste mix microstructure is coarser than the SRA admixed test series. The pore sizes about which the

101

respective mixes cluster are: 500 angstroms and 270 angstroms. These pore sizes exert the largest potentials for drying shrinkage of any discussed yet. So we expect the associated shrinkage behavior to be large. This is verified with results from the drying shrinkage study. The improvement in drying shrinkage should be fairly low at this low water-to-cementitious ratio since the relative shift of the curve barely clears the reference paste curve.

Figure 4.4.11on the other hand again demonstrates that for the silica fume admixed
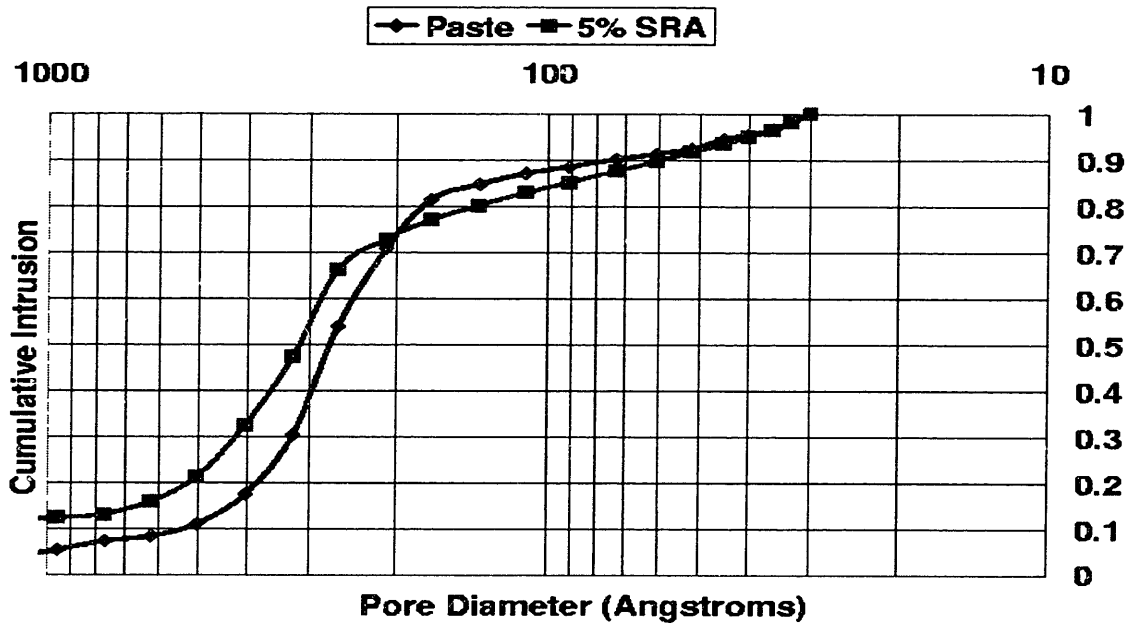
Figure 4.4.11 The normalized cumulative distribution of pores for the W/C = 0.25 silica fume mixes with and without the SRA.

testing series there is little difference between the two types of mixes. The pore structure is refined as expected. Unlike the reference paste mix, the SRA causes a coarser microstructure to develop. So it is expected that there will be significant reductions in drying shrinkage strains experienced between the two mixes. This behavior does occur in the drying shrinkage specimens tested.

4.5 Moisture Profile Study

4.5.1 Introduction

As described earlier in the experimental methodology section, it is important to under-

stand how moisture leaves a slab system due to evaporation, capillary suction, and/or diffusion. As the top surface dries at an increased rate compared to the insulated bottom surface, the internal moisture distributes itself in a very non-uniform manner. The difference in moisture content then results in a variation in strain causing the curling deformation. This is a very size dependent phenomena, because internal movement of water is governed by diffusion. The larger the specimen the longer it takes to move to the surface. Therefore, there are uneven layers of hydration products which may affect the bulk behavior of the system. In order to understand curling, it is important to describe the shape and change in shape of the moisture profile with time. This section presents the results obtained from the application of the electrochemical impedance spectroscopy technique to three different mix designs at three different surface to volume ratios.

4.5.2 EIS Background

This is a quick review of the key concepts described in the experimental methodology section pertaining to the use of the EIS techniques to determine moisture content as a function of depth in cement slabs. When the neat cement specimens are first mixed, the constituents are in a water-colloidal suspension and the electrochemical response is best represented as a di-electric electrolyte dispersed between the two electrodes. The sample is considered fully saturated. An equivalent circuit model of this system would best be represented by a series of resistors and the high frequency response depicted in a Nyquist plot is not semi-circular in shape. As the hydration reactions proceed and the water is consumed, the microstructure starts to develop interfaces between the hydration products and the unhydrated cement. Water is also lost after initial curing due to evaporation and subsequent drying. Therefore, the once fully saturated material develops a porous network and becomes unsaturated as drying proceeds.

There are three types of water present in the porous network: chemically adsorbed, physically adsorbed, and free water. Depending on the pore size distribution of the specimen, each type of water will affect the determination of the moisture content of the sample [Gu et al., 1986]. The two competing sources of moisture loss in the material are hydration and drying. For the purposes of this study, drying is the primary source addressed. For the higher water-to-cementitious ratios, full hydration, i.e. greater than 80%, may take up to a month to occur. However, the lower water-to-cementitous ratios achieve the same level of

hydration as soon as 2-7 days and hence the majority of moisture loss is associated with drying.

Terrill et al., conducted a study on ascertaining the moisture profile of rectangular specimens using crack initiators and relative humidity probes, and determined that the relative humidity probes are unable to accurately ascertain changes in moisture content in gel pores and may be only applicable to meso-to-macro porous systems [Terrill et al., 1986]. The advantage of using a.c. electrochemical measurement techniques is the fact that these types of measurements are very sensitive to moisture content in any of the available forms/types.

A small perturbing a.c. signal is applied across the set of electrodes and the salt ions in solution in the porous network respond by fluctuating in response to the field until they reach their relaxation time which is the time to required to fluctuate in phase with the applied field at the given frequency. The relaxation time is dependent on the source of water responding, i.e., free water has the fastest response while chemically adsorbed water has the slowest response. As described earlier, the spread in relaxation times of the material is depicted in the Nyquist plot as a depression of the semi-circle below the real component of the impedance.

Since the real component of the impedance is composed of the resistance's of elements in the porous network and the electrolytic material, the phase angle of these components are small near $0°$. Therefore for the fully saturated case, in the earliest times after mixing, there is no formation of a high frequency arc [Gu et al., 1986]. Later as pores start to empty and interfaces start to develop the high frequency response evolves. When a pore is completely empty of water it acts as a leaky capacitor and maintains a phase angle close to $-90°$. Therefore by plotting phase angle as a function of depth for the profile specimens one is able to ascertain a qualitative moisture profile.

Several preliminary tests were conducted on paste and SRA admixed specimens to determine what the optimum frequency is for choosing phase angle as a descriptor for moisture content. These tests were conducted both on the cylindrical specimens as well as the platelet specimens described in the drying shrinkage study. The characteristic range for obtaining information about bulk paste properties for all mixes tested lay between 10^4

and 10^7 Hz. The best suited frequency was 10^6 Hz, and hence all data presented in the upcoming sections are measured at this frequency.

4.5.3 One-half inch moisture profile EIS specimens
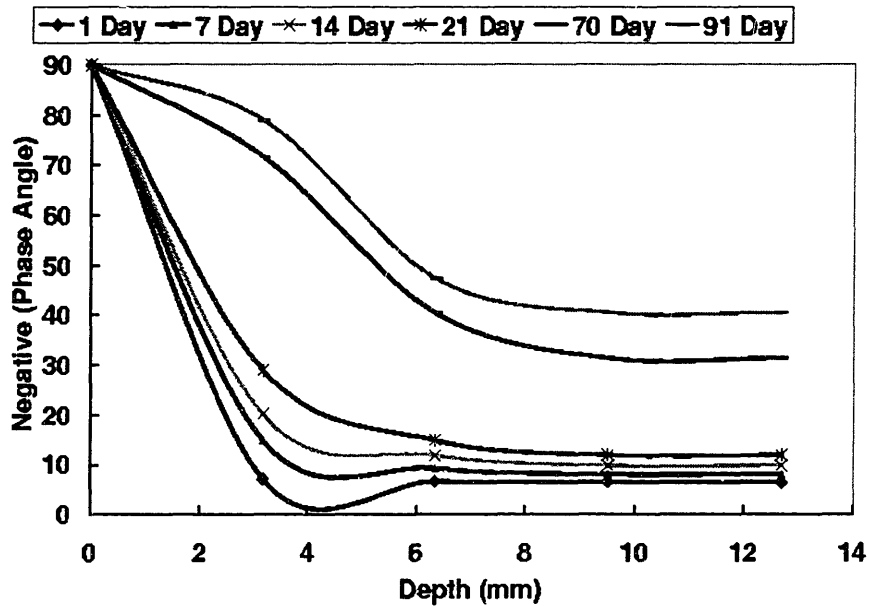
Figure 4.5.1. Measured moisture profiles of paste and admixed one-half inch
W/C = 0.45 SRA admixed specimens.

Figure 4.5.1 depicts the profiles of the W/C = 0.45 with 5% SRA one-half inch specimen at various ages.The data points have been fitted using a higher order polynomial. The datum, zero, occurs at the top surface of the specimen which is exposed to the ambient 50% RH environment. The first point is artificially set to -90° corresponding to a fully dry condition. As expected the shape of the curve steadily shifts towards higher negative phase angles as time proceeds indicating that drying is occurring.

At early ages there is a large gradient in the measured phase angle. The magnitude of the gradient decreases with time as expected, because most of the material reaches its equilibrium moisture content. Nevertheless, there is still a gradient present at 91 days which implies that there should still be some curling deformation present. This is substantiated with the experimental results obtained in the curling deformation study.

Figure 4.5.2 depicts the changes in profiles of the one-half inch paste specimens. Note that the magnitudes of the phase angles are higher at all testing stations for the SRA admixed specimens. This is consistent with the mass loss data obtained in the drying

shrinkage study. The SRA mixes consistently lose more water than the reference mixes, and hence the measured di-electric properties should be higher. Despite the difference in
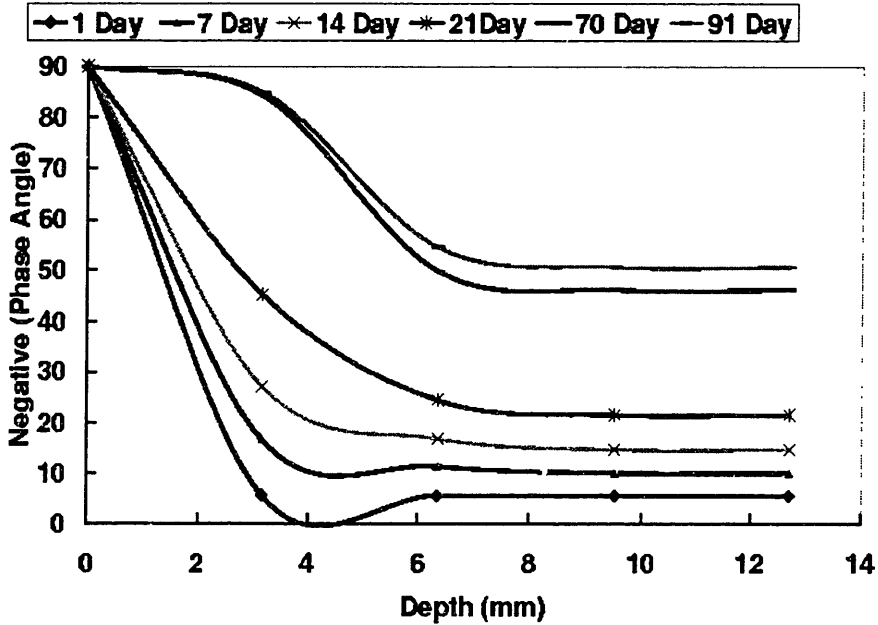
Figure 4.5.2. Measured moisture profiles of W/C = 0.45 paste specimens.

magnitudes, the shapes of the curves are also different. There is a slower change in the moisture profile as a function of time. Note how much more uniform the moisture content is through the thickness of the material (the negative of the phase angle is taken as a descriptor of moisture content, and hence the moisture profiles are only qualitative) for the SRA admixed series. Since a larger portion of the material is maintained at a constant moisture content, it serves as a restraint thereby reducing curling deformations. This is indeed the behavior exhibited by the curling specimens.

Figure 4.5.3 depicts the behavior exhibited by the W/C = 0.55 SRA admixed specimen. The slope of the curve initially is greater than the corresponding W/C = 0.45 SRA admixed mix. This is expected because the microstructure is coarser and so there is more moisture lost for the higher water-to-cement ratio mix. The uniformity after the first station remains. The overall shapes remain similar with greater disparity at later ages. It is interesting to note that the magnitudes of the phase angles are similar for both mixes at later ages, with smaller phase angles for the higher water-to-cement ratio mix. This seems contrary to the expected results, but because the microstructure is different, i.e. coarser, the measured resistive and capacitive responses change. That is, not only is the pore solu-

tion different but the distance between capacitive plates is greater. This implies that the method can only be used to compare mixes of similar design with changes only in the addition of the SRA.
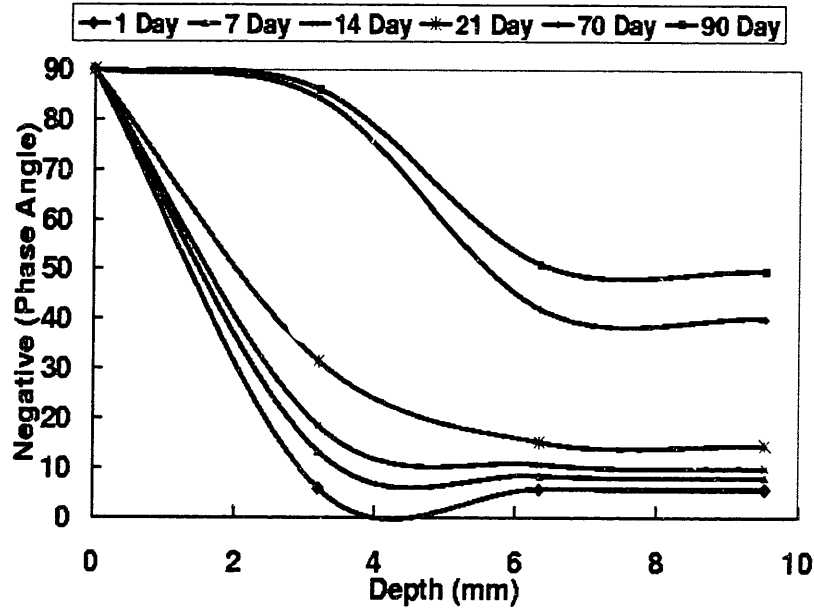
Figure 4.5.3. Measured moisture profiles of the W/C = 0.55 SRA one-half inch EIS specimens.

Figure 4.5.4 shows how the phase angle changes with time for the associated reference W/C = 0.55 paste mix. There is a greater difference in shape between this mix design and
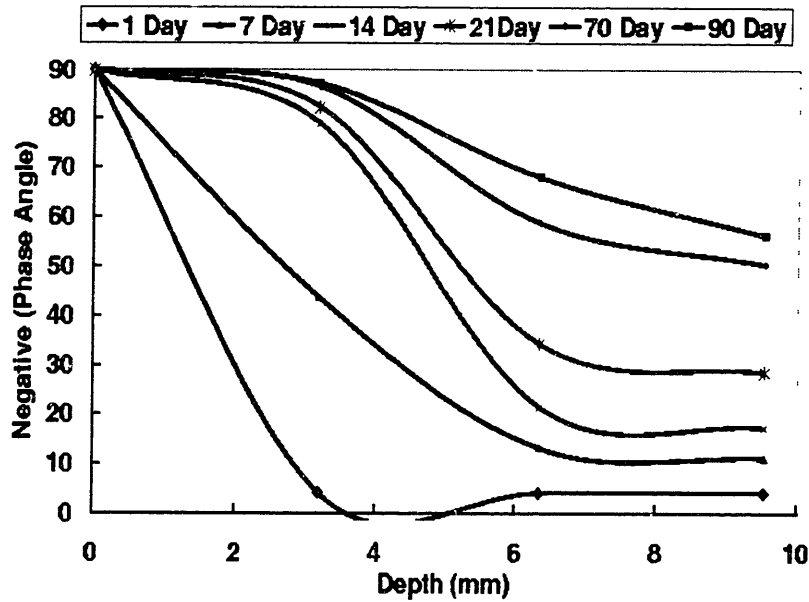
Figure 4.5.4 The measured moisture profile for the W/C = 0.55 reference one-half inch paste EIS specimen.

the SRA mix design at the same water-to-cement ratio then for the W/C = 0.45 mixes. Another interesting trend in the data is that the magnitudes of the phase angles are greater for the paste mix then for the SRA mix. There is still much larger gradients through the full thickness of the specimen. This implies that this mix should experience greater curling deformations. Again this observation is substantiated with the results from the curling deformation study. From the microstructural analysis we know that the difference in pore structure measured, i.e. paste finer than SRA admixed mix, is opposite to that experienced by the W/C = 0.45 mixes. This may explain why the paste mix is know showing higher phase angle magnitudes then the SRA mix. Further work is required to fully explain this behavior.

The finest pore structure mixes, W/C = 0.45 with the addition of 7.5% silica fume with and without the SRA are expected to demonstrate similar behavior as the W/C = 0.45 mixes based upon the microstructural analysis. Figure 4.5.5 shows the SRA admixed
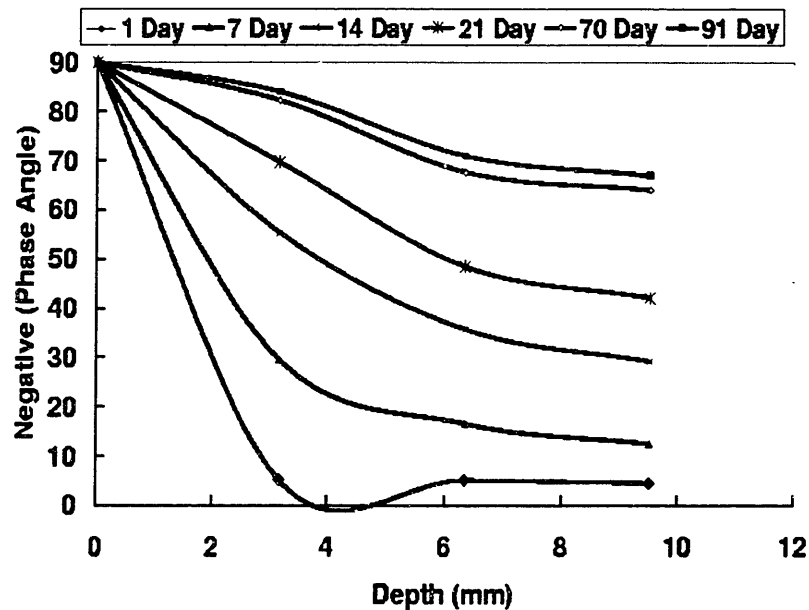
Figure 4.5.5 The measured EIS response of the W/C = 0.45 with a 7.5% silica fume and 5% SRA addition.

response. There is a very large gradient in the curve for early ages, progressively decreasing at later ages. There is little difference between the 70 and 91 day response. At these ages there is a small gradient present which should correspond to reduced curling tendencies. The measured center line deflections of this mix at these two ages substantiate this behavior.

Figure 4.5.6 depicts the change in EIS response for the reference paste mix. As expected the magnitudes of the phase angles for the paste mix are smaller than the associated SRA measured response. This supports the notion that whether the SRA admixed mix produces a coarser or finer microstructure will affect the magnitude of the phase angle measured. The gradient in phase angle is greater for the paste mix, indicating that the measured curling deformations should be larger. This is substantiated with data from the curling study.
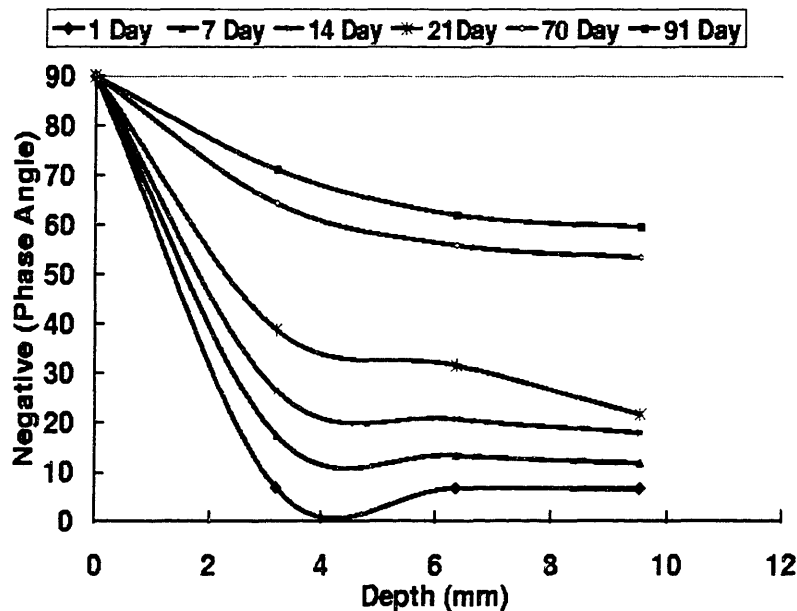
Figure 4.5.6 The measured EIS response for the W/C = 0.45 with a 7.5% silica fume addition.

In summary, the response of each test mix correlates well with the measured curling behavior. Since these mixes have the smallest exposed surface area to volume ratios, it is expected that they will experience the most changes in di-electric properties in the time frame of the test.

4.5.4 One inch moisture profile EIS specimens

For this set of specimens, only the W/C = 0.45 mix is presented because the same trends established for the one-half inch specimens also occur with all the one inch specimens. What is interesting is the change in magnitudes of the measured phase angles. Figures 4.5.7 and 4.5.8 depict the change in measured phase angle with time for the W/C = 0.45 test mixes with and without the addition of the 5% SRA. Again the shape of the curves are very similar with the reference specimen exhibiting a steeper gradient at the later ages.

The 70 and 91 day curves show that the SRA specimen maintains a uniform moisture profile, while the reference specimen has an almost linear gradient through most of its thickness and a higher gradient between the first station and the top surface.
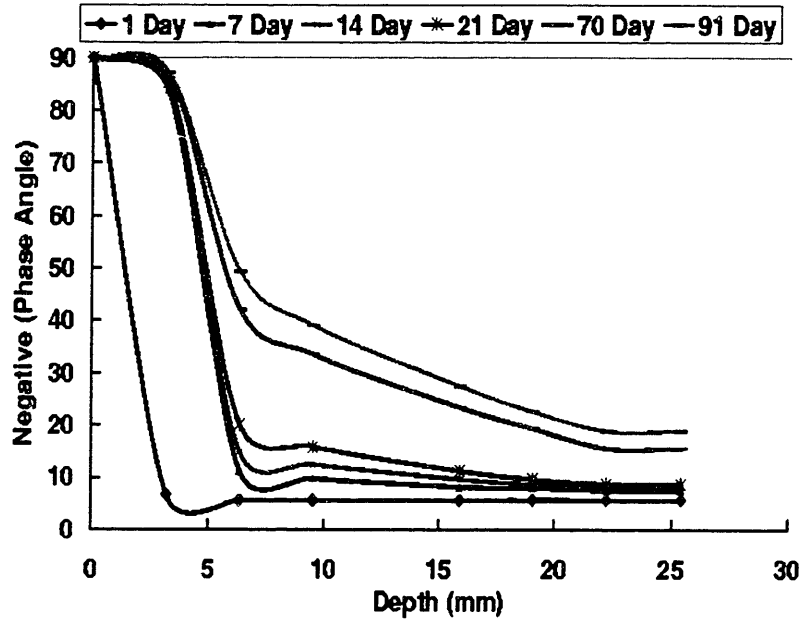
Figure 4.5.7 The measured changes in phase angle with time for the W/C = 0.45 reference one inch EIS specimen.
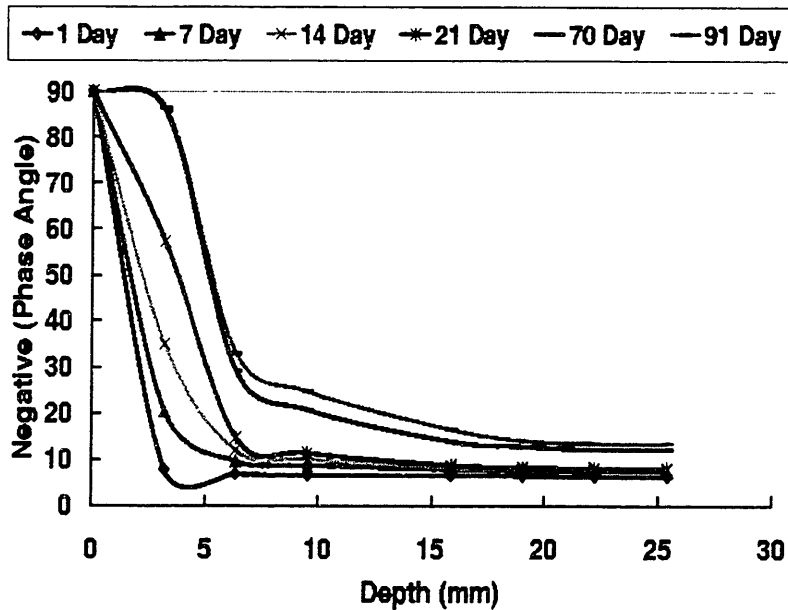
Figure 4.5.8 The measured changes in phase angle with time for the W/C = 0.45 SRA admixed one inch EIS specimen.

This implies that the tendency to curl is larger for the reference mix than for the SRA mix which is substantiated with the trends in curling data presented earlier for the one-half inch specimens. These test were conducted after the curling tests, and so later age infor-

mation is not available yet. What is required is the correlation between moisture content at a given level and the measured EIS response in order to quantitatively assign moisture values in the specimen using this technique. Theses tests are ongoing and will be reported elsewhere. Since the relative difference in phase angle magnitudes through the thickness of the samples for the one-half inch and the one inch specimens are fairly large, one must expect that the curling behavior of thicker specimens will take longer to fully develop. If, as presented in the curling deformation study, there is a tendency for the reference mixes to relax due to creep then the measured reductions are expected to decrease.

4.5.5 Two inch moisture profile EIS specimens

Following similar trends as established earlier for the one-half inch and one inch specimens, only the W/C = 0.45 specimen responses will be presented as representative behavior for the two inch specimens. The three different thicknesses were tested to obtain information on size effect problems. One problem mentioned in the mechanical property section of the thesis is that without any restraining inclusions in the paste matrix, there is a greater tendency to crack for larger specimens than smaller specimens. This will of course affect the way that moisture leaves the system, i.e. a change from diffusional flow to capillary suction. Also, if the change encountered is small, then the rate of flow out of the system is expected to be dramatically lower the smaller the exposed surface area to volume ratio. This is due to the increased internal reservoir of moisture.

Figures 4.5.9 and 4.5.10 depict the changes in measured phase angle experienced by the two inch EIS specimens as a function of time. The same trends, reference paste exhibiting higher phase angles than the SRA for the W/C = 0.45 and 0.45 with a 7.5% addition of silica fume occur. The W/C = 0.55 trend is still opposite to the other two mixes. The greater uniformity in the moisture content for the SRA mixes should cause a larger portion of the slab thickness to resist curling deformations and hence produce smaller measured center line deflections. This type of behavior is exhibited in the one-half inch specimens. Several tests have been initiated varying the thickness of the cement slab for particular

111

mixes and will be presented elsewhere. Initial data does support the hypothesis that larger

thickness samples take longer to curl than thinner specimens [Dallaire et al., 1997].
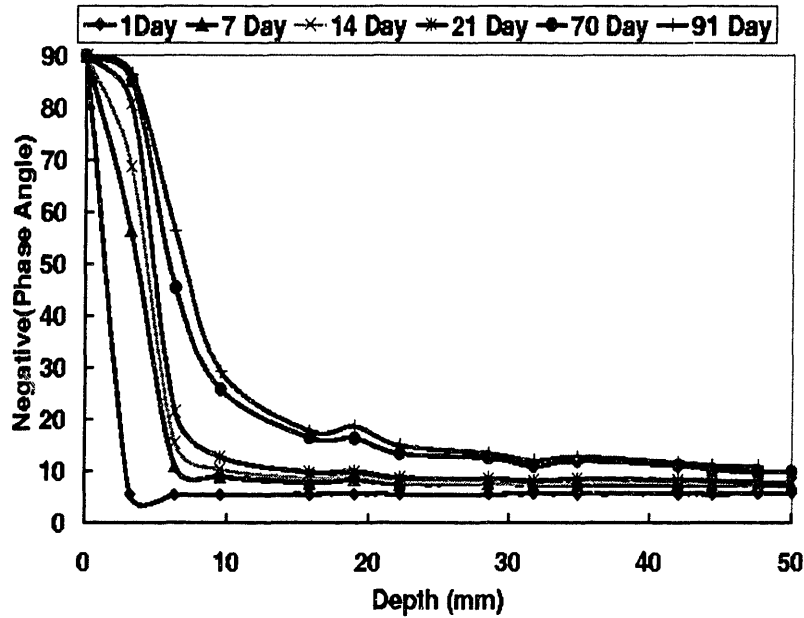
Figure 4.5.9 The measured changes in phase angle with maturity for the W/C = 0.45 two inch reference paste specimen.
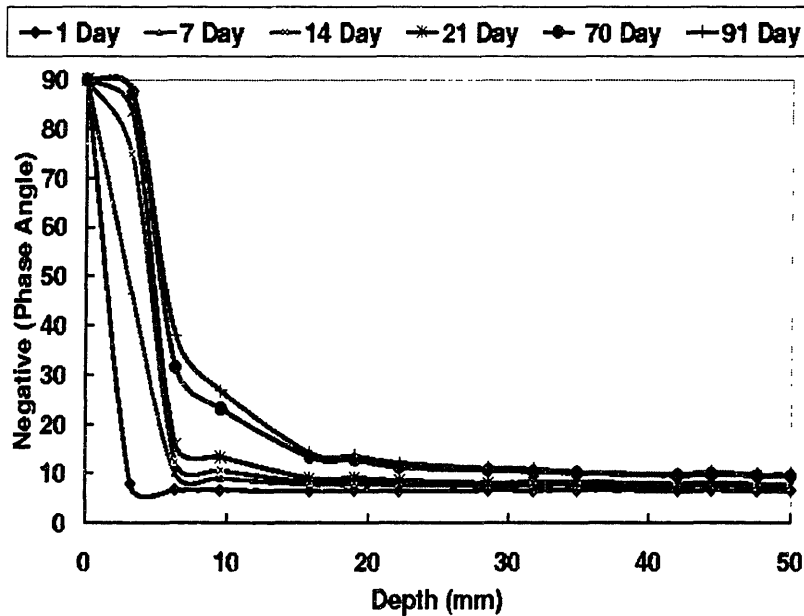
Figure 4.5.10 The measured changes in phase angle with maturity for the W/C = 0.45 two inch SRA specimen.

The mass loss information obtained for these specimens substantiate that the higher

the exposed surface area to volume ratio the greater the mass loss. Figure 4.5.11 depicts

this type of behavior. This type of behavior was followed by all the test mixes tested.

Notice that the slopes of the mass loss curve for the one inch and the two inch reference past specimens have not leveled off. That is because there is still plenty of moisture in both systems. The one-half inch specimen however, has leveled off and is near equilibrium. Similar behavior is exhibited by the SRA mixes. Chapter 5 will discuss this behavior in greater detail.
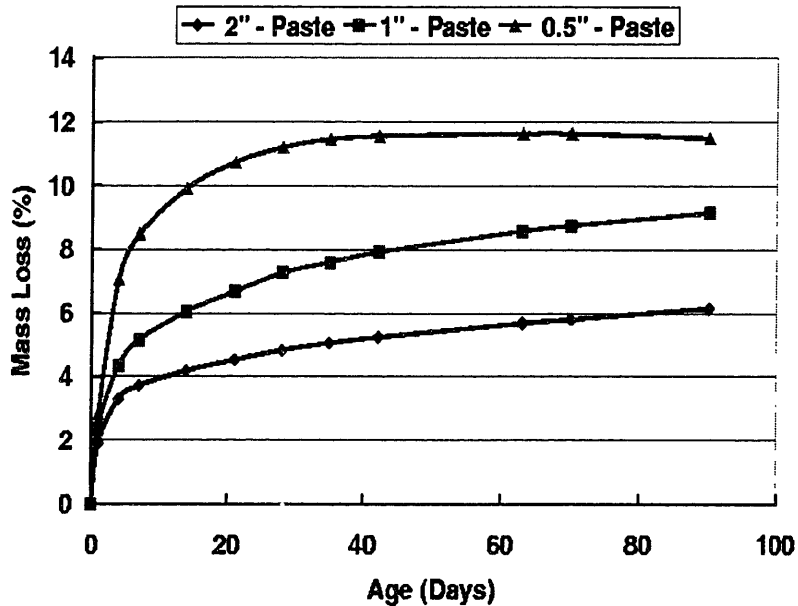
Figure 4.5.11 The mass loss behavior of the EIS moisture profile samples, W/C = 0.45.

4.5.6 Cylindrical EIS Specimens

'There were some problems encountered with these specimens in the lower relative humidity environments. Shrinkage cracking occurred at ages greater than 28 - 35 days which dramatically altered the response of the specimens. Therefore the discussion of these results will not be presented. There was to much scatter in the data and hence a new set of specimens need to be tested. The purpose of these specimens were to correlate moisture content at a given environmental condition with the measured EIS response.

It was decided that sectional analysis would provide more accurate information for slab specimens because the same mold shapes could be used. Sectional analysis is the splitting of specimens of a given thickness at a preset age and measuring the change in moisture content as a function of depth. Final moisture content is determined by baking specimens at an elevated temperature for a short period of time and measuring the final

mass loss. These types of tests are currently being conducted, but will not be presented in this report. Therefore the results obtained using the EIS technique provide only a qualitative measure of moisture.

4.6 Summary

The results presented in this section of the thesis provide the necessary background empirical data with which to correlate findings determined from the analytical and computational model to be discussed in Chapter 5. There are benefits in using the SRA to reduce not only drying shrinkage strains at low relative humidity environments but also curling deformations in cement slabs. In particular, the drying shrinkage strains are reduced between 30 - 46% depending on the mix design. Typical magnitudes of reductions in curling deformations exceed that amount and hence lead to the concept of an additional mechanism occurring simultaneously with the reductions in drying shrinkage at a given moisture content. Based upon the results obtained using the electrochemical impedance technique, the second mechanism is a change in the shape of the moisture profile. The addition of the shrinkage reducing admixture produces a more uniform moisture profile through time. The greater the uniformity, the greater the reductions in curling behavior expected. This has been substantiated with the one-half inch curling specimens.

The newly developed testing technique to determine moisture content as a function of depth and time still requires additional tests to correlate change in phase angle with moisture content. These tests are currently being conducted, but will not be presented in this report. Due to the exaggerated behavior of both drying shrinkage and curling for paste, it is expected that reduced effects will occur in mortar and concrete. This is an area of research that needs to be studied applying the same basic testing procedures established in this study. These types of tests are currently being conducted but will not be presented in this report.

Chapter 5

Analytical Modeling

5.1 Introduction

This section of the thesis presents the required analytical developments of moisture movement and drying shrinkage and relates this information to the curling deformation problem. Again, curling in cement slabs occurs due to the formation of a non-uniform moisture profile. The non-uniform moisture profile develops due to differences in drying rates between the exposed upper surface of the slab and the insulated bottom surface as depicted in Figure 5.1.1. Cement paste shrinks in drying environments, so the non-uniform mois-

Evaporation from the top surface of the slab
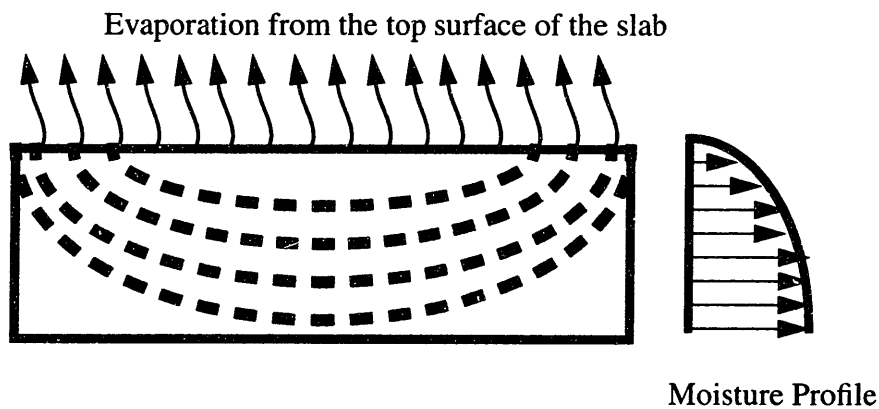
Moisture Profile

Figure 5.1.1 Changes in moisture content through slab thickness due to uneven drying rates between top and bottom surfaces of slabs.

ture profile results in differential shrinkage strains through the slab thickness. Unrestrained slabs experience curling deformations, and restrained slabs experience high tensile stresses and may crack extensively. The cracks reduce the serviceability of the structure.

The purpose of the experimental section of the thesis was to develop in an evolutionary fashion a set of data capable of explaining some of the fundamental mechanisms occurring. The use of a newly developed shrinkage reducing admixture was also tested and changes in the drying shrinkage, the moisture profile, and curling behavior were observed.

115

This information is now used to help develop a computational model. Earlier research initiatives which tried to explain changes in the curling phenomena are presented and used.

5.2 Drying Shrinkage

5.2.1 Introduction

This portion of the analytical section provides the necessary theoretical development explaining how the SRA affects drying shrinkage. The environmental conditions of interest are those that lie between 40% - 100% RH, above freezing temperatures. In this range of relative humidity environments capillary tension theory applies. Therefore, this is the main mechanism used to describe changes in the drying shrinkage behavior of specimens with the SRA.

As described earlier in the literature review section of this report, capillary tension theory has been used by many researchers in the past to describe how changes in mix design, such as cement and water content, affect drying shrinkage. The key equations applied are the Kelvin equation and the Laplace equation which describe the relations of moisture content, surface tension and pore radii, with the compressive elastic stresses developed in the paste matrix. Coupled with these equations are moisture transport laws. Size effect is a considerable problem which needs to be addressed. By combining these different aspects of this complex problem, one is able to develop a rational theory to describe drying shrinkage. What follows is the development of this theory.

Drying shrinkage as described by Neville is due to the movement of moisture from a paste sample [Neville 1996]. The types of moisture loss from the system include: internal hydration, evaporation at surfaces, capillary suction, and internal diffusion. Of the mentioned types, internal diffusion governs for large samples, and at later ages. Hydration may cause problems in systems prior to setting in the form of plastic shrinkage and thermal cracking. With sufficient care when casting, these problems are easily overcome by changing curing times, methods, and temperatures. Therefore it plays a small role in the drying shrinkage process. The rates of evaporation from the exposed surfaces are important in

determining how the system interacts with the ambient environment and should be considered. Capillary suction may be important for very coarse sized pore structures, but play a lesser role for high strength pastes and lower water-to-cementitious material ratio mixes. For concrete systems where bleed channels develop between particle inclusions and the bulk matrix, capillary suction may prove to be important, but because the system analyzed is neat cement paste devoid of entrained air, this mechanism is not included. Neat paste mixes after sufficient hydration do not have interconnected pores of sufficient size to warrant the use of capillary suction. Instead the movement of water in these systems is through vapor diffusion. So the governing mechanism associated with moisture movement in paste at later ages is diffusional flow.

5.2.2 Moisture Transfer in Cementitious Slabs

Diffusional flow is dependent on the diffusivity of the material, which may be constant or concentration dependent. This type of flow may occur either in a steady state manner, or under transient conditions. Transient conditions are often characterized by changes in concentration of the liquid of interest in both position and time. The basic equations used to describe simple diffusional flow derive from the work of Fick in 1855. The first equation is called Fick's law of diffusional flow which mimics the flow of heat. It states that the rate of transfer of a liquid through a unit area of an isotropic section is proportional to the concentration gradient measured normal to the surface [Sih et al. 1986, Vergnaud 1992]:

$$f = -D\frac{\partial C}{\partial x} \tag{5.1}$$

where f is the rate of transfer per unit area of section or flux, C is the concentration of the diffusing liquid, x is the spacial position measured normal to the section surface, and D is the diffusivity of the material.

There are two types of evaporation of interest in the modeling of drying systems, a finite rate of evaporation and an infinite rate of evaporation. A finite rate of evaporation from the surface of a material is proportional to the difference between the actual concentration at the surface and the concentration which is in equilibrium with ambient conditions remote from the surface [Scherer 1992, Sih et al 1986, Vergnaud 1992]. The proportionality coefficient is given by the rate of evaporation of a pure liquid exposed to the same conditions. This is typically written:

$$E = E_o(C_s - C_{amb}) \tag{5.2}$$

where E is the finite evaporation rate, E_o is the rate of evaporation of a pure liquid, C_s represents the surface concentration, and finally C_{amb} represents the remote ambient concentration. For processes where the evaporation rate is dependent on diffusion, one can combine equations (5.1) and (5.2) to obtain:

$$-D\left(\frac{\partial C}{\partial x}\right)_s = E_o(C_s - C_{amb}). \tag{5.3}$$

From this expression one observes that the rate of evaporation from the surface increases with the rate of evaporation of the pure liquid. The dependence on temperature for the rate of evaporation is introduced using the well known Clausius-Clapeyron equation [Vergnaud 1992]:

$$\ln\left(\frac{E_{T1}}{E_{T2}}\right) = -\frac{\Delta H_v}{R}\left(\frac{1}{T1} - \frac{1}{T2}\right) \tag{5.4 a}$$

where E_{T1} and E_{T2} are the rates of evaporation of the pure liquid at temperatures T1 and T2, R is the ideal gas constant, and ΔH_v is the enthalpy of vaporization of the pure liquid. The other typical equation used to describe the dependence of moisture transfer on temperature is the Arrhenius relation [Sih et al. 1986]:

$$D = D_o \exp\left(-\frac{E_d}{RT}\right). \tag{5.4 b}$$

where D is the diffusivity of the material, D_o is the proportionality constant, E_d is the activation energy, R is the universal gas constant, and finally T is the temperature measured in the Kelvin scale.

For infinite rates of evaporation, the exposed surfaces of the solid reach equilibrium with the surrounding atmosphere immediately. Typically strong convective currents and a much larger ambient environment volume than material volume is required. This type of evaporation is usually characterized as a boundary condition in the form:

$$C_s = 0. \tag{5.5}$$

Either type of evaporation mechanism strongly influences the ease of calculating system response to different drying conditions. From an analytical standpoint equation (5.5) is the simplest type of boundary condition to address.

For cement slabs, the assumption required to begin a simplified analysis is that the slab is a thin isotropic plate which is subjected to different initial and boundary conditions. The analysis of drying shrinkage conducted in this report follows the assumptions stated by

Pickett in 1946, namely that the functional form of drying shrinkage is related to moisture loss, and hence a detailed description of several classic drying initial and boundary conditions are presented. Then due to the similarities of the problem statements, the shrinkage problem will be answered after new descriptions of certain parameters and their dimensions are defined.

5.2.3 Transient Constant Diffusivity Analyses with an Infinite Rate of Evaporation

The simplest case to begin with is the analysis of the constant diffusivity non-steady state with infinite evaporation scenario. The equation for diffusion in one dimension with a constant diffusivity follows Fick's second law [Powers 1987, Sih et al. 1986, Vergnaud 1992]:

$$\frac{\partial C}{\partial t} = D\frac{\partial^2 C}{\partial x^2} \tag{5.6}$$

with initial conditions: $\quad t = 0, 0 < x < L, C = C_{in}$ (slab)

and boundary conditions: $\quad x = 0, x = L, C = 0$ (exposed surfaces).

The slab is initially at a uniform concentration C_{in}, and because there is infinite evaporation at the two exposed faces the concentration there is zero. For a perfectly insulated slab on a single side with one exposed surface at the opposite side, the analysis is similar due to symmetry. Half the double exposed slab gives the appropriate solution. A solution to the partial differential equation given above is easily determined by assuming that the solution is separable in space and time respectively.

$$C_{x,t} = C_x C_t \tag{5.7}$$

substituting this expression into equation (5.6) yields:

$$\frac{1}{C_t}\frac{\partial C_t}{\partial t} = \frac{D}{C_x}\frac{\partial^2 C_x}{\partial x^2}. \tag{5.8}$$

Notice that the expression on either the left or right hand side are solely dependent on a single variable, t or x respectively, and are therefore equal to a constant which we shall conveniently choose as $-\lambda^2 D$. The problem has been simplified to two differential equations:

$$\frac{1}{C_t}\frac{\partial C_t}{\partial t} = -\lambda^2 D, \frac{D}{C_x}\frac{\partial^2 C_x}{\partial x^2} = -\lambda^2 D. \tag{5.9}$$

The solutions for these two differential equations are:

$$C_t = \exp(-\lambda^2 Dt) + Ct \tag{5.10}$$

and $\quad\quad\quad C_x = A\sin(\lambda x) + B\cos(\lambda x) \tag{5.11}$

which therefore leads to the solution:

$$C_{x,t} = (A\sin(\lambda x) + B\cos(\lambda x))\exp(-\lambda^2 Dt) \qquad (5.12)$$

where A and B are constants of integration. The most general solution is obtained in a trigonometric series format:

$$C_{x,t} = \sum_{n=1}^{\infty} ((A_n\sin(\lambda_n x) + B_n\cos(\lambda_n x))\exp(-\lambda_n^2 Dt)). \qquad (5.13)$$

The assumption that the liquid in the slab is initially uniformly distributed and that the surfaces are kept at zero concentration are defined by the initial and boundary conditions given above. The general equation (5.13) has constants A_n, B_n, and λ_n which may be determined using the boundary and initial conditions. To begin, applying the boundary condition $C = 0$ for $x = 0$ leaves $B_n = 0$, while the condition $C = 0$ at $x = L$ leaves $\lambda_n = \frac{n\pi}{L}$. The initial condition becomes:

$$C_{in} = \sum_{1}^{\infty} A_n\sin\left(\frac{n\pi x}{L}\right) \qquad (5.14)$$

in the region defined between $0 < x < L$. Using the orthogonality relations from Fourier analysis, equation (5.14) is multiplied by $\sin\left(\frac{n\pi x}{L}\right)$ and integrated from 0 to L. Recalling that:

$$\int_0^L \sin\left(\frac{p\pi x}{L}\right)\sin\left(\frac{n\pi x}{L}\right)dx = \begin{cases} 0 \\ \left(\frac{L}{2}\right) \end{cases} \qquad (5.15)$$

when $p \neq n$ and when $p = n$ respectively.

The equation now has the form:

$$C_{in}\int_0^L \sin\left(\frac{n\pi x}{L}\right)dx = A_p\int_0^L \sin\left(\frac{p\pi x}{L}\right)\sin\left(\frac{n\pi x}{L}\right)dx + A_n\int_0^L\left(\sin\left(\frac{n\pi x}{L}\right)\right)^2 dx \qquad (5.16)$$

A useful relation that will provide an answer in a better format is given by [Vergnaud 1992]:

$$2\sin\left(\frac{p\pi x}{L}\right)\sin\left(\frac{n\pi x}{L}\right) = \cos\left(\frac{(n-p)\pi x}{L}\right) - \cos\left(\frac{(n+p)\pi x}{L}\right). \qquad (5.17)$$

Applying this to equation (5.16) and reducing one obtains the following:

$$\left[-\frac{C_{in}L}{n\pi}\cos\left(\frac{n\pi x}{L}\right)\right]_0^L = \frac{C_{in}L}{n\pi}[1-(-1)^n] = \frac{A_n L}{2}. \qquad (5.18)$$

Note that all terms where n is even equal zero, and where n is odd A_n becomes:

$$A_n = \frac{4C_{in}}{(2n+1)\pi}. \qquad (5.19)$$

Therefore the final solution is given by:

$$C_{x,t} = \frac{4C_{in}}{\pi}\sum_{n=0}^{\infty}\frac{1}{(2n+1)}\sin\left(\frac{(2n+1)\pi x}{L}\right)\exp\left(\left(-\frac{(2n+1)^2\pi^2}{L^2}\right)Dt\right). \qquad (5.20)$$

120

A useful quantity to know based upon this analysis is how much liquid is expected to leave one side of the slab of exposed area A at a given time t, $F_{0,t}$. Choosing the face $x = 0$, the quantity may be calculated from:

$$F_{0,t} = A\int_0^t D\left|\frac{\partial C}{\partial x}\right|dt$$

(5.21)

At $x = 0$ equation (5.20) yields after differentiation:

$$\left|\frac{\partial C}{\partial x}\right| = \frac{4C_{in}}{\pi}\sum_{n=0}^{\infty}\exp\left(\left(-\frac{(2n+1)^2\pi^2}{L^2}\right)Dt\right).$$

(5.22)

Substituting this relation into equation (5.21) and reducing the result to the simplest form gives:

$$F_{0,t} = \frac{C_{in}LA}{2}\sum_{n=0}^{\infty}\left\{1 + \left(-\frac{8}{\pi^2}\right)\frac{1}{(2n+1)^2}\right\}\exp\left(\left(-\frac{(2n+1)^2\pi^2}{L^2}\right)Dt\right).$$

(5.23)

Of course, the total loss for two exposed faces is just two times the above quantity. Finally, after a sufficiently long time, all of the liquid which can leave the slab has and the calculated value is then given by (for moisture loss from two faces):

$$F_{\infty} = C_{in}LA.$$

(5.24)

This relation enables us to describe the moisture loss at anytime from the slab in terms of the absolute total moisture loss possible:

$$\frac{F_{\infty}-F_t}{F_{\infty}} = \frac{8}{\pi^2}\left\{\sum_{n=0}^{\infty}\left\{\frac{1}{(2n+1)^2}\right\}\exp\left(\left(-\frac{(2n+1)^2\pi^2}{L^2}\right)Dt\right)\right\}.$$

(5.25)

After a sufficiently long period of time, $0.5 < \frac{F_t}{F_{\infty}} < 1$, this relation can be further reduced to:

$$\frac{F_{\infty}-F_t}{F_{\infty}} = \frac{8}{\pi^2}\exp\left(\left(-\frac{\pi^2}{L^2}\right)Dt\right).$$

(5.26)

This relation is very useful in determining the diffusivity of a material from experimental data. When the diffusivity becomes constant, one can calculate it assuming that this occurs around the time $0.5 = \frac{F_{\infty}-F_t}{F_{\infty}}$ of equation (5.25).

Now if the slab has an alternative initial concentration, i.e. not quite saturated, and the surfaces are at a concentration different from the slab but held constant, C_{ext}, the solution becomes:

$$\frac{C_{ext}-C_{x,t}}{C_{ext}-C_{in}} = \frac{4}{\pi}\sum_{n=0}^{\infty}\frac{1}{(2n+1)}\sin\left(\frac{(2n+1)\pi x}{L}\right)\exp\left(\left(-\frac{(2n+1)^2\pi^2}{L^2}\right)Dt\right).$$

(5.27)

121

Another alternative case occurs if the surface concentrations are held constant at a given concentration while there is an initial distribution through the slab thickness. Then the same procedure is followed with only changes in the initial condition. This solution is also represented in the form of a trigonometric series:

$$C_{x,t} - C_{ext} = \frac{2C_{ext}}{\pi} \sum_{n=1}^{\infty} \frac{\cos n\pi - 1}{n} \sin\left(\frac{n\pi x}{L}\right) \exp\left(\left(-\frac{n^2\pi^2}{L^2}\right)Dt\right) \tag{5.28}$$

$$+ \left(\frac{2}{L}\right) \sum_{n=1}^{\infty} \sin\left(\frac{n\pi x}{L}\right) \exp\left(-\frac{n^2\pi^2}{L^2}\right)Dt \int_0^L f(x_p) \sin\left(\left(\frac{n\pi x_p}{L}\right)\right)dx_p \tag{5.28 cont-}$$

Using the relations established by these analyses one is able to determine the diffusivity of a slab under the following assumptions: constant diffusivity with an infinite volume of the surrounding atmosphere and an infinite rate of evaporation. The three relations applicable to these conditions are [Vergnaud 1992]:

for short time periods
$$\frac{F_t}{F_\infty} = \frac{4}{L}\sqrt{\frac{Dt}{\pi}} \tag{5.29}$$

at the half life of the process
$$\frac{Dt}{L^2} = 0.0498, \tag{5.30}$$

and for long time periods
$$\ln\left(\frac{F_\infty - F_t}{F_\infty}\right) = -\pi^2\frac{Dt}{L^2} + \ln\left(\frac{8}{\pi^2}\right) \tag{5.31}$$

5.2.4 Diffusion from a Permeable Layer on the Bottom Face and Infinite Evaporation on the Exposed Upper Face

The next analysis of interest stems from observation in the experimental program, where sealed specimens did not act perfectly sealed. To treat this case analytically, we assume that there is a diffusing layer on the base of the slab that is permeable and that the top exposed face experiences infinite evaporation. The only difference in the analysis is the presence of the thin permeable layer. The boundary conditions are written to address this layer. The same governing one dimensional flow equation holds as stated in (5.6). The boundary conditions are:

$$t = 0, \quad 0 < x < h, \quad C = C_{in} \quad \text{(permeable layer)}$$

$$0 < x < L, \quad C = 0 \quad \text{(slab)}$$

$$t > 0, \quad C_{0,t} = C_{L,t} = 0 \quad \text{(exposed surfaces)}$$

where t is time, x is spatial location, h is the thickness of the permeable coating, L is the thickness of the slab, and the concentrations are as defined earlier.

The solution for the concentration is then given by:

$$C_{x,t} = \frac{4C_{in}}{\pi}\sum_{n=1}^{\infty}\frac{1}{n}\sin\left(\frac{n\pi h}{2L}\right)\sin\left(\frac{n\pi x}{L}\right)\exp\left(-\frac{n^2\pi^2}{L^2}Dt\right) \tag{5.32}$$

Therefore, the amount of liquid remaining in the slab after some time period is given by the following:

$$F_t^p = \int_0^L C_{x,t}dx \tag{5.33}$$

where $C_{x,t}$ is given by (5.32). This is again similar to the analysis conducted earlier. As time approaches infinite extent, the amount in the permeable layer becomes constant at: $F_\infty = C_{in}h$. Like the earlier analysis it is appropriate to write the final content as a normalized quantity [Vergnaud 1992]:

$$\frac{F_t^p}{F_\infty} = \frac{8L}{h\pi^2}\left\{\sum_{n=0}^{\infty}\left\{\frac{1}{(2n+1)^2}\right\}\left\{\sin\left(\frac{(2n+1)\pi xh}{2L}\right)\right\}^2\exp\left(\left(-\frac{(2n+1)^2\pi^2}{L^2}\right)Dt\right)\right\} \tag{5.34}$$

There the total amount of liquid which has left the permeable layer and the slab is:

$$F_\infty = F_t + F_{t^p}. \tag{5.35}$$

The problem with many of the trigonometric series solutions is that they converge very slowly and may require very high n values. For problems where the diffusivity is not constant then numerical solutions must be relied upon.

5.2.5 Finite Rates of Evaporation

The next types of problems of interest are those where the rate of evaporation is not infinite and the process is transient. This type of problem occurs when the surrounding atmosphere is larger than the slab, and the amounts of evaporated material does not change the ambient concentration. Another scenario occurs when the ambient environment is not large but the external conditions are forced to a constant condition. The one dimensional flow equation again applies as given by equation (5.6), and the boundary conditions are now given by:

$$t = 0, \quad -L > x > L, \qquad C = C_{in} \qquad \text{(Slab)}$$

$$x < -L \text{ or} \qquad C = C_{ext} \qquad \text{(Air)}$$

$$x > L$$

123

These conditions show that the rate of evaporation is equal to the rate that the liquid in the slab reaches the surface. Therefore, internal diffusion governs. As described earlier the rate of evaporation is proportional to the difference in concentrations of the surface and the ambient environment. Earlier the concentration on the surface was denoted by a sub-scripted o. Without further derivations, the solution to the posed problem is:

$$\frac{C_{ext} - C_{x,t}}{C_{ext} - C_{in}} = \sum_{n=1}^{\infty} \frac{2S\cos\frac{\beta_n x}{L}}{(\beta_n^2 + S^2 + S)\cos\beta_n} \exp\left(-\frac{\beta_n^2}{L^2}Dt\right).$$

(5.36)

where the β_n s are the positive roots of the equation $\beta_n \tan\beta_n = S$, and S is a dimensionless number given by: $S = \frac{E_o L}{D}$. The roots of the β_n equation are easily determined using a MATLAB script or from published tables. The total amount of liquid that leaves the slab at time t is again expressed as a fraction of the infinite loss:

$$\frac{F_\infty - F_t}{F_\infty} = \sum_{n=1}^{\infty} \left\{\frac{2S^2}{\beta_n^2(\beta_n^2 + S^2 + S)}\right\} \exp\left(\left(-\frac{\beta_n^2}{L^2}\right)Dt\right).$$

(5.37)

It is easy to ascertain that if the ambient concentration is lower than the slab concentration evaporation occurs, or if the ambient concentration is higher than the slab concentration that condensation occurs. The kinetics of the process are again studied applying the same principles already outlined above.

5.2.6 Steady State Analyses

For the steady state response to either the infinite or non-infinite rates of evaporation problems the solution process is simplified because the transient term in equation (5.6) becomes zero. Double integration of the equation and then application of the appropriate boundary conditions yield the solution.

$$\frac{C_{ext} - C_{x,t}}{C_{ext}} = \frac{x}{L}$$

(5.38)

and the rate of moisture loss is given by:

$$F = \frac{DC_{ext}}{L}$$

(5.39)

The second problem of interest is that of the steady-state constant diffusivity with constant concentration on one exposed surface and a finite rate of evaporation on the other exposed surface. Choose the datum surface, $x = 0$, to correspond to the constant concentration side, C_i, and the opposite face at $x = L$ as the one with finite evaporation. The concen-

124

tration at the surface is denoted as C_o while the ambient concentration is C_{ext}. The conditions at $x = L$ yield:

$$-D\frac{\partial C}{\partial x} = E_o(C_o - C_{ext})$$
(5.40)

For the steady state condition the concentration gradient is constant in the slab, and after integration the above relation yields:

$$D\left(\frac{C_i - C_o}{L}\right) = E_o(C_o - C_{ext}),$$
(5.41)

and the surface concentration is given by:

$$C_o = \frac{DC_i - E_oLC_{ext}}{D + LE_o}.$$
(5.42)

Using this expression one can derive the rate of transfer of the liquid through the slab as:

$$F = (C_i - C_{ext})\frac{DE_o}{D + E_oL}$$
(5.43)

where F is the rate of flow of material, and the other variables have been defined above.

5.2.7 Summary of Simplified Analytical Analyses

Now the drying problem of constant diffusivity with both finite and infinite rates of evaporation have been addressed. These problems constitute some of the classic partial differential equation problems where separation of variables and the use of Fourier analysis and orthogonal functions are used. Applying these means to solve the problems leaves solutions in trigonometric series that may rely on a large number of terms to converge. For problems of varying diffusivity numerical methods must be used and checked based upon these analytical expressions. A finite difference code was developed to calculate the response of a slab with varying diffusivities. The results correlate well with the analytical solutions presented.

5.2.8 Numerical Analyses

Figure 5.2.1 depicts the change in moisture in a slab with a diffusivity of 3.0E-4 in^2/day for the SRA mix and 5.0E-4 in^2/day for the reference paste mix, both with a W/C = 0.45. The diffusivity values were calculated from the mass loss data of the EIS moisture profile

specimens. The measured moisture content at the first station is in very good agreement with the calculated response, however because hydration was not taken into account there is no other manner in which moisture can be consumed and the calculated response has the moisture content near the insulated surface approach fully saturated conditions. Another problem which needs to be addressed is the fact that the insulated face indeed lost moisture, albeit at a much lower rate then the exposed surface due to improper sealing. The calculated response made use of the earlier developed solutions for a slab subjected to an infinite rate of evaporation with a constant external concentration of moisture. Hydration can be modeled in two separate stages, initially an almost linear relation holds in terms of moisture consumption and then a dormant period ensues when diffusion governs [Neville 1996]. This is easily incorporated in the numerical model provided that the certain material parameters are known from experimental techniques. This is not reported further here.
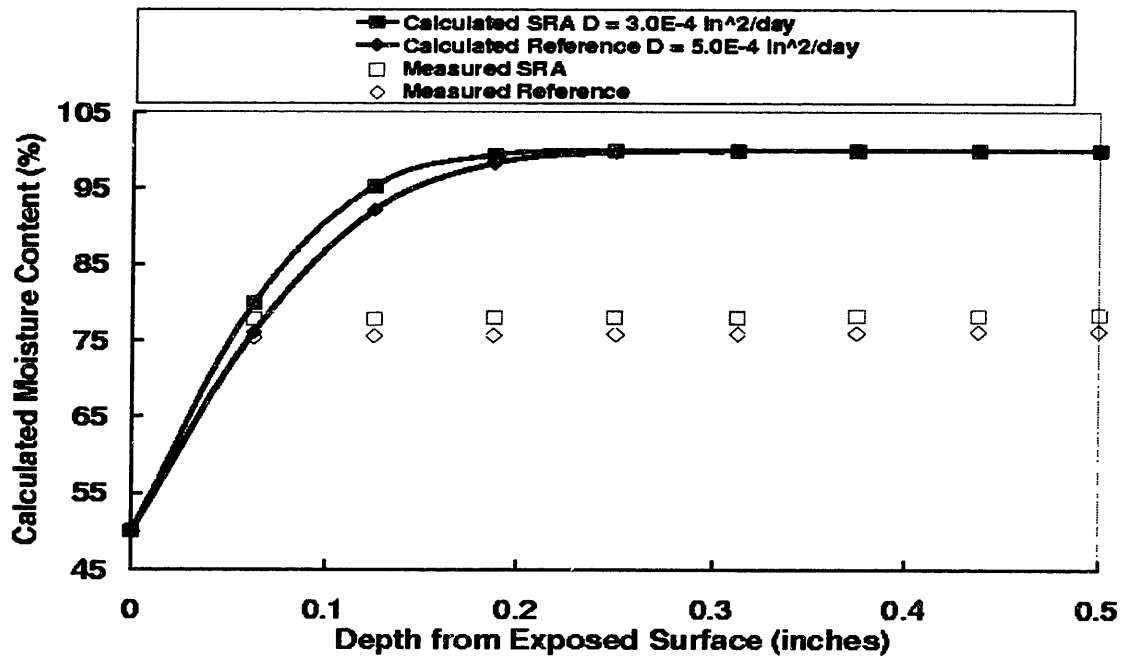
Figure 5.2.1 The 7 day moisture profile measured and calculated for the W/C = 0.45 mix.

The one and three day calculated responses are closer to the measured results. As time progresses it becomes increasingly evident that there are two distinct moisture loss fronts.

Figure 5.2.2 depicts the changes in the moisture profile as a function of a wide range of values for the diffusivity, and Figure 5.2.3 shows how the moisture varies in a single sample through time. The diffusivity has units of $\frac{in^2}{day}$, and the normalized time scale is dimensionless. Note that at the later stages of drying the steady state moisture gradient is linear through the thickness which causes uniform curling deformations. It is interesting to recall that the measured di-electric response for the one-half inch specimen also demonstrated linear behavior for the upper measuring stations. The drying front extending from the bottom changed the response such that it will induce even greater curling deformations do to the increased non-linearity of the moisture content. Also based upon those results it was apparent that there was more moisture in the system in general, hence the drying shrinkage strains experienced by the SRA admixed series would be even less then expected if the two moisture profiles had been the same and the dominant mechanism was just the reduction of drying shrinkage at a particular moisture content.
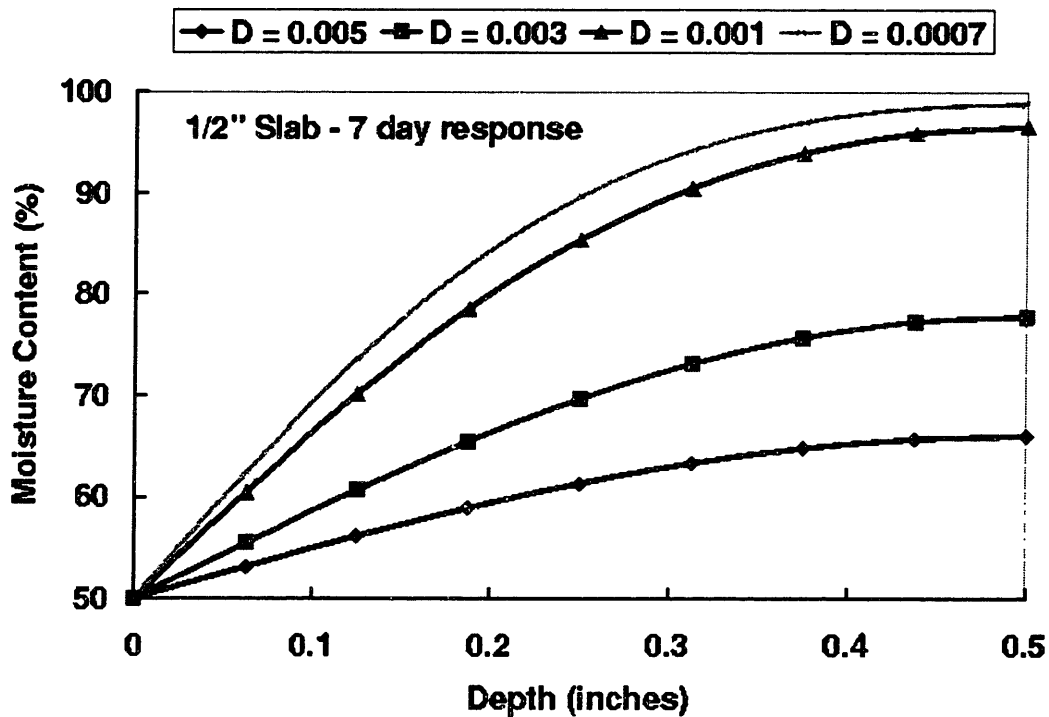
Figure 5.2.2 The calculated moisture profiles for a 1/2" cement slab with varied values of diffusivity.

5.2.9 Shrinkage Functional

Since the shrinkage in cement paste follows the movement of moisture from the slab system, these analyses are applicable to that problem with some slight modification of defini-
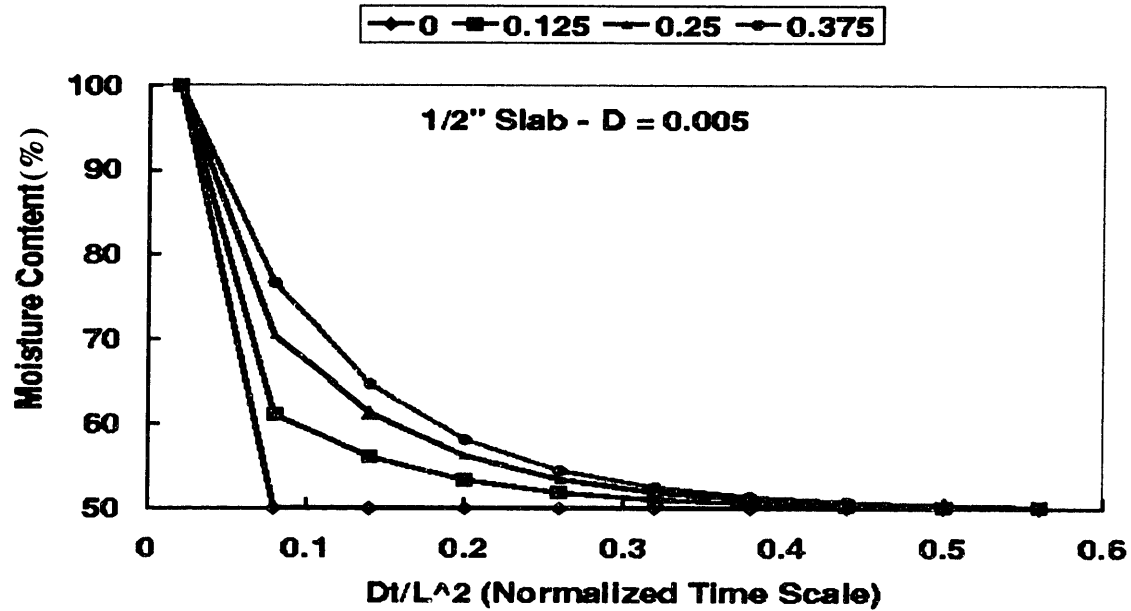
Figure 5.2.3 Changes in the calculated moisture content at particular depths of a
1/2" cement slab through time.

tions of terms. Pickett conducted such an analysis and found good correlation between these types of expressions and drying shrinkage [Pickett, 1946]. Some experimental data is required to obtain estimates of some of these parameters. A shrinkage functional replaces the concentration in equation (5.6) and the boundary conditions are defined similarly. The diffusivity now becomes the diffusivity of shrinkage. It is expected based upon the results presented in the experimental results section that the value of the diffusivity changes with the addition of the SRA, because the measured moisture profiles are different.

With the developed expressions for shrinkage following the movement of moisture in the system, we are now capable of calculating how drying shrinkage changes with external environmental conditions. For a general analysis, a computational scheme is desired using the finite difference or finite element approach. The numerical technique used for this study was the finite difference technique. As this approach is well documented in the literature or covered in most undergraduate curricula no background information concerning the technique is presented. The program was developed using MATLAB, an available

commercial mathematical software package. The finite difference approach is able to account for varying boundary conditions in a very efficient manner. The governing differential equations are discretized using the calculus of finite differences, and variable diffusivity attributed with concentration changes can easily be modeled for moisture movement. In order to develop a understanding of shrinkage phenomena a fundamental understanding of the mechanisms involved is required. So for the purposes of this paper only constant diffusivity analyses are conducted, and if the results are in considerable error, then the possibilities of concentration dependence will have to be addressed.

In these analyses an implicit assumption made is the independence of moisture flow from temperature effects. For typical operational environments this is warranted. However, for structures that experience large changes in temperature or moisture in a very short period of time need to account for the coupled phenomena. Luckily in the field of heat and mass transfer many researchers have studied these effects and their work may be applicable to the current study.

So applying the concepts developed by Pickett, a new functional is defined in terms of shrinkage and the diffusivity of interest is then associated with drying shrinkage. For the purposes of brevity, only the one dimensional analysis is presented. The same relations then developed earlier are now applicable to the shrinkage problem with the new definitions for the evaporative constant and initial and final equilibrium shrinkage values. These are easily determined experimentally and so the model is semi-empirical in nature. The complimentary evaporative coefficient accounts for the geometry of the specimen involved and should be related to the governing dimension, as well as the exposed surface area to volume ratio. Figure 5.2.4 depicts the new problem in similar form to the one already solved. The solution to this problem is of course composed of both the steady state and transient solution. The final form of the shrinkage functional is:

$$S(x, t) = \frac{S_o + xE(S_{inf} - S_o)}{(k + Eh_x)} + \sum_{n = 1}^{\infty} b_n \sin\lambda_n x \exp(-\lambda^2_n kt). \qquad (5.44)$$

By using the orthogonality relations one is able to determine the values for b_n and the roots of the equation $\tan(\lambda b) = -\frac{k}{E}\lambda$ then give the correct values of λ_n. Here E is the proportionality constant associated with the convective term, and not the compressive modulus elasticity.
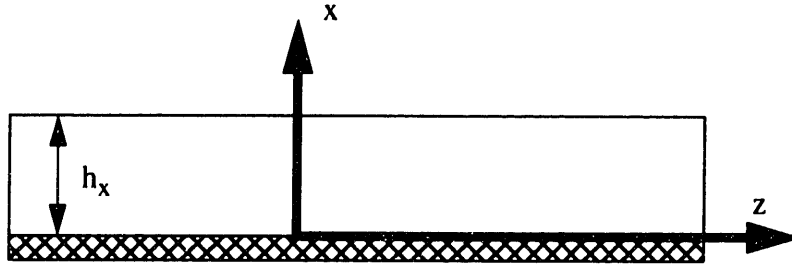
Problem Statement:

$$\frac{\partial^2 S}{\partial x^2} = \frac{1}{k}\frac{\partial S}{\partial t} \quad , \qquad 0 < x < h_x; \qquad 0 < t$$

Initial Condition: $\quad S(0,t) = So, \qquad 0 < t$

Boundary Conditions: $\quad -kdS/dx(h_x,t) = E(S(h_x,t) - S_{inf}), \quad 0 < t$

$$S(x,0) = f(x), \qquad\qquad 0 < x < h_x$$

Figure 5.2.4 Description of the shrinkage functional following diffusional behavior.

5.2.10 Application of the Kelvin and Laplace Equations

An alternative approach to the one taken by Pickett is to directly apply moisture movement analyses coupled with an understanding of microstructural information with the Kelvin and Laplace equations to directly calculate the shrinkage strains induced on the system. Again, for the ease of the discussion the Kelvin and Laplace equation are given below:

$$\ln\left(\frac{P}{P_o}\right) = \frac{2\gamma_{LV}}{RT\rho r} \tag{2.5}$$

$$\sigma' = -2\frac{\gamma_{LV}}{r} \tag{2.4}$$

where all the terms have been defined in Chapter 2. Table 5.1 depicts the calculated magnitudes of stresses for various sized capillary pores filled with water:

Pore Radius (microns)	Stress (pascals)	Stress (psi)	Vapor Pressure P/P_o
5000	30	0.00	1.0000

Table 5.1: Theoretical magnitudes of stress calculated using the Kelvin and Laplace equations.

130

Pore Radius (microns)	Stress (pascals)	Stress (psi)	Vapor Pressure P/P_o
2500	59	0.01	1.0000
1250	118	0.02	0.9999
625	236	0.03	0.9998
312.5	472	0.07	0.9997
78.125	1889	0.27	0.9986
39.0625	3778	0.55	0.9973
19.53125	7556	1.10	0.9945
9.76562	15111	2.19	0.9891
4.88281	30222	4.38	0.9782
2.44141	60455	8.77	0.9569
1.22070	120890	17.53	0.9157
0.61035	241780	35.07	0.8385
0.30518	483560	70.13	0.7031
0.15259	967120	140.27	0.4943

Table 5.1: Theoretical magnitudes of stress calculated using the Kelvin and Laplace equations.

Note how the stress increases with decreasing pore size as discussed earlier. This information may be of use if the water filled pores at a given equilibrium moisture content are determined from the moisture analysis. A critical pore size range must be defined with which to average the hydrostatic stress. There are certain pores which under the conditions stipulated in the drying shrinkage study will never empty, and may therefore play a larger role in the drying shrinkage strains experienced. Obviously the larger pores which are empty play no role at all. Therefore a critical pore size range is defined as made up of all the gel pores that do not empty under normal drying environments to the upper pore limit composed of those pores just about to empty. This pore range is used to determine the average stress and strain that a specimen experiences. The only way to conduct this analysis is through the use of the mercury intrusion poresimetry data, where we have information concerning the pore structure of each mix design.

An example calculation is illustrative. Let us examine the pore size distribution of the W/C = 0.45 reference paste mix and the companion 5% SRA admixed design mix. Figure 4.4.6 in the microstructural analysis section presented the normalized pore distribution for these test mixes. From the table above it is apparent that pores greater then 1000 angstroms do not actively participate in inducing drying shrinkage strains. For a particular relative humidity we can calculate which is the upper limit for the pore range. As an example let us assume that the ambient condition is at 50% RH, therefore by applying Kelvin's equation the pores that are still active are smaller than or equal to 16 angstroms. We can calculate what the active pore volume is by taking a the ratio of the evaporable water to the remaining water after a long time period [Nagataki et al., 1982, Nagataki et al., 1983]. To obtain this information we must have some experimental information because the mercury poresimetry technique is unable to measure pores typically below 20 - 30 angstroms. Old samples, in excess of 90 days may be baked in an oven at a low enough temperature to obtain the required evaporable water content without degrading the delicate CSH sheets. Using this information along with the assumption that the difference in pore solution surface tensions remain relatively constant through time we can calculate the predicted response for this system. Typically it is useful to normalize the pore volume by dividing through with the unit cement paste volume [Nagataki et al., 1982, Nagataki et al., 1983]. If all other parameters are comparable we can expect the reduction in shrinkage to be close to the ratio of the surface tensions. Indeed the long term benefits comparing these two mixes are very close to that value. The small difference calculated may occur due the second order pore wall-vapor interfacial energy effects. Due to results from wetting-rewetting experiments it is apparent that the shrinkage reducing admixture comes out of solution and may coat the pore walls [Dallaire et al. 1997]. Comparison of residual compressive strengths and by applying a Griffith type relation, one should be able to calculate the differences in the solid-vapor interfacial energies. However these types of analyses have not been conducted yet.

5.3 Curling Deformations

The curling deformations in slabs may be caused by nonuniform distributions of temperature and moisture. This non-uniformity causes internal stresses to develop due to restraint

between different regions of the slab. The slab expands or contracts due to the local internal moisture content. These strains occur even when no external forces are applied to the system, i.e. gravity, tires, and/or external restraints. Provided that the stresses do not institute any changes in the diffusion process, classical linear elastic analysis holds and drying shrinkage or thermal stresses are super-positionable.

For the problem of a slab drying from one surface, i.e. a plate resting on the ground, one dimensional moisture flow is expected as discussed in the last section. Typically the deformations are small on the scale of the length of the slab, so small deformation theory applies. The following relations for strain apply [Pickett 1946, Sih et al. 1986]:

$$\varepsilon_y = {}^o\varepsilon_y + {}^o\kappa_y x$$

$$\varepsilon_z = {}^o\varepsilon_z + {}^o\kappa_z x \tag{5.45}$$

$$\gamma_{yz} = {}^o\gamma_{yz} + {}^o\kappa_{yz} x.$$

In equation (5.46), ${}^o\varepsilon_y$, ${}^o\varepsilon_z$, and ${}^o\gamma_{yz}$ are the strain components, while ${}^o\kappa_y$, ${}^o\kappa_z$, and ${}^o\kappa_{yz}$ are the curvatures experienced at the mid-plane of the slab. The coordinate system is defined as y, and z lying in the plane of the slab while the x-direction is in the direction of the top surface. This is a right handed coordinate system. The mid-plane of the plate is defined at $x = 0$. The strains may be weighted through the slab thickness $-h_x < x < h_x$ and are defined as follow:

$$ {}^o\varepsilon_z = \frac{1}{2h_x} \int_{-h_h}^{h_h} \varepsilon_z(x) dx \tag{5.46}$$

and

$$ {}^o\kappa_z = \frac{1}{2h_x} \int_{-h_h}^{h_h} x\kappa_z(x) dx. \tag{5.47}$$

Of course similar expressions apply for the other strains and curvatures. From linear elasticity, we know that:

$$\varepsilon_y = \frac{1}{E}(\sigma_y - \upsilon\sigma_z) + \alpha(T - T_o) + S \tag{5.48}$$

$$\varepsilon_z = \frac{1}{E}(\sigma_z - \upsilon\sigma_y) + \alpha(T - T_o) + S \tag{5.49}$$

and

$$\gamma_{yz} = \frac{2(1 + \upsilon)}{E}\sigma_{yz} \tag{5.50}$$

where υ and E are the Poisson's ratio and modulus of elasticity respectively, α is the coefficient of thermal expansion, T is the temperature, and S is the shrinkage strain determined from the analyses conducted above. Next one calculates the resulting temperature and shrinkage forces through the slab thickness as:

$$^TN = \frac{\alpha E}{(1-v)} \int_{-h_h}^{h_h} (T - T_o)dx \qquad (5.51)$$

$$^SN = \frac{E}{(1-v)} \int_{-h_h}^{h_h} Sdx. \qquad (5.52)$$

The moments caused by these forces are determined by multiplying equations (5.51) and (5.52) by x within the integral. The results are:

$$^TM = \frac{\alpha E}{(1-v)} \int_{-h_h}^{h_h} x(T - T_o)dx \qquad (5.53)$$

and

$$^SM = \frac{E}{(1-v)} \int_{-h_h}^{h_h} xSdx. \qquad (5.54)$$

Therefore the general expressions for strains and curvatures the midpoint of the slab are given by:

$$^o\varepsilon_y = {}^o\varepsilon_z = \frac{(1-v)}{2Eh_x}[{}^TN + {}^SN];{}^o\gamma_{yz} = 0 \qquad (5.55)$$

$$^o\kappa_y = {}^o\kappa_z = \frac{3(1-v)}{2Eh_x}[{}^TM + {}^SM];{}^o\kappa_{yz} = 0. \qquad (5.56)$$

Using the above expressions and enforcing global equilibrium one is able to establish the equations for the general strain components:

$$\varepsilon_y = \varepsilon_z = \frac{(1-v)}{2Eh_x}\left\{ {}^TN + {}^SN + \frac{3x}{(h_x)^2}[{}^TM + {}^SM] \right\};\gamma_{yz} = 0. \qquad (5.57)$$

This describes a one dimensional analyses which is applicable due to the symmetry of the system, the strain varies solely in the x-direction. Using these expressions, it is easy to then compute the internal stresses induced on the solid due to the temperature and shrinkage. These stresses are given by:

$$\sigma_y = \frac{E}{(1-v^2)}[\varepsilon_y + v\varepsilon_z - \alpha(1+v)(T - T_o) - (1+v)S] \qquad (5.58)$$

$$\sigma_z = \frac{E}{(1-v^2)}[\varepsilon_z + v\varepsilon_y - \alpha(1+v)(T - T_o) - (1+v)S] \qquad (5.59)$$

$$\sigma_{yz} = \frac{E}{2(1+v)}\gamma_{yz}. \qquad (5.60)$$

Next substitute the expressions determined above for the shrinkage strains and note that the shear stress vanishes as it must, to yield:

$$\sigma_y = \sigma_z = \frac{1}{2h_x}[{}^TN + {}^SN] + \frac{3x}{2(h_x)^3}[{}^TM + {}^SM] - \frac{\alpha E}{(1-v)}(T - T_o) - \frac{E}{(1-v)}S. \qquad (5.61)$$

With this, the stresses and strains have been defined and the elastic analysis is conducted easily with the introduction of the strain field associated with the drying shrinkage determined in the previous analysis including uncoupled temperature effects if necessary.

To begin let us assume that temperature plays a lesser role and the problem of interest is the deformation induced in the cement slab due solely to the non-uniform distribution of moisture through it thickness caused by the one dimensional flow out the top surface. Since the flow of moisture in a cement slab drying from only one surface is believed to be the same as that occurring in either half of a slab of twice the thickness drying from two surfaces, it is logical to assume that the expressions developed for the drying shrinkage of the slab drying from only one surface will apply equally well for either half of the slab drying from two exposed surfaces. Therefore, the plane which lies mid-way between the two faces is taken as the datum $x = 0$ (See Figure 5.2.4). For a slab drying from two sides with equal rates of evaporation, the two sides experience symmetric curling forces and hence restrain each other from curling. This is substantiated with the small drying shrinkage prisms that had two sides exposed in multiple environmental conditions with no out of plane deformations. They experienced uniform shrinkage strains.

However for the slab with a single exposed surface, there are no restraining forces present and curling deformations are expected. If the slab is completely unrestrained lying on an infinitely hard surface, neglecting friction between the slab and the interface and gravity loads, then the only contributing source for the unbalanced curling forces are due to the differential strains induced by drying shrinkage. A simplified analysis is to address the longitudinal strains first and then expand the analysis to include the lateral portion. Similar to the heat transfer problem, the first step is to determine the stress which occurs due to complete longitudinal support/restraint. This stress is defined as:

$$^{P}\sigma_{z} = \frac{E}{(1-\upsilon)}S.$$ (5.62)

The average value of $^{P}\sigma_{z}$ is determined by:

$$^{P}\overline{\sigma}_{z} = \frac{E}{(1-\upsilon)h_{x}}\int_{0}^{h_{x}}Sdx$$ (5.63)

and so the sum of these two parts of the stress is:

$$^{PP}\sigma_{z} = \frac{E}{(1-\upsilon)}\left[S - \frac{1}{h_{x}}\int_{0}^{h_{x}}Sdx\right].$$ (5.64)

135

The moment that is produced by this stress is of course determined by multiplying the stress by x and integrating through the thickness. This is the moment which occurs to prevent curling deformations and is given by:

$$M = \int_0^{h_x} {}^{pp}\sigma_z x\, dx.$$ (5.65)

Of course for the case of interest there is no external restraint and so this moment must be removed by adding an equal but oppositely signed moment. Using this moment expression and the expressions for longitudinal restraint and average longitudinal restraint one is able to determine the stress which occurs by applying elementary beam theory:

$$\sigma_z = \frac{E}{(1-\upsilon)}\left\{ S + \left(6\frac{x}{h_x} - 4\right)\frac{1}{h_x}\int_0^{h_x} S\, dx + \left(6 - 12\frac{x}{h_x}\right)\left(\frac{1}{(h_x)^2}\int_0^{h_x} Sx\, dx\right)\right\}.$$ (5.66)

For slabs with comparable length to width ratios, σ_y is of similar form. If one applies simple beam theory using these expressions it is possible to calculate the expected curling deformations. Since the system is symmetric about the center-line of the longitudinal axis of the slab, then the maximum curling deformation occurs at the center and is calculated by:

$$u_{max} = \frac{3(l)^2}{2h_x}\left[\frac{1}{(h_x)^2}\int_0^{h_x} Sx\, dx - \frac{1}{2h_x}\int_0^{h_x} S\, dx\right]$$ (5.67)

where l is the length of the slab and the rest of the terms are already defined above.

The slightly more complicated analysis including curvature effects follows a similar analysis and is not presented in full. Using these developed expressions, one is able to calculate the expected curling deformations for slabs with and without the addition of the SRA. The key differences in the analyses are the determination of the diffusivities of each slab respectively for input into the shrinkage model discussed above. If the analysis for the drying shrinkage strain is conducted using the Kelvin and Laplace equations following the one dimensional flow of water from the system and using a critical pore size range, then that is what is used as the shrinkage functional.

An illustrative example is helpful to describe the performance of the analysis compared to actual experimental results. For early time periods the variation of strain through the thickness of a sample may be modeled using a second order function. At later ages when the steady state solution governs, the behavior is better approximated with a linear variation in strain through the thickness of the member. So two time periods are then con-

sidered, and early age response around 28 days and the response at the later age of 90 days. The second age was picked based upon the qualitative results described in the moisture profile study. The slope at that point in time would have been linear if not for the presence of the second drying front. Figure 5.3.1 depicts the variation in moisture content for the slab at 28 and 90 days. Based upon the response of the system, correlations between
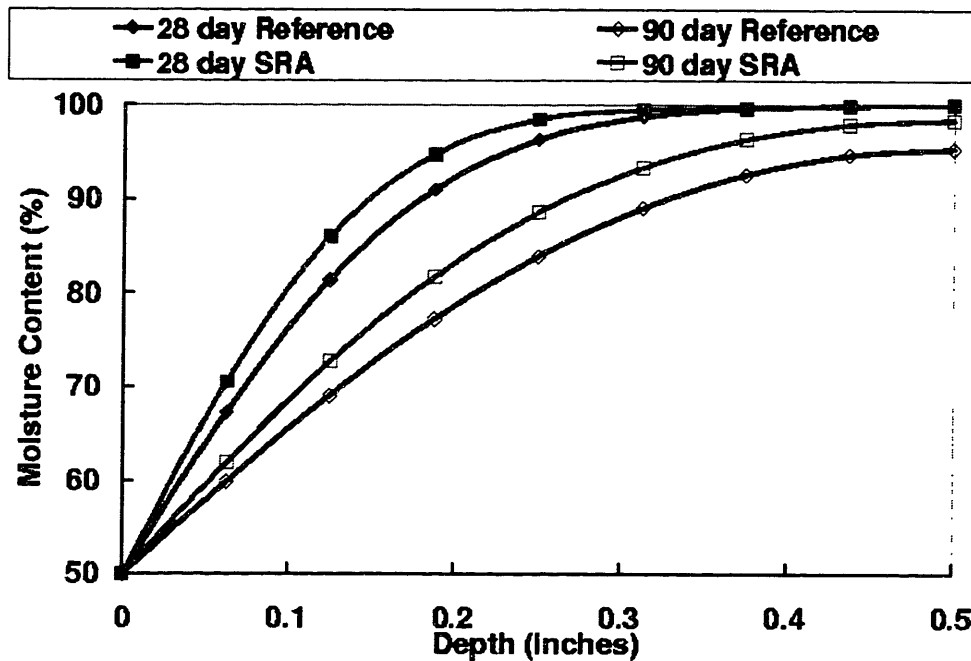
Figure 5.3.1 The calculated moisture profiles for a 1/2" cement slab with a W/C = 0.45.

the drying shrinkage behavior at a particular environmental condition and the shape of the moisture profile may be used to map the strain field. A second order polynomial is fitted to the strain field and then used for the functional of strain in the analyses described above. Comparisons between the center-line deflections in time for the reference paste and 5% SRA admixed mixes are presented in Table 5.2 below.

	Calculated	Deflections (inches)	Measured	Deflections (inches)
Age	28 Day	90 Day	28 Day	90 Day
Reference	0.551	0.712	0.205	0.65
SRA	0.34	0.508	0.095	0.33

Table 5.2: Comparison of model and experimental center-line deflections at 28 and 90 days for the W/C = 0.45 reference and SRA admixed mixes.

137

As described earlier, there is a problem with calculating the response of the system when the hydration reactions are still actively occurring. The early age response should take moisture loss into account. Still the differences experienced by the SRA admixed series at 28 days is larger than one would expect. In order to accurately describe the moisture profile for these types of mixes, one may have to account for inter-diffusional flow induced by the concentration gradients that arise as drying occurs. As the moisture content reaches a critical concentration, the SRA comes out of solution and establishes a secondary potential field for moisture movement. This can easily be incorporated in the computational model. The results at 90 days are better for the reference mix with differences in the measured and calculated response of nine percent. It is hypothesized that the results would be even closer if the effects of creep due to self weight are accounted for. The later age response for the SRA admixed mix experience differences of about thirty five percent. Again I strongly believe that one must account for the inter-diffusion of water and the concentrated SRA through the thickness of the slab.

5.4 Summary

The fundamental theory of capillary tension and its effect on the drying shrinkage response of drying systems was presented. This information was required to establish the relative changes in the differential strains through the cement paste slab thickness. The key assumptions required to model the curling phenomena are that the system acts in a linear elastic manner, and the shape of the strain field follows the shape of the moisture profiles established using a one dimensional fluid flow analysis. Temperature and moisture are assumed to be uncoupled and the stresses arising from curling restraint or self weight do not affect the manner in which diffusion occurs. The expressions developed are for a one dimensional analysis, but extrapolation of the procedure to multi-dimensions is easily accomplished. The results of calculated drying shrinkage strains versus the measured strains are fairly good. Yet the curling model is found to have some deficiencies in accounting for changes in the shape of the moisture profile established by inter-diffusional

flow of pore water and the SRA polymer. Further work in accounting for the separate periods of hydration and the subsequent removal of moisture as well as the inter-diffusional flow problem are currently being addressed but will not be included in this thesis.

Chapter 6

Conclusions and Future Research Needs

6.1 Summary

The problem addressed in this thesis is that of curling deformations induced in cement slabs cast on grade. As a result of the differential drying rates from the top to the bottom surfaces, a non-uniform moisture profile develops. Since cement paste experiences changes in volume depending on the ambient environmental conditions, this non-uniform moisture profile produces differential strains through the thickness of the slab and curling deformations occur. For symmetrically exposed systems no out of plane deformations occur. However there are still differential strains through the thickness which may cause microcracking depending on the rigidity of the system.

To address this complex problem, a multiphased study combining experimental tests and analytical developments was conducted. The benefits gained from using the shrinkage reducing admixture for drying shrinkage strains have magnitudes related to the ratio of the pore solution surface tensions. Reductions in shrinkage strains varied somewhat with mix design, but the optimal benefits occurred in the mid to high water-to-cementitious material ratios. For these mixes the range in long term reductions in drying shrinkage are from 35 - 45%.

The mechanical property tests demonstrated that there is a variable effect on compressive strength and compressive modulus of elasticity due to the addition of the shrinkage reducing admixture depending on the mix design. Generally with the addition of the shrinkage reducing admixture in concrete samples, a five to ten percent reduction in compressive strength with little change in modulus of elasticity occurs. The results from the

paste study provide no such clear indication. For many of the mixes the strength increased, perhaps due to the reduction in internal microcracking caused by self desiccation and differential shrinkage from the interior to the exterior walls of a specimen.

The microstructural analyses provided very useful information concerning changes induced in the pore size distributions of both reference and SRA admixed mixes. As expected the pore structure is refined with decreases in water-to-cementitious ratio. Greater refinement occurs for the silica fume admixed mixes. Variable changes in terms of refinement/coarsening of the microstructure occurred for the neat cement paste mixes with the addition of the shrinkage reducing admixture. The technique used was unable to provide detailed information about the smallest pore sizes in any given mix.

The flow of moisture from the SRA admixed test specimens was different then the companion reference as determined using the newly developed electrochemical impedance spectroscopy technique. Samples with the SRA exhibited more uniform moisture content through a majority of the thickness with slightly higher gradient occurring at the exposed surface. The greater uniformity through the thickness provided additional restraint against curling deformations. This occurs because a greater proportion of the slab is shrinking at the same rate, which then acts like a monolithic slab restraining the curling tendencies of the non-uniform moisture gradient above it. The measured center-line curling deformations for the specimens admixed with the SRA were less than the companion reference specimens. The magnitudes of reductions are greater then those predicted due to drying shrinkage reduction alone. The change in the moisture content may occur due to an additional mechanism. As the SRA reaches a critical concentration in the pore solution it is believed that SRA then precipitates out and coats the pore walls. This then may cause not only a change in the surface tension exhibited within the pore but also a change in the contact angle. Absorption/desorption tests should be conducted to exam changes in the

141

rates of adsorption and desorption with time. Changes in both types of behavior should occur if the tendency of the SRA is to remain adsorbed on the pore wall as opposed to going back into solution.

The elastic analyses of a cement slab subjected to one dimensional moisture flow from the upper exposed surface was conducted and compared with experimental results. Linear elasticity is a simplified assumption for cementitious composites which exhibit very non-linear material response due to internal microcracking and differences in the tensile and compressive strengths. Therefore the simplified analyses is able to model the deformation characteristics of a cement slab cast on an infinitely hard foundation without accounting for creep, interfacial friction between slab and subgrade, and cracking. However within these limitations the modeled deformations match fairly well with the experimental results at later ages for the reference mixes but less well for the SRA admixed mixes. Shrinkage was said to follow the movement of moisture from the slab with a constant diffusivity and the moisture transport is governed by diffusional flow. Some complications experienced were that the seal on the experimental samples was permeable and drying occurred from the bottom and side faces at a reduced rate compared to the exposed upper surface. The difference in experimental versus analytical results probably partially stem from this occurrence. Other possible causes for differences in behavior could be attributable to the internal sink of moisture due to hydration. This is especially true for lower water-to-cementitious materials where self-desiccation is sure to occur.

6.2 Conclusions

The conclusions drawn based upon both the experimental and analytical developments are:

- The introduction of a drying shrinkage reducing admixture into a wide variety of mix designs reduces the long term drying shrinkage strains experienced in low relative

humidity environments. The reductions in shrinkage strains become less significant at very high relative humidities.

- The presence of the shrinkage reducing admixture has variable effects on the compressive strength and compressive modulus of elasticity. Many of the test mixes had improved strengths with reduced compressive moduli.

- The use of a drying shrinkage reducing admixture changes the curling behavior of neat cement paste slabs. Reductions in curling are typically in excess of 60% within the first 90 days and then decrease at later ages.

- Based upon the extensive microstructural analysis conducted on both reference and shrinkage reducing admixed mixes there is a variable effect on the pore size distributions. Typically silica fume mixes with and without the SRA have very similar distributions, but the neat paste mixes with and without the SRA experience both refined and coarsened microstructures depending on the particular mix design.

- The measured and calculated curling deformations suggest that there are other mechanisms involved besides the reduction in drying shrinkage at a given depth and moisture content.

- The shape of the moisture profile becomes more uniform due to the addition of the shrinkage reducing admixture. Since a greater portion of the slab is subjected to similar shrinkage strains, that portion acts as a restraint against any curling tendencies induced by high gradients present at the exposed surface.

- The newly developed testing technique to determine moisture content as a function of time and environmental history applying electrochemical impedance spectroscopy is very efficient and sensitive to changes in moisture content and damage propagation.

6.3 Future Research Needs

Based upon the conclusions drawn at the close of this study, it is evident that more work is required to fully characterize the effects of using the shrinkage reducing admixture to reduce curling deformation. Tests with curling specimens with greater length to width ratios should be conducted to examine edge effects. The analyses conducted were for one dimensional flow and deformation, two and three dimensional analyses should also be conducted. The effects in changes of the subgrade modulus with the slab response should also be tested. Creep is an important phenomena that all cementitious composites exhibit and needs to be accounted for. The constant diffusivity and uncoupled temperature and moisture flow conditions should be re-examined. Many structural elements in the field may experience sufficient transient temperature and moisture changes that there is a cou-

pling effect.

Further tests are required with the electrochemical impedance spectroscopy measuring technique to obtain the correlation between changes in dielectric response with moisture content. It is suggested that larger samples be tested to ascertain the extents of size dependence on deformations and moisture transport response.The addition of restraining particle inclusion such as coarse and fine aggregate should be modeled with changes in the moisture and shrinkage models to account for bleed pathways and increased overall porosity. Finally, similar tests and analyses for mortar and concrete samples are needed. These tests would be more representative of real applications.

References

Al-Nasara, M., and Wang, R. L., *"Parametric Study of Slab-on-Grade Problems due to Initial Warping and Point Loads,"* ACI Structural Journal, Vol. 91, No. 1, March-April 1994, pp. 198-210.

Annual Book of ASTM Standards (1996) Concrete and Aggregates, Section C-39, *Standard Test Method for Compressive Strength of Cylindrical Concrete Specimens,* Vol 4.02

Annual Book of ASTM Standards (1996) Concrete and Aggregates, Section C 157 *"Standard Test Method for Length Change of Hardened Hydraulic-Cement Mortar and Concrete,"* Vol 4.02

Annual Book of ASTM Standards (1996) Concrete and Aggregates, Section C192-95a *"Making and Curing Concrete Specimens in the Laboratory,"* Vol 4.02

Annual Book of ASTM Standards (1996) Concrete and Aggregates, Section C-469, *Standard Test Method for Static Modulus of Elasticity and Poisson's Ratio of Concrete in Compression,* Vol 4.02

Annual Book of ASTM Standards (1996) Concrete and Aggregates, Section C-617, *Standard Practice for Capping Cylindrical Concrete Specimens, Vol 4.02*

Berke, N. S., Dallaire, M. P., Hicks, M. C., and A. Kerkar, *"New Developments in Shrinkage Reducing Admixtures"* pre-print of paper, Grace Construction Products, Cambridge, MA, USA, 1996.

Bazant, Z. P., and Wittman, F. H., *"Creep and Shrinkage in Concrete Structures,"* John Wiley & Sons, New York, 1982.
Bradbury, R. D., *"Reinforced Concrete Pavements,"* Wire Reinforcement Institute, Washington, 1938

Christensen B. J., Mason T. O., and Jennings H. M., 1992, *"Influence of Silica Fume on the Early Hydration of Portland Cements Using Impedance Spectroscopy"*, J. Am. Ceram. Soc., Vol. 75, No. 4, pp. 939-945.

Czernin, W., *"Cement Chemistry and Physics for Civil Engineers,"* Chemical Publishing Company, New York, 1962

Dallaire, M. P., Private conversation concerning Shrinkage Reducing Admixture and Concrete Curling Behavior, 1997.

Fujiwara, H., Tomita R., and Shimoyama, Y., "*A Study of Frost Resistance of Concrete Using an Organic Shrinkage-Reducing Agent,*" ACI SP 145-34, American Concrete Institute, Detroit, MI, 1994, pp. 643 - 655.

Griffith, A. A., "*The Phenomena of Rupture and Flow in Solids,*" The Royal Society, 221A, 1920

Gu P., Xie P., Beaudion J. J., and Brousseau R., 1992, "*A.C. Impedance Spectroscopy (I): A New Equivalent Circuit Model fro Hydrated Portland Cement Paste*", Cem. Conr. Res., Vol. 22, No. 5, pp. 833-840.

Gu P., Xie P., Beaudion J. J., and Brousseau R., 1993 A, "*A.C. Impedance Spectroscopy (II): Microstructural Characterization Hydrating Cement-Silica Fume Systems*", Cem. Conr. Res., Vol. 23, No. 1, pp. 157-168.

Gu P., Xie P., and Beaudion J. J., 1993 B, "*Microstructural Characterization of the Transition Zone in Cement System by Means of A.C. Impedance Spectroscopy*", Cem. Conr. Res., Vol. 23, No. 3, pp. 581-591.

Gu P., Xie P., Xu Z., and Beaudoin J. J., 1993 C, "*Application of A.C. Impedance Techniques in Studies of Porous Cementitious Materials, (I): Influence of Solid Phase and Pore Solution on High Frequency Resistance*", Cem. Conr. Res., Vol. 23, No. 3, pp. 531-540.

Harr, M. E., and Leonards, G. A., "*Warping Stresses and Deflections in Concrete Pavements,*" HRB Proc. 38:286, 1959

McCarter W. J., Gearing S. and Buzzed N., 1988, "*Impedance Measurements on Cement Pastes*", J. Mater. Sci. Lett., Vol. 7, No. 10, pp. 1056-1057.

McCarter W. J. and Brousseau R., 1990 "*The A.C. Response of Hardened Cement Paste*", Cem. Conr. Res., Vol. 20, No. 6, pp. 891-900.

Nagataki S., and Yonekura, A., "*Properties of Drying Shrinkage and Creep of High-Strength Concrete,*" Transactions of the Japan Concrete Institute, Vol. 4, III - 18 - A, 1982, pp. 223 - 236.
Nagataki S., and Yonekura, A., "*The Mechanisms of Drying Shrinkage and Creep of Concrete,*" Transactions of the Japan Concrete Institute, Vol. 5, III - 3 - A, 1983, pp. 127 - 140.

Neville, A. M., "*Properties of Concrete,*" Fourth Edition, John Wiley & Sons, New York, 1996.

Ogawa, A. and Tomita, R., "*Crack Control of Reinforced Concrete Structures by Using Shrinkage Reducing Agents in Combination with Expansive Additives,*" International Conference - 2000, Economical and Durable Construction Through Excellence, Dundee, UK, September 1993.

Pickett, G., "*Shrinkage Stresses in Concrete,*" Journal of the American Concrete Institute, Vol. 42, No. 3, January 1946. pp. 165 - 204.

Powers, D. L., "*Boundary Value Problems,*" Harcourt Brace Jovanovich, Publishers, 1987.

Scherer, G. W., A, "*Drying of Ceramics Made by Sol-Gel Processing,*" Drying 1992,edited by A.S. Mujumdar, pp. 92-113.

Scherer, G. W., B, "*Crack-tip stress in gels*" Journal of Non-Crystalline Solids, Vol. 144 1992 pp. 210-216.

Scherer, G. W., "*Drying Gels - III. Warping plate,*" Journal of Non-Crystalline Solids Vol. 91 1987, pp. 83-100.

Shah, S. P., Marikunte, S., Yang, W., and Aldea, C., "*Control of Cracking with Shrinkage-Reducing Admixtures,*" Transportation Research Record 1574, 1997 pp. 25 - 36.

Shah, S. P., Kraguler, M. E., and Sarigaphuti, M., "*Effects of Shrinkage Reducing Admixture on Restrained Shrinkage Cracking of Concrete,*" ACI Materials Journal, Vol. 89, No. 3, May-June 1992, pp. 289- 295.

Shoya, M. and Sugita, S., A, "*Application of Special Admixture to Reduce Shrinkage Cracking of Air-Dried Concrete,*" Hachinoche Institute of Technology, Hachinoche, Japan, pp. 1 -11.

Shoya, M. and Sugita, S., B, "*Improvement of Drying Shrinkage and Shrinkage Cracking of Concrete By Special Surfactants,*" Proceedings of the International RILEM Symposium, 1990, pp. 484-495.

Sih, G. C., Michopoulos, J. G., Chou, S. C., "*Hygorthermoelastcicty,*" Martinus Nijhoff Publishers, 1986

Soroka, I., "*Portland Cement Paste and Concrete,*" MacMillian Press LTD, London, 1979.

Terrill, J. M., Richardson, M., and Selby, A. R., "*Non-linear Moisture Profiles and Shrinkage in Concrete Members,*" Magazine of Concrete Research, Vol. 38, No. 137, December 1986, pp. 220 - 225.

Tomita, R., Simoyama, Y., and Inoue, K., "*Properties of Hardened Concrete Impregnated with Cement Shrinkage Reducing Agent,*" CAJ Review, 1986, pp. 314 - 317.

Uchikawa, H., "*Hydration of Cement and Structure Formation and Properties of Cement Paste in the Presence of Organic Admixture,*" Invited Paper at the Conference of Concrete Canada, Quebec, Canada, October 6, 1994.

Vergnaud, J. M., "*Drying of Polymeric and Solid Materials, Modeling and Industrial Applications,*" Springer-Verlag, 1992

Ytterberg, R. F., A, "*Shrinkage and Curling of Slabs on Grade - Part 1 - Drying Shrinkage,*" Concrete International, April 1987, pp. 22-31.

Ytterberg, R. F., B, "*Shrinkage and Curling of Slabs on Grade - Part II- Warping and Curling,*" Concrete International, May 1987, pp. 54-61.

Westergaard, H. M., "*Stresses in Concrete Pavements Computed by Theoritical Analysis,*" Public Roads, April 1926.

Westergaard, H. M., "*Analysis of Stresses in Concrete Roads caused by Variations of Temperatures,*" Public Roads, 1927

Xie P., Gu P., Xu Z., and Beaudoin J. J., 1993, "*A Rationalized A.C. Impedance Model for Microstructural Characterization of Hydrating Cement Systems*", Cem. Conr. Res., Vol. 23, No. 2, pp. 359-367.

Xie P., Gu P., Fu Y., and Beaudoin J. J., 1994, "*A.C. Impedance Phenomena in Hydrating Cement Systems: Origin of the High Frequency Arc*", Cem. Conr. Res., Vol. 24, No. 4, pp. 704-706.

Xu Z., Gu P., Xie P., and Beaudoin J. J., 1993, "*Application of A.C. Impedance Techniques in Studies of Porous Cementitious Materials, (II): Relationship between ACIS Behavior and the Porous Microstructure*", Cem. Conr. Res., Vol. 23, No. 4, pp. 853-862.

Appendix I

The tables attached in this Appendix are those which are referenced in the body of the text of this report. Tables A.1.1 through A.1.20 provide the shrinkage data obtained from the testing of the platelet cement paste specimens at various constant relative humidity environments. The shrinkage values are presented in terms of percentage shrinkage and the age is given in days. TablesA.1.21 through A.1.40 provide the companion mass loss information from the same specimens used in the shrinkage study. Mass loss is presented in terms of a percentage, while again the age is given in terms of days from casting. The last three tables included provide a succinct summary of the mechanical properties obtained from the different mix designs. The units appropriate for each table are presented in the table itself.

Table A.1.1 Shrinkage values of the W/C=0.65 Reference test series.

Shrinkage is presented in (%)

Age (days)	100% RH	88% RH	75% RH	63 % RH	42% RH
7	-0.01	0.06	0.15267	0.182	0.24133
14	-0.02	0.071	0.17933	0.215	0.282
21	-0.023	0.097	0.19267	0.225	0.29867
28	-0.028	0.096	0.20133	0.234	0.31667
35	-0.035	0.102	0.20733	0.235	0.33667
42	-0.011	0.128	0.226	0.256	0.36667
56	-0.031	0.105	0.21733	0.265	0.394
70	-0.016	0.13	0.24133	0.265	0.406
90	-0.02	0.132	0.24733	0.281	0.40667

Table A.1.2 Shrinkage Values of the W/C=0.65 5% SRA test series.

Shrinkage is presented in (%)

Age (days)	100% RH	88% RH	75% RH	63 % RH	42% RH
7	-0.002	0.02733	0.094	0.09733	0.128
14	-0.013	0.04733	0.115	0.11867	0.15067
21	-0.013	0.06867	0.122	0.132	0.15933
28	-0.017	0.07133	0.13	0.13867	0.16067
35	-0.019	0.08867	0.132	0.13867	0.16867
42	-0.783	0.098	0.14	0.158	0.17867
56	-0.809	0.083	0.158	0.16333	0.19467
70	-0.797	0.1	0.161	0.16267	0.202
90	-0.811	0.107	0.175	0.17133	0.216

Table A.1.3 Shrinkage values of the W/C=0.65 7.5% SF test series.
Shrinkage is presented in (%)

Age (days)	100% RH	88 % RH	75% RH	63 % RH	42% RH
7	-0.039333	0.048	0.150667	0.168	0.27133
14	-0.030667	0.0906667	0.232	0.275333	0.348
21	-0.039333	0.0986667	0.246	0.298667	0.37267
28	-0.033667	0.1193333	0.27	0.312	0.41667
35	-0.028	0.1083333	0.280667	0.325	0.44267
42	-0.053333	0.0973333	0.291333	0.331333	0.472
56	-0.018	0.1413333	0.296667	0.329333	0.49333
70	-0.034	0.176	0.32	0.334667	0.51067
90	-0.027333	0.126	0.331333	0.339333	0.50467
120	-0.044667	0.1146667	0.329333	0.345333	0.53533

Table A.1.4 Shrinkage values of the W/C=0.65 7.5% SF & 5% SRA test series
Shrinkage is presented in (%)

Age (days)	100% RH	88 % RH	75% RH	63 % RH	42% RH
7	-0.029333	0.01	0.074	0.056667	0.14667
14	-0.024	0.0613333	0.114667	0.134667	0.19
21	-0.029333	0.0646667	0.122	0.144	0.202
28	-0.024	0.08	0.135333	0.149	0.22533
35	-0.018667	0.07	0.142667	0.157	0.236
42	-0.038667	0.06	0.15	0.161333	0.24667
56	-0.023333	0.0886667	0.153333	0.161333	0.24867
70	-0.022	0.086	0.149333	0.17	0.26667
90	-0.030667	0.078	0.148	0.163333	0.25867
120	-0.034	0.074	0.150667	0.170667	0.25533

Table A.1.5 Shrinkage values of the W/C=0.55 Reference test series.
Shrinkage is presented in (%)

Age (days)	100% RH	88% RH	75% RH	63% RH	42% RH
0	0	0	0	0	0
7	0.001117	0.02255	0.06681	0.10589	0.16437
14	-0.003318	0.04565	0.10575	0.16241	0.23508
21	0.000547	0.04841	0.11343	0.17503	0.24761
30	-0.002224	0.05061	0.1255	0.18548	0.26992
37	-0.002192	0.05226	0.13591	0.19208	0.28025
42	-2.2E-06	0.05171	0.14305	0.19151	0.28349
54	0.000564	0.05501	0.16883	0.19977	0.30035
63	0.001643	0.06162	0.17103	0.20417	0.30851
102	-0.006074	0.07537	0.19353	0.20855	0.34172

Table A.1.6 Shrinkage values of the W/C=0.55 & 5% SRA test series.
Shrinkage is presented in (%)

Age (days)	100% RH	88% RH	75% RH	63% RH	42% RH
0	0	0	0	0	0
7	0.004356	0.02285	0.0341	0.05042	0.10357
14	0.004377	0.02269	0.03369	0.04979	0.15515
21	0.004377	0.02265	0.03359	0.04969	0.16502
30	0.004399	0.02262	0.03345	0.04963	0.16888
37	0.004421	0.02261	0.03335	0.04961	0.17436
42	0.00441	0.0226	0.03328	0.04961	0.17436
54	0.004415	0.02257	0.03309	0.04955	0.1804
63	0.004399	0.02252	0.03305	0.04952	0.18259
102	0.004432	0.02245	0.0329	0.04947	0.19302

Table A.1.7 Shrinkage values of the W/C=0.55 & 7.5% SF test series.
Shrinkage is presented in (%)

Age (days)	100% RH	93 % RH	78% RH	66 % RH	42% RH
0	0	0	0	0	0.0000
7	-0.01	0.098	0.20933	0.25933	0.3630
14	-0.03867	0.110667	0.25133	0.29733	0.4110
21	-0.02767	0.132	0.25533	0.30333	0.4250
28	-0.01667	0.145333	0.266	0.30667	0.4390
35	-0.018	0.138	0.26467	0.31467	0.4630
42	-0.01	0.134333	0.294	0.31533	0.4800
56	-0.00867	0.135333	0.302	0.34	0.4870
70	-0.01333	0.128	0.30733	0.328	0.4910
90	-0.022	0.122667	0.30667	0.33333	0.4940

Table A.1.8 Shrinkage values of the W/C=0.55 & 7.5% SF & 5% SRA test series.
Shrinkage is presented in (%)

Age (days)	100% RH	93 % RH	78% RH	66 % RH	42% RH
0	0	0	0	0	0
7	-0.008	0.077333	0.138	0.14933	0.184
14	-0.03333	0.087333	0.16533	0.17	0.21333
21	-0.02333	0.108667	0.16333	0.172	0.21933
28	-0.01333	0.106667	0.16733	0.17133	0.22267
35	-0.014	0.104667	0.16867	0.17733	0.232
42	-0.01333	0.104667	0.18533	0.17733	0.24467
56	-0.016	0.104667	0.19333	0.19533	0.254
70	-0.01733	0.097333	0.20533	0.18867	0.25067
90	-0.02267	0.092667	0.206	0.19333	0.24067

Table A.1.9 Shrinkage values of the W/C=0.45 Reference test series.

Shrinkage is presented in (%)

Age (days)	100% RH	88% RH	75% RH	63% RH	42 % RH
0	0	0	0	0	0
7	-0.009924	0.033678	0.07438	0.143418	0.2083
14	-0.011581	0.038643	0.08958	0.168172	0.23439
21	-0.01544	0.03809	0.08306	0.164887	0.23387
28	-0.013784	0.041962	0.09827	0.181941	0.25181
35	-0.018764	0.048035	0.10806	0.187439	0.2578
42	-0.017636	0.047501	0.10968	0.188538	0.26215
49	-0.018748	0.041964	0.11457	0.192401	0.27193
56	-0.019297	0.0486	0.1249	0.195148	0.27467
70	-0.013236	0.046382	0.13795	0.202341	0.28064
130	-0.022069	0.052454	0.14122	0.204506	0.28445

Table A.1.10 Shrinkage values of the W/C=0.45 & 5% SRA test series.

Shrinkage is presented in (%)

Age (days)	100% RH	88% RH	75% RH	63% RH	42 % RH
0	0	0	0	0	0
7	-0.013672	0.029526	0.05024	0.094634	0.11373
14	-0.01586	0.036628	0.06718	0.112807	0.13154
21	-0.019685	0.035568	0.06771	0.107831	0.12776
28	-0.017497	0.041581	0.07701	0.12326	0.14071
35	-0.016947	0.046508	0.08301	0.127114	0.14448
42	-0.021319	0.044852	0.08574	0.126577	0.14503
49	-0.020772	0.040474	0.09394	0.131511	0.14826
56	-0.020228	0.048669	0.0994	0.135418	0.14827
70	-0.018581	0.046484	0.11196	0.138702	0.15366
130	-0.027859	0.051411	0.11579	0.143093	0.16663

Table A.1.11 Shrinkage Values of the W/C=0.45 + 7.5% SF test series.
Shrinkage is presented in (%)

Age (days)	100% RH	88 % RH	75% RH	63 % RH	39% RH
0	0	0	0	0	0
7	-0.038667	0.065333	0.17	0.21267	0.27867
14	-0.024667	0.096667	0.215333	0.24333	0.31933
21	-0.024	0.099333	0.226667	0.26133	0.34867
28	-0.023333	0.1	0.233333	0.262	0.368
35	-0.027333	0.100667	0.235333	0.27933	0.372
42	-0.031333	0.108667	0.234	0.266	0.382
56	-0.035333	0.125333	0.238667	0.28667	0.416
70	-0.034667	0.098	0.245333	0.28667	0.41733
90	-0.043333	0.092667	0.244667	0.27933	0.42267

Table A.1.12 Shrinkage Values of the W/C=0.45 + 7.5% SF & 5% SRA test series.
Shrinkage is presented in (%)

Age (days)	100% RH	88 % RH	75% RH	63 % RH	39% RH
0	0	0	0	0	0
7	-0.022667	0.06	0.133333	0.16267	0.172
14	-0.002667	0.088667	0.170667	0.18733	0.209
21	-0.001667	0.096667	0.184	0.2	0.218
28	-0.000667	0.094667	0.186667	0.20267	0.229
35	-0.005333	0.098667	0.185333	0.206	0.229
42	-0.01	0.104667	0.185333	0.20133	0.232
56	-0.012667	0.114667	0.192667	0.21067	0.238
70	-0.014	0.092667	0.196667	0.22067	0.242
90	-0.020667	0.086	0.198	0.218	0.25

Table A.1.13 Shrinkage values of the W/C=0.35 Reference test series.
Shrinkage is presented in (%)

Age (days)	100% RH	88 % RH	75% RH	63 % RH	42% RH
0	0	0	0	0	0
7	-0.009873	0.046748	0.091415	0.15572	0.23175
14	-0.007675	0.053355	0.110152	0.19154	0.25973
21	-0.002737	0.053919	0.12448	0.20253	0.27128
28	-0.00768	0.051694	0.136608	0.20638	0.2795
35	-0.000545	0.057743	0.140472	0.21135	0.28555
42	-0.000547	0.062153	0.153707	0.21633	0.28828
49	-0.008222	0.052248	0.160874	0.21741	0.29323
97	-0.008771	0.061055	0.184039	0.22679	0.31354

Table A.1.14 Shrinkage values of the W/C=0.35 & 5% SRA test series.
Shrinkage is presented in (%)

Age (days)	100% RH	88 % RH	75% RH	63 % RH	42% RH
0	0	0	0	0	0
7	-0.012024	0.032396	0.068718	0.10979	0.14105
14	-0.016939	0.035654	0.084657	0.12956	0.16732
21	-0.012548	0.0373	0.099505	0.13834	0.17389
28	-0.015848	0.038405	0.109418	0.14438	0.17937
35	-0.014757	0.046602	0.113816	0.14767	0.18155
42	-0.019672	0.040578	0.122626	0.15042	0.1843
49	-0.021863	0.034542	0.13088	0.15372	0.18648
97	-0.028428	0.044436	0.144638	0.16197	0.19524

Table A.1.15 Shrinkage values of the W/C=0.35 + 7.5% SF test series.

Shrinkage is presented in (%)

Age (days)	100% RH	88 % RH	75% RH	63 % RH	42% RH
0	0	0	0	0	0
14	-0.050667	0.05933	0.188	0.232	0.288
21	-0.042	0.07933	0.20667	0.248	0.31
28	-0.042	0.07867	0.204	0.25533	0.322
35	-0.042	0.078	0.226	0.262	0.334
42	-0.046	0.08	0.21133	0.25733	0.32867
56	-0.052667	0.078	0.226	0.26333	0.34
70	-0.075333	0.056	0.214	0.238	0.32933
90	-0.058	0.06467	0.236	0.26267	0.348

Table A.1.16 Shrinkage values of the W/C=0.35 & 7.5% SF & 5% SRA test series.

Shrinkage is presented in (%)

Age (days)	100% RH	88 % RH	75% RH	63 % RH	42% RH
0	0	0	0	0	0
14	-0.023333	0.05333	0.13867	0.14867	0.18133
21	-0.012	0.078	0.154	0.156	0.204
28	-0.006667	0.08533	0.16467	0.17333	0.21333
35	-0.006	0.08	0.16333	0.174	0.222
42	-0.012	0.08133	0.156	0.172	0.22467
56	-0.019333	0.07867	0.16267	0.172	0.226
70	-0.058667	0.052	0.15	0.15133	0.20867
90	-0.023333	0.068	0.174	0.17267	0.22733

Table A.1.17 Shrinkage values of the W/C=0.25 Reference test series.

Shrinkage is presented in (%)

Age (days)	100% RH	88% RH	75 % RH	63% RH	42% RH
0	0	0	0	0	0
7	-0.162209	0.014911	0.30457	0.328347	0.3543012
14	-0.187453	0.015367	0.29342	0.332764	0.3684439
21	-0.202395	0.004724	0.30396	0.363038	0.3879343
28	-0.202395	0.012293	0.31292	0.379721	0.3960869
35	-0.222102	0.030506	0.31437	0.380957	0.402457
42	-0.202474	0.052987	0.3466	0.401706	0.4188798
49	-0.232723	0.034717	0.3114	0.366571	0.4068996
56	-0.159362	0.054865	0.34964	0.413178	0.4421977
70	-0.150279	0.047468	0.35197	0.410706	0.4527754

Table A.1.18 Shrinkage Values of the W/C=0.25 & 5% SRA test series.

Shrinkage is presented in (%)

Age (days)	100% RH	88% RH	75 % RH	63% RH	42% RH
0	0	0	0	0	0
7	0.0000	0.0000	0.0000	0.0000	0.0000
14	-0.1096	0.0696	0.2113	0.2364	0.2820
21	-0.1574	0.0643	0.2229	0.2528	0.3065
28	-0.1791	0.0569	0.2312	0.2792	0.3164
35	-0.1765	0.0718	0.2407	0.2924	0.3242
42	-0.1726	0.0858	0.2504	0.2990	0.3286
56	-0.1625	0.1117	0.2744	0.3211	0.3495
70	-0.1726	0.1204	0.2738	0.3343	0.3629
90	-0.1344	0.1289	0.2807	0.3331	0.3673

Table A.1.19 Shrinkage values of the W/C=0.25 & 7.5% SF test series.

Shrinkage is presented in (%)

Age (days)	100% RH	88% RH	75 % RH	63% RH	42% RH
0	0	0	0	0	0
7		0.01133	0.011	0.164	0.22
14	-0.074667	0.02267	0.038	0.18467	0.24267
21	-0.076	0.026	0.051	0.19	0.256
28	-0.065333	0.03733	0.067	0.21067	0.268
35	-0.064	0.04333	0.075	0.21333	0.278
42	-0.063333	0.04133	0.081	0.21533	0.28133
49	-0.064667	0.05133	0.081	0.21933	0.282
57	-0.069333	0.04533	0.082	0.21733	0.28933
71	-0.074	0.05867	0.085	0.22867	0.28467
91	-0.073333	0.03867	0.092	0.22067	0.28

Table A.1.20 Shrinkage values of the W/C=0.25 & 7.5% SF & 5% SRA test series.

Shrinkage is presented in (%)

Age (days)	100% RH	88% RH	75 % RH	63% RH	42% RH
0	0	0	0	0	0
7	-0.02	0.0273	0.0887	0.13067	0.15867
14	-0.04	0.0427	0.1173	0.146	0.18
21	-0.04	0.0473	0.1280	0.15133	0.188
28	-0.024	0.0633	0.1447	0.16867	0.202
35	-0.024667	0.0593	0.1513	0.17667	0.21
42	-0.021333	0.0640	0.1640	0.178	0.21333
56	-0.024667	0.0647	0.1680	0.17667	0.21333
70	-0.034667	0.0710	0.1730	0.186	0.21233
90	-0.039333	0.0680	0.1740	0.18267	0.21133

Table A.1.21 Mass loss valuse of W/C = 0.65 Reference test series.

Mass loss is presented in (%)

Age (days)	100% RH	88 % RH	75% RH	63 % RH	42% RH
0	0	0	0	0	0
7	-6.88036	6.22164	9.79633	11.8689	13.5694
14	-8.12017	6.29313	10.3386	12.4357	14.4019
21	-8.52103	7.25209	10.6139	12.8285	14.5594
28	-8.21586	7.20529	10.8099	13.1868	14.4414
35	-8.28763	7.22145	10.8726	13.2908	14.237
42	-8.36344	7.30052	10.9414	13.4066	13.954
49	-8.41629	7.1198	10.8935	13.5219	13.828
52	-8.52716	7.20624	10.8225	13.5676	13.8044
70	-8.81842	7.14401	10.6238	13.4975	13.7651
90	-8.93123	7.15903	11	13.6359	14.1189

Table A.1.22 Mass loss valuse of W/C = 0.65 & 5% SRA test series.

Mass loss is presented in (%)

Age (days)	100% RH	88 % RH	75% RH	63 % RH	42% RH
0	0	0	0	0	0
7	-4.44023	8.47231	12.9401	13.0478	15.643
14	-5.0948	8.8462	13.4551	14.0621	16.5793
21	-5.3203	9.5698	13.9384	14.6584	16.7973
28	-5.35154	9.62752	14.0572	14.9258	16.8747
35	-6.63481	9.63672	14.0416	14.9564	16.8976
42	-5.35154	9.73381	14.0768	15.0478	16.8499
49	-4.82678	8.80951	14.0172	15.0937	16.889
56	-4.82648	9.63753	13.9456	15.5	16.8413
70	-5.14452	10.3856	13.7911	15.124	16.5745
90	-5.14452	10.3856	13.7911	15.124	16.5745

Table A.1.23 Mass loss valuse of W/C = 0.65 & 7.5% SF test series.

Mass loss is presented in (%)

Age (days)	100% RH	88 % RH	75% RH	63 % RH	42% RH
0	0	0	0	0	0
7	-6.1945094	4.868945	10.983844	10.66712	16.23715
14	-6.7254566	6.431939	12.363948	14.58529	17.50086
21	-6.5150251	6.552423	12.70953	13.49003	17.60756
28	-6.8178895	6.697683	12.89385	13.84	17.49636
35	-7.1207539	6.701608	12.912776	13.96	17.19309
42	-7.1269853	6.705532	12.931703	14.14814	17.1008
70	-7.2753221	7.197329	13.407644	14.47253	17.32266
90	-7.468096	6.592077	14.34205	14.60547	17.02828
120	-7.5969364	6.003245	13.658749	13.72485	15.39215

Table A.1.24 Mass loss valuse of W/C = 0.65 & 7.5% SF & 5% SRA test series.

Mass loss is presented in (%)

Age (days)	100% RH	88 % RH	75% RH	63 % RH	42% RH
0	0	0	0	0	0
7	-5.1770669	7.386721	13.291048	11.24956	22.2071
14	-5.6915704	9.477709	14.62426	15.06717	23.26786
21	-5.7476175	9.541693	15.106624	15.54615	23.35286
28	-5.9641634	9.647783	15.313911	15.553	23.2955
35	-6.1807093	9.667863	15.291845	15.679	23.22864
42	-6.1240081	9.687944	15.269779	15.87901	23.16808
49	-6.4773971	9.647276	15.27777	15.87074	22.30983
56	-6.3096734	9.793935	15.210567	15.93582	22.98662
70	-6.397463	10.07935	15.567925	15.98463	22.95241

Table A.1.25 Mass loss values of the W/C=0.55 Reference test series.

Mass loss is presented in (%)

Age(days)	100% RH	88% RH	75% RH	63% RH	42% RH
0	0	0	0	0	0
7	-0.969469	3.0815	6.33328	9.59104	12.374
14	-1.150874	3.83847	7.75988	11.6024	14.4904
21	-1.436165	4.07578	8.01931	12.1013	14.8752
30	-1.496758	4.15171	8.38305	12.434	14.7936
37	-1.716429	3.96084	7.61167	12.2752	14.5562
42	-2.140185	4.06174	7.44798	12.4793	14.6603
54	-2.382984	3.81709	7.21836	12.5473	14.5935
63	-2.200736	3.92403	7.27754	12.5246	14.5416
102	-2.054557	3.29513	6.75016	12.5853	14.1039

Table A.1.26 Mass loss values of the W/C=0.55 & 5% SRA test series.

Mass loss is presented in (%)

Age(days)	100% RH	88% RH	75% RH	63% RH	42% RH
0	0	0	0	0	0
7	-0.552097	3.12614	6.84214	10.9228	13.2385
14	-0.656897	5.11825	9.95955	13.3557	15.2229
21	-0.812787	5.64185	10.3553	13.8129	15.6875
30	-0.940234	5.94474	10.1062	14.108	15.8097
37	-1.328578	5.70057	9.82684	13.9233	15.6799
42	-1.941987	5.8704	9.66564	14.1374	15.8549
54	-1.796971	5.58246	9.38615	14.1301	15.8855
63	-1.885878	5.76653	9.47463	14.3143	15.9084
102	-1.301469	5.38241	8.85756	14.3807	15.7941

Table A.1.27 Mass loss values of the W/C=0.55 & 7.5% SF test series.

Mass loss is presented in (%)

Age(days)	100% RH	88 % RH	75% RH	63 % RH	42% RH
0	0	0	0	0	0
7	-5.075874	5.243947	9.928009	12.031	14.3985
14	-5.721096	6.367355	10.40248	12.6812	15.1118
21	-5.99626	6.312861	10.62265	12.983	15.3368
28	-5.818916	6.499837	10.71442	13.1496	15.2259
35	-5.907363	6.320285	10.79057	13.285	14.906
42	-5.996016	6.763254	11.13421	13.4907	15.1632
56	-6.117692	6.27244	11.3535	13.8473	15.0958
70	-6.26268	5.798022	11.5728	13.4502	14.3404
90	-6.256044	5.471708	11.78196	13.116	13.6946

Table A.1.28 Mass loss values of the W/C=0.55 & 7.5% SF & 5% SRA test series.

Mass loss is presented in (%)

Age(days)	100% RH	88 % RH	75% RH	63 % RH	42% RH
0	0	0	0	0	0
7	-3.496008	6.820557	11.73081	13.3081	14.7215
14	-5.143611	7.685961	12.37387	14.18	15.5006
21	-5.675449	7.670225	12.57254	14.4313	15.6344
28	-5.735902	7.902782	12.65981	14.5808	15.5871
35	-5.812568	7.717784	12.7234	14.6674	15.3824
42	-5.876029	8.183803	13.05707	14.62	15.343
56	-5.889978	7.678248	12.88657	14.58	15.39
70	-6.108118	7.26086	12.71607	14.558	15.28
90	-6.169937	7.003905	12.54129	14.181	15.34

Table A.1.29 Mass Loss values of the W/C=0.45 Reference test series.
Mass loss is presented in (%)

Age(days)	100% RH	88 % RH	75% RH	63 % RH	42% RH
0	0	0	0	0	0
7	-3.92458948	1.68994112	4.3872314	8.2828063	10.697699
14	-4.0528644	1.54466356	4.6399327	8.9308616	11.280552
21	-4.17334694	1.32587156	4.3855628	8.9438295	11.353844
28	-4.21855209	1.25316248	4.4819802	9.2747285	11.644922
35	-4.2418093	1.2759568	4.6684387	9.3950703	11.797708
42	-4.36132395	1.47185446	4.6968714	9.6504208	11.542554
49	-4.50451979	1.22446369	4.4988108	9.6498267	11.542072
56	-4.44367465	1.19513251	4.4680065	9.6350728	11.411378
70	-4.27065538	1.04237214	4.1817581	9.7610367	11.309709

Table A.1.30 Mass Loss values of the W/C=0.45 & 5% SRA test series.
Mass loss is presented in (%)

Age(days)	100% RH	88 % RH	75% RH	63 % RH	42% RH
0	0	0	0	0	0
7	-2.92679224	2.77412115	7.1102893	10.342115	12.657251
14	-3.14668208	2.88418285	7.6850592	11.295259	13.317263
21	-3.23034802	2.72299379	7.5647125	11.214157	13.403078
28	-3.32988057	2.74465399	7.6642449	11.612849	13.826579
35	-3.27382682	2.83252404	7.7796959	11.77191	13.920024
42	-3.44317035	3.0095514	7.7288266	11.931756	13.948514
49	-3.54200791	2.73723776	7.5424723	11.916442	14.005839
56	-3.4144365	2.84016368	7.4116609	11.865417	13.962778
70	-3.28792566	2.54616228	7.2759639	12.010343	14.027413

Table A.1.31 Mass loss values of the W/C = 0.45 &7.5% SF test series.
Mass loss is presented in (%)

Age(days)	100% RH	88 % RH	75% RH	63 % RH	42% RH
0	0	0	0	0	0
7	-6.675871	3.282639	5.953545	8.49013	11.0201
14	-6.932551	3.565328	6.500531	9.15406	11.5508
21	-6.474587	3.594206	6.757669	9.44574	11.5344
28	-6.967785	3.565059	6.991769	9.65008	11.5578
35	-7.018984	3.631367	7.021688	9.78086	11.5493
42	-7.027355	3.776869	7.079779	10.0064	11.45
56	-7.144752	4.023038	7.738079	10.1449	11.456
70	-7.163693	3.724798	7.956904	10.2615	11.3198
90	-7.219203	3.461184	7.994764	9.70779	11.2214

Table A.1.32 Mass loss values of the W/C = 0.45 & 7.5% SF & 5% SRA test series.
Mass loss is presented in (%)

Age(days)	100% RH	88 % RH	75% RH	63 % RH	42% RH
0	0	0	0	0	0
7	-6.981327	4.437046	7.186548	9.95621	11.53
14	-7.453082	5.436103	7.900007	10.5195	11.974
21	-7.461928	4.827137	8.092858	10.7596	12.0091
28	-7.29656	4.768059	8.188504	10.9084	12.0311
35	-7.427094	4.871179	8.254972	10.9544	11.9872
42	-7.427551	5.011046	8.254299	11.0747	11.9363
56	-7.604945	5.18	8.615231	11.1722	11.8188
70	-7.638165	4.841417	8.609163	11.2692	11.6222
90	-7.714297	4.443882	8.354473	10.9908	11.4251

Table A.1.33 Mass loss values of the W/C=0.35 Reference test series.

Mass loss is presented in (%)

Age(days)	100% RH	88 % RH	75% RH	63 % RH	42% RH
0	0	0	0	0	0
7	-0.990453	1.084698	2.789963	6.14895	9.15441
14	-1.523158	1.032573	3.190725	6.98597	10.2618
21	-1.236232	1.080552	3.217806	7.3106	10.5559
28	-1.229722	1.059065	3.395312	7.49872	10.6163
35	-2.303301	0.956897	3.27937	8.24992	10.9451
42	-1.948342	0.828585	3.449909	8.00719	10.7366
49	-2.107666	0.699356	3.442505	7.66805	10.7844
97	-1.676174	0.407339	3.803043	8.12931	10.757

Table A.1.34 Mass loss values of the W/C=0.35 & 5% SRA test series.

Mass loss is presented in (%)

Age(days)	100% RH	88 % RH	75% RH	63 % RH	42% RH
0	0	0	0	0	0
7	-2.513526	0.933177	3.498437	6.30037	8.66437
14	-3.474185	0.919855	3.917713	7.39051	9.71939
21	-2.780161	0.858867	3.917855	7.79184	10.0425
28	-2.961636	0.906282	4.180369	7.9514	10.2136
35	-3.7587	0.743306	3.944301	7.99187	10.2997
42	-3.269847	0.647493	3.910029	7.88509	10.2507
49	-4.053086	0.309745	3.964706	7.95177	10.3378
97	-3.366785	0.024881	4.355801	8.30596	10.5381

Table A.1.35 Shrinkage values of the W/C=0.35 + 7.5% SF test series.

Mass loss is presented in (%)

Age(days)	100% RH	88 % RH	75% RH	63 % RH	42% RH
0	0	0	0	0	0
14	-4.198562	1.17423	3.49821	5.66123	7.85504
21	-4.750202	1.20188	3.72768	5.98913	8.2823
28	-4.476164	1.13273	4.03671	6.16414	8.46102
35	-4.760886	1.16041	3.9353	6.35978	8.59525
42	-4.666344	1.20172	3.97817	6.39481	8.72948
56	-4.748388	1.29843	4.12923	6.58984	8.63974
70	-4.756296	1.44326	4.33496	6.7244	9.00456
90	-4.973342	1.17419	4.29865	6.80422	8.51806

Table A.1.36 Shrinkage values of the W/C=0.35 + 7.5% SF & 5% SRA test series.

Mass loss is presented in (%)

Age(days)	100% RH	88 % RH	75% RH	63 % RH	42% RH
0	0	0	0	0	0
14	-4.602522	1.79035	5.0679	7.3445	8.38689
21	-4.789354	1.87383	5.36693	7.67097	8.79266
28	-4.782501	1.90182	5.74178	7.80699	8.93125
35	-5.030758	1.90872	5.87923	7.93672	9.04223
42	-4.925388	1.95733	6.0084	7.94302	9.11142
56	-5.058766	2.06879	6.16541	8.09332	9.05638
70	-4.999002	2.22195	6.45067	8.30433	9.21576
90	-5.084335	1.91554	6.49914	8.14773	8.69605

Table A.1.37 Mass loss values of the W/C=0.25 Referece test series.
Mass loss is presented in (%)

Age(days)	100% RH	88 % RH	75% RH	63% RH	42% RH
0	0	0	0	0	0
7	-3.336621	-0.18537	3.34356	3.127394	4.4410144
14	-3.659473	-0.52625	3.18526	4.267384	5.0289414
21	-4.223454	-0.66438	3.19789	3.89154	5.4491856
28	-4.099011	-0.78886	3.21057	3.962938	5.6714579
35	-3.805118	-0.74303	3.23588	4.05235	5.8818835
42	-3.785616	-0.74977	3.24857	4.075753	6.0114203
49	-3.704758	-0.74341	3.25488	4.033549	6.1223837
56	-3.895387	-0.35711	3.28019	4.01547	6.2152501
70	-3.913759	-0.27903	3.25488	4.080159	6.6562416
90	-3.920436	-0.3647	3.22319	4.035311	6.7606092

Table A.1.38 Mass loss values of the W/C=0.25 & 5% SRA test series.
Mass loss is presented in (%)

Age(days)	100% RH	88 % RH	75% RH	63% RH	42% RH
0	0.0000	0.0000	0.0000	0.0000	0.0000
7	-3.4629	0.9862	3.9797	4.1696	5.1615
14	-3.5576	0.5829	3.9291	4.6294	5.7078
21	-3.8645	0.4482	4.0111	4.8222	6.0858
28	-3.9487	0.3841	3.9733	4.8782	6.2354
35	-3.6427	0.4424	4.0425	4.9403	6.4049
42	-3.6482	0.4682	4.0358	4.9589	6.4962
49	-3.6668	0.4885	4.0463	4.9029	6.5676
56	-3.8097	0.5081	4.0751	4.8843	6.6327
70	-4.0341	0.6656	4.0463	4.8045	6.6781
90	-3.8676	0.5590	4.0174	4.7002	6.6586

Table A.1.39 Mass loss values of the W/C=0.25 & 7.5% SF test series.

Mass loss is presented in (%)

Age(days)	100% RH	88 % RH	75% RH	63% RH	42% RH
0	0	0	0	0	0
7	-3.049104	-0.23562	0.83114	1.61194	3.49213
14	-3.653722	-0.2553	1.147956	2.15187	4.32533
21	-3.883706	-0.29468	1.230844	1.80123	4.70325
28	-3.844096	-0.39312	1.379832	2.57485	4.87934
35	-3.86359	-0.37343	1.398449	2.69207	5.00301
42	-3.949756	-0.38005	1.417794	2.75068	5.09429
57	-3.978271	-0.34069	1.501444	2.86773	5.1536
71	-3.949964	-0.14379	2.248439	3.10217	5.68027
91	-3.997765	-0.29488	2.350517	3.11504	5.19795

Table A.1.40 Mass loss values of the W/C=0.25 & 7.5% SF & 5% SRA test series.

Mass loss is presented in (%)

Age(days)	100% RH	88 % RH	75% RH	63% RH	42% RH
0	0	0	0	0	0
7	-5.471055	0.24756	2.008461	3.39513	4.3439
14	-4.798823	0.28088	2.50355	4.12959	4.96912
21	-4.856494	0.17118	2.774493	4.38508	5.21787
28	-5.768195	0.24739	3.073922	4.47683	5.32569
35	-5.729772	0.24126	3.012635	4.53591	5.41994
42	-5.118024	0.02542	3.045744	4.54889	5.46699
49	-5.322632	0.03455	3.098655	4.60126	5.44708
58	-5.259876	0.32555	3.105461	4.60126	5.47397
70	-5.188001	0.54599	3.12	4.80457	5.68251
90	-5.201401	0.20805	3.11	4.67996	5.18526

Table A.1.41 Summary of Cube Strength, All Mixes

Compressive Strength in units of psi

	7	14	28	56
w/c=0.25	15862	16558	19278	
w/c=0.25, 5% SRA	13383	14143	17496	
w/c=0.25 & 7.5% SF	15448	14950	17899	
w/c=0.25 & 7.5% SF, 5% SRA	13542	12959	15725	
w/c=0.35	12717	12650	9175	10064
w/c=0.35, 5% SRA	11775	13167	8758	12826
w/c=0.35 & 7.5% SF	10117	9850	7792	8208
w/c=0.35 & 7.5% SF, 5% SRA	9425	10875	7142	8208
w/c=0.45	8167	8900	6625	9638
w/c=0.45, 5% SRA	7308	8383	6167	8110
w/c=0.45 & 7.5% SF	7450	9017	5967	9853
w/c=0.45 & 7.5% SF, 5% SRA	7517	8800	6233	9138
w/c=0.55	5633	4799	4936	
w/c=0.55, 5% SRA	6025	6872	7195	
w/c=0.55 & 7.5% SF	4917	6163	6907	
w/c=0.55 & 7.5% SF, 5% SRA	5817	6864	7936	
w/c=0.65	4608	5608	6188	
w/c=0.65, 5% SRA	5033	5488	5949	
w/c=0.65 & 7.5% SF	3325	4424	5130	
w/c=0.65 & 7.5% SF, 5% SRA	4183	4740	5895	

Table A.1.42 Compressive Moduli of Elasticty, All Mixes

All units in 10^6 psi

Age	w/c=0.25	w/c=0.25, 5% SRA	w/c=0.25 + 7.5% SF	w/c=0.25 + 7.5% SF, 5% SRA
1	1.0347813	1.012890193	3.72303833	3.694379125
7	1.1829602	1.034216129	4.251666979	4.142160429
14	1.2600797	0.966632589	3.843553316	3.83108325
28	1.3496099	1.199432074	4.382309469	3.93069815
56	1.425768	1.255287925	3.925446	4.563576258
90	1.7363833	1.683205592		4.27077049

Age	w/c=0.35	w/c=0.35, 5% SRA	w/c=0.35 + 7.5% SF	w/c=0.35 + 7.5% SF, 5% SRA
1			0.735938916	0.731618284
7			0.818197783	0.99107779
14			0.787169966	0.980297568
28			1.100371162	0.847490084
56			1.055615564	1.030243734
90			0.947067621	0.913867019

Age	w/c=0.45	w/c=0.45, 5% SRA	w/c=0.45 + 7.5% SF	w/c=0.45 + 7.5% SF, 5% SRA
1	2.4171784	2.044596849	2.216728215	1.868658884
7	2.5007223	2.184950928	2.209667788	2.248053005
14	2.9212259	2.407699278	2.588479374	2.492367848
28	2.8714193	2.714106252	2.818613226	2.660424679
56	2.8991428	2.870477006	3.147591328	3.043057101
90	3.2146529	3.024867847	3.017735035	2.919034552

Age	w/c=0.55	w/c=0.55, 5% SRA	w/c=0.55+7.5% SF	w/c=0.55 + 7.5% SF, 5% SRA
2	1.0443266	1.488376099	1.346	1.416937875
7	1.9902635	1.674955244	1.590	1.506160872
14	2.0851689	1.898046931	1.726	2.58168565
28	2.4052743	2.107420387	2.163	2.409539348
56	2.1089351	1.947598822	2.137	2.74407534
90	2.4033803	2.448813682	2.395	2.531

Age	w/c=0.65	w/c=0.65, 5% SRA	w/c=0.65+7.5% SF	w/c=0.65 + 7.5% SF, 5% SRA
2	0.5097791	0.523774593	0.959652313	1.026663058
7	0.491458	0.584411875	1.071635206	1.25230012
14	0.5681664	0.540886059	1.290325199	1.510955598
28	0.5892971	0.520701198	1.757559159	1.688779986
56			1.736997873	2.051211288
90	0.9658293	0.833228629	1.913520751	1.869491326

Table A.1.43 Curling Center-Line-Deflections, All Mixes

Deflections measured in inches, Age in days

w/c	SF%	%SRA	7	28	56	90
0.25	0	0	0.055	0.05	0.065	0.09
0.25	0	5	0.055	0.085	0.11	0.145
0.25	7.5	0	0.06	0.04	0.065	0.105
0.25	7.5	5	0.05	0.075	0.11	0.14
0.35	0	0	0.115	0.095	0.14	0.18
0.35	0	5	0.085	0.06	0.105	0.145
0.35	7.5	0	0.15	0.175	0.285	0.365
0.35	7.5	5	0.075	0.11	0.17	0.25
0.45	0	0	0.22	0.205	0.35	0.46
0.45	0	5	0.095	0.05	0.12	0.18
0.45	7.5	0	0.295	0.38	0.635	0.8
0.45	7.5	5	0.21	0.13	0.18	0.295
0.55	0	0	0.13	0.295	0.59	0.77
0.55	0	5	0.11	0.115	0.195	0.3
0.55	7.5	0	0.265	0.385	0.65	0.785
0.55	7.5	5	0.165	0.12	0.17	0.295
0.65	0	0	0.21	0.355	0.615	0.765
0.65	0	5	0.2	0.125	0.195	0.3
0.65	7.5	0	0.265	0.445	0.68	0.74
0.65	7.5	5	0.155	0.075	0.18	0.3